Scientific Aspects of Polymer Electrolyte Fuel Cell Durability and Degradation

Rod Borup,* Jeremy Meyers,[‡] Bryan Pivovar,[†] Yu Seung Kim,[†] Rangachary Mukundan,[†] Nancy Garland,[§] Deborah Myers,[||] Mahlon Wilson,[†] Fernando Garzon,[†] David Wood,[†] Piotr Zelenay,[†] Karren More,[⊥] Ken Stroh,[†] Tom Zawodzinski,[⊗] James Boncella,[†] James E. McGrath,[○] Minoru Inaba,[#] Kenji Miyatake,[▽] Michio Hori,[◆] Kenichiro Ota,[△] Zempachi Ogumi,[£] Seizo Miyata,[+] Atsushi Nishikata,[¶] Zyun Siroma,[∞] Yoshiharu Uchimoto,[◇] Kazuaki Yasuda,[+] Ken-ichi Kimijima,[∞] and Norio Iwashita[∞]

Los Alamos National Laboratory, Los Alamos, New Mexico 87545, University of Texas at Austin, Austin, Texas 78712-0292, U.S. Department of Energy, Washington, DC 20585, Argonne National Laboratory, Argonne, Illinois 60439, Oak Ridge National Laboratory, Oak Ridge, Tennessee 37831-6064, Case Western Reserve University, Cleveland, Ohio 44120, Virginia Tech University, Blacksburg, Virginia 24061, Doshisha Univerisy, Kyotanabe, Kyoto 610-0321, Japan, University of Yamanashi, Kofu, Yamanashi 400-8510, Japan, Daido Institute of Technology, Nagoya, Aichi 457-8530, Japan, Yokohama National University, Hodogaya-ku, Yokohama 240-8501, Japan, Kyoto University, Nishikyo-ku, Kyoto 615-8510, Japan, New Energy and Industrial Technology Development Organization, Kawasaki City, Kanagawa 212-8554, Japan, Tokyo Institute of Technology, Meguro-ku, Tokyo 152-8552, Japan, AIST, Tokyo 135-0064, Japan, and Kyoto University, Sakyo-ku, Kyoto 606-8501, Japan

Received April 17, 2007

Contents

1. Introduction 3905
- 1.1. Durability Targets for Stationary and Transportation Applications 3907
  - 1.1.1. U.S. DOE Fuel Cell Programs 3907
  - 1.1.2. Japanese NEDO Fuel Cell Programs 3908
  - 1.1.3. European Hydrogen and Fuel Cell Technology Platform 3908
- 1.2. PEM Fuel Cell Materials 3908
- 1.3. Durability Tests 3909

2. Operational Effects on Fuel Cell Durability 3910
- 2.1. Impurity Effects 3911
  - 2.1.1. Fuel Impurities 3911
  - 2.1.2. Air Impurities 3913
- 2.2. Subfreezing Effects in PEM Fuel Cells 3914
  - 2.2.1. Effect of Subfreezing Temperatures on PEM Fuel Cells and Components 3914
  - 2.2.2. Start-up Characteristics of Fuel Cells at Subfreezing Temperatures 3915
  - 2.2.3. Mitigation Strategies Utilized To Avoid Degradation Due to Subfreezing Temperatures 3916
- 2.3. Other Operating Conditions 3916
  - 2.3.1. Load Cycling: Potential 3916
  - 2.3.2. Fuel Starvation 3916
  - 2.3.3. Start/Stop Cycling 3918
  - 2.3.4. Temperature and Relative Humidity 3918

3. Membrane Degradation 3918
- 3.1. Discussion of Polymer Electrolyte Membranes (PEMs) 3918
- 3.2. *In Situ* PEM Durability Evaluation 3919
  - 3.2.1. Life Test 3919
  - 3.2.2. Accelerated Life Test 3920
- 3.3. Chemical Degradation 3921
  - 3.3.1. Peroxide/Radical Degradation 3921
  - 3.3.2. Hydrolytic Degradation 3924
  - 3.3.3. Efforts to Improve Chemical Properties 3925
- 3.4. Physical Degradation 3925
  - 3.4.1. Membrane Creep 3925
  - 3.4.2. Microcrack Fracture 3927
  - 3.4.3. Structural/Morphological Changes 3928
  - 3.4.4. Efforts To Improve Physical Properties 3929

4. Electrocatalyst Stability 3930
- 4.1. Chemical State of Platinum under PEMFC Cathode Conditions 3930
  - 4.1.1. Thermodynamics 3930
- 4.2. Spectroscopic Analysis of Pt in the Electrochemical Environment 3930
  - 4.2.1. Bulk Electrodes 3930
  - 4.2.2. Carbon-Supported Nanoparticles in Aqueous Electrolyte 3930
  - 4.2.3. Carbon-Supported Platinum Nanoparticles in an MEA 3931
  - 4.2.4. Pt Solubility—Equilibrium 3931
- 4.3. Pt Dissolution under Nonequilibrium Conditions 3932
  - 4.3.1. Aqueous Electrolyte 3932
  - 4.3.2. Phosphoric Acid Fuel Cells 3932
  - 4.3.3. Polymer Electrolyte Fuel Cells 3932
  - 4.3.4. Alloy Effects 3933
- 4.4. Platinum Particle Growth Analysis 3934
  - 4.4.1. Particle Growth Analysis by XRD 3934
  - 4.4.2. Glancing Angle X-ray Diffraction Studies 3935
  - 4.4.3. Particle Growth Analysis by TEM Imaging 3935

* Corresponding author: Rod Borup, MPA-11, MS J579, P.O. Box 1663, Los Alamos National Laboratory, Los Alamos, New Mexico 87545. Phone (office): (505) 667-2823. Fax: (505) 665-9507. E-mail: borup@lanl.gov.
[†] Los Alamos National Laboratory.
[‡] University of Texas at Austin.
[§] U.S. Department of Energy.
[||] Argonne National Laboratory.
[⊥] Oak Ridge National Laboratory.
[⊗] Case Western Reserve University.
[○] Virginia Tech University.
[#] Doshisha Univerisy.
[▽] University of Yamanashi.
[◆] Daido Institute of Technology.
[△] Yokohama National University.
[£] Kyoto University, Nishikyo-ku.
[+] New Energy and Industrial Technology Development Organization.
[¶] Tokyo Institute of Technology.
[∞] AIST.
[◇] Kyoto University, Sakyo-ku.

10.1021/cr050182l CCC: $65.00
Published on Web 09/13/2007

4.4.4. Particle Growth Mechanism 3936
4.5. Corrosion of Catalyst Support 3937
4.5.1. Carbon Corrosion in PEMFCs 3937
4.5.2. Carbon Corrosion in PAFCs 3937
4.5.3. Carbon Corrosion in Aqueous Solutions 3938
4.5.4. Novel Support Materials 3938
4.6. Novel Materials: Nonprecious Catalysts for PEMFC Cathodes 3940
4.6.1. Carbides, Oxides, Oxynitrides, and Carbonitrides 3940
4.6.2. Catalysts Derived from Macrocycles, Porphyrins, and Composites 3941
5. Gas Diffusion Layer (GDL) 3942
5.1. Modeling of Transport Processes 3942
5.2. Saturation and GDL Surface Properties 3942
5.3. Degradation of Mass Transport with Operation 3943
5.3.1. GDL Hydrophobicity Loss 3943
5.3.2. GDL Carbon Corrosion and Loss 3943
5.3.3. Mechanical Degradation of GDLs 3944
6. Summary 3944
7. Acknowledgments 3944
8. References 3944

1. Introduction

Polymer electrolyte membrane (PEM) fuel cells have the potential to alleviate major problems associated with the production and consumption of energy. Fuel cells operate as energy conversion devices, and when supplied with hydrogen derived from renewable energy sources (solar, wind, biomass, *etc.*), they have the potential to substantially and positively impact many areas, including environmental, economic, and energy security. For operation with hydrogen as the fuel, the only chemical byproduct is water; thus, the process is clean. The fuel cell is also more efficient in its conversion of chemical energy to electrical energy than present technologies. Together, these features suggest that fuel cells can reduce the problems associated with petroleum based energy production, which include air pollution, greenhouse-gas emissions, and economic dependence on petroleum. For this reason, industrial developers and world governments have shown great interest in developing fuel cell power sources.

PEM fuel cells are being developed as electrical power sources for vehicles and for stationary and portable power applications. Fuel cell development for use in light-duty vehicles has focused on polymer electrolyte membrane fuel cells (PEMFCs) because they operate at relatively low temperatures and have short start-up and transient-response times compared to other types of fuel cells that operate at higher temperatures (200 °C to 800 °C). Higher-temperature fuel cells are not as amenable to transient behavior required for transportation propulsion, including start-up and shut-down, and do not typically have as high a power density or specific power nor as low a cost. For these reasons, nearly all the major automakers have fuel cell projects based on PEM technology. While there is a concentration on PEMFCs for transportation technologies, other types of fuel cells have been and are currently in development based on other technologies. For a retrospective look at the development of fuel cell technologies over the past 100 years, the reader should see Perry and Fuller.[1]

Rod Borup is a Team Leader in the fuel cell program at Los Alamos National Lab in Los Alamos, New Mexico. He received his B.S.E. in Chemical Engineering from the University of Iowa in 1988 and his Ph.D. from the University of Washington in 1993. He has worked on fuel cell technology since 1994, working in the areas of hydrogen production and PEM fuel cell stack components. He has been awarded 12 U.S. patents, authored over 40 papers related to fuel cell technology, and presented over 50 oral papers at national meetings. His current main research area is related to water transport in PEM fuel cells and PEM fuel cell durability. Recently, he was awarded the 2005 DOE Hydrogen Program R&D Award for the most significant R&D contribution of the year for his team's work in fuel cell durability and was the Principal Investigator for the 2004 Fuel Cell Seminar (San Antonio, TX, USA) Best Poster Award.

Jeremy Meyers is an Assistant Professor of materials science and engineering and mechanical engineering at the University of Texas at Austin, where his research focuses on the development of electrochemical energy systems and materials. Prior to joining the faculty at Texas, Jeremy worked as manager of the advanced transportation technology group at UTC Power, where he was responsible for developing new system designs and components for automotive PEM fuel cell power plants. While at UTC Power, Jeremy led several customer development projects and a DOE-sponsored investigation into novel catalysts and membranes for PEM fuel cells. Jeremy has coauthored several papers on key mechanisms of fuel cell degradation and is a co-inventor of several patents. In 2006, Jeremy and several colleagues received the George Mead Medal, UTC's highest award for engineering achievement, and he served as the co-chair of the Gordon Research Conference on fuel cells. Jeremy received his Ph.D. in Chemical Engineering from the University of California at Berkeley and holds a Bachelor's Degree in Chemical Engineering from Stanford University.

Automobile manufacturers and fuel cell developers have produced PEMFCs for many years, but recent significant technological advances have left two major remaining challenges to widespread fuel cell use: cost and lifetime, which are interrelated. For example, adding more catalyst to a fuel cell increases catalyst lifetime but increases fuel cell cost. Similarly, increasing a fuel cell membrane's thickness increases its lifetime but also increases its cost by

Bryan Pivovar received his B.S. in Chemical Engineering from the University of Wisconsin in 1994. He completed his Ph.D. in Chemical Engineering at the University of Minnesota in 2000 under the direction of Profs. Ed Cussler and Bill Smyrl, studying transport properties in fuel cell electrolytes. He continued working in the area of polymer electrolyte fuel cells at Los Alamos National Laboratory as a post-doc (2000–2001), as a technical staff member (2001–2005), and in his current position as a team leader (2005–present). In this time, Bryan's research has expanded to include further aspects of fuel cell operation, including electrodes, subfreezing effects, alternative polymers, hydroxide conductors, fuel cell interfaces, impurities, water transport, and high-temperature membranes. Bryan has served at various levels in national and international conferences and workshops, including organizing a DOE sponsored workshop on freezing effects in fuel cells and an ARO sponsored workshop on alkaline membrane fuel cells, and he was co-chair of the 2007 Gordon Research Conference on Fuel Cells.

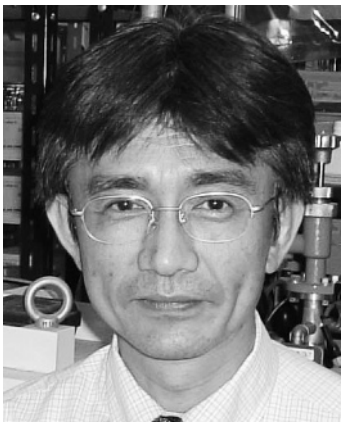

Minoru Inaba is a Professor at the Department of Molecular Science and Technology, Faculty of Engineering, Doshisha University, Japan. He received his B.Sc. from the Faculty of Engineering, Kyoto University, in 1984 and his M.Sc. in 1986 and his Dr. Eng. in 1995 from the Graduate School of Engineering, Kyoto University. He has worked on electrochemical energy conversion systems including fuel cells and lithium-ion batteries at Kyoto University (1992–2002) and at Doshisha University (2002–present). His primary research interest is the durability of polymer electrolyte fuel cells (PEFCs), in particular, membrane degradation, and he has been involved in NEDO R&D research projects on PEFC durability since 2001. He has authored over 140 technical papers and 30 review articles.

adding material and lowering specific performance. Thus, a complex balance exists between the cost and lifetime of a PEM fuel cell. However, since PEM fuel cells currently are not cost competitive for most applications and still do not have sufficient durability, measures to increase fuel cell lifetime that also add expense are not an option. To improve the durability of PEM fuel cells, researchers are studying the factors that determine a PEM fuel cell's lifetime, so that the lifetime can be increased without increasing cost or losing performance.

Kenichiro Ota is a Professor of the Chemical Energy Laboratory at the Graduate School of Engineering, Yokohama National University, Japan. He received his B.S.E. in Applied Chemistry from the University of Tokyo in 1968 and his Ph.D. from the University of Tokyo in 1973. He has worked on hydrogen energy and fuel cells since 1974, working on materials science for fuel cells and water electrolysis. He has published more than 150 original papers, 70 review papers, and 50 scientific books. He is now the president of the Hydrogen Energy Systems Society of Japan, the chairman of the Fuel Cell Research Group of the Electrochemical Society of Japan, and the chairman of the National Committee for the Standardization of the Stationary Fuel Cells. He is also a member of the National Committee for Nuclear Safety.

Zempachi Ogumi is a Professor of the Electrochemistry Laboratory at the Graduate School of Engineering, Kyoto University, Japan. He received his Ph.D. from Kyoto University in 1975 after finishing Bachelor and Master courses in the Department of Industrial Chemistry, Graduate School of Engineering, Kyoto University. He has worked on lithium batteries and fuel cells, focusing on materials science and reactions in electrochemical energy conversion and storage. He is now the president of the Electrochemical Society of Japan.

Studies have shown that several factors can reduce the useful life of a PEM fuel cell, including platinum-particle dissolution and sintering, carbon-support corrosion, and membrane thinning.[2−4] Lifetime can also be reduced by efforts to maximize the initial performance of a fuel cell component. For example, decreasing the equivalent weight of the polymer electrolyte typically increases the membrane's proton conductivity but also increases its water uptake and gas permeability—and degrades its mechanical properties.

The conditions under which a fuel cell operates or to which it is exposed can also affect its performance and lifetime. Important operating conditions include impurities in the fuel or oxidant streams, the fuel cell's temperature, its voltage and current, the pressures of the fuel and oxidant streams, and whether it operates continuously or transiently—as occurs during start-up and shutdown.

The failure modes of PEM fuel cells have recently received much attention;[4−6] the causes and mechanisms of fuel cell degradation have received less attention. The intent of this paper is to review the current understanding of hydrogen-fueled PEMFC degradation.

Typically, a PEMFC exhibits a gradual decline in power output during operation. Initially, the cumulative effect of this gradual decline is acceptable; that is, the power output of the cell or stack is still high enough to effectively operate the device to which it provides power. But with time, the cumulative effect of this gradual decline can become so large that the cell or stack can no longer deliver the required power. The degradation is then unacceptable. The causes of the gradual performance decline are not completely understood, especially the degradation mechanisms that occur in the fuel cell's different components and the relative contribution of each component's degradation to the degradation of the entire fuel cell. However, such understanding is required for PEMFC developers to develop new materials that last longer but are not prohibitively expensive. As mentioned, in the past few years, much progress has been made in understanding how the polymer electrolyte membrane and platinum electrocatalyst degrade and the carbon supports corrode.

Because other concerns were more pressing at the time, only a few PEMFC researchers studied lifetime issues before the early 2000s. Now, however, the emphasis has shifted from designing fuel cell systems and improving their short-term performance to improving fuel cell reliability and lifetime and making fuel cells cost competitive. As a result, the number of published studies of fuel cell reliability, lifetime, and cost has increased dramatically, as was first noted in 2003.[5] Some of these studies revealed severe degradation of PEMFC materials previously thought to be immune to corrosion and decomposition, and it is now recognized that lifetime problems had been previously underestimated because it was thought—incorrectly—that key PEMFC materials such as platinum (the metal catalyst), proton-conducting ionomer (used in the membrane and catalyst layer), carbon/graphite [used in the catalyst support, the GDL (gas-diffusion layer), and the bipolar plate], and Teflon (used in the GDL) would not suffer extensive chemical/physical degradation during fuel cell operation leading to unacceptable performance losses.

Within a PEMFC, the individual components are exposed to an aggressive combination of strong oxidizing conditions, liquid water, strongly acidic conditions, high temperature, high electrochemical potentials, reactive intermediate reaction products, a chemically reducing atmosphere at the anode, high electric current, and large potential gradients. In recent years, researchers have realized the importance of trying to understand the roles of these various conditions in the degradation process and to reduce their negative effects.

Figure 1 shows the number of literature hits for the topics of PEMFC degradation and PEMFC durability as functions of time. We obtained these results using SciSearch, a common database of scientific literature. Spikes in publications on PEMFC degradation and durability occur in 2004 and 2005. Since 1989, 58% of the hits on these topics occurred in 2005 and 2006. Before 2004, comparatively little had been published on these topics because, until then, most of the emphasis had been on improving the initial—"beginning-of-life" (BOL)— performance of a stack or a fuel cell component. In the past few years, research in these areas, especially membrane durability, catalyst durability, membrane electrode assembly (MEA) durability, and the effects of operating conditions, has increased significantly. In fact, symposia and sessions dealing with durability are now regular events at two of the most prominent PEMFC R&D meetings—the Electrochemical Society Joint International Meeting and the Fuel Cell Seminar. Such symposia and sessions did not exist before 2005. There is even a new conference in its second year—on Fuel Cells Durability & Performance—that deals only with these topics.

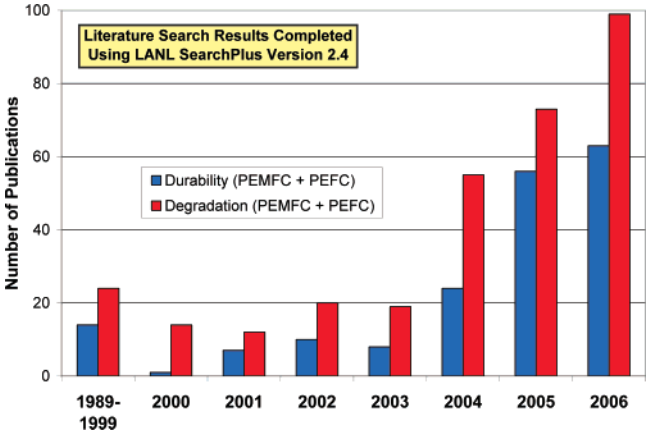

Figure 1. Trend in published literature for PEMFC long-term durability and degradation studies (1989−2006). The search criteria were "Proton Exchange Membrane Fuel Cell" plus "Polymer Electrolyte Fuel Cell (PEFC)" and "durability" for the blue bars. The searches were repeated, substituting "degradation" for "durability", and these totals correspond to the red bars.

Although research on fuel cell durability has clearly increased in recent years, to date, no review paper has covered this research. Our intent is to correct this situation. We first review durability targets (subsection 1.1), durability testing methods (subsection 1.3), and the effect of operating conditions on durability (section 2). We then focus on components: membranes (section 3), electrocatalysts and supports (section 4), and gas-diffusion media (section 5). To limit the paper's scope, we exclude from our discussion bipolar plates/flow fields, gaskets, stacks, and other system components. Moreover, details about these components are often proprietary.

1.1. Durability Targets for Stationary and Transportation Applications

The governments of the U.S., Japan, Europe, and other countries promote PEMFC development by funding certain R&D programs. In particular, the U.S. Department of Energy (DOE), Japan's Ministry of Economy, Trade, and Industry (METI), and the European Commission are supporting the development of PEMFCs for transportation and stationary applications. These programs have established targets for commercializing fuel cells for transportation and stationary applications. Subsections 1.1.1, 1.1.2, and 1.1.3 discuss these targets.

1.1.1. U.S. DOE Fuel Cell Programs

The U.S. DOE Office of Energy Efficiency and Renewable Energy's Hydrogen, Fuel Cells and Infrastructure Technologies (HFCIT) Program is facilitating the research and technology development efforts needed for fuel cell technology readiness. The DOE is working closely with its national laboratories, universities, and industry partners to overcome

critical technical barriers to fuel cell commercialization. The Hydrogen, Fuel Cells and Infrastructure Technologies Program's Multi-Year RD&D plan is built upon several predecessor planning documents and is integrated with other DOE office plans. The Plan describes the details of research and technology development, requirements, and schedule.[6]

Automotive fuel cell systems need to be as durable and reliable as current automotive engines. Thus, automotive fuel cell systems will have to last for at least 5,000 h (equivalent to 150,000 driven miles) and be able to function properly over the full range of external ("ambient") temperatures (−40 °C to +40 °C). Membranes, which are critical components of the fuel cell stack, must be able to perform over the full range of system operating temperatures with less than 5% performance loss at the end of life—without external humidification, which adds cost and complexity to the system. Catalyst lifetime is also important and can be compromised by platinum sintering and dissolution, especially under load cycling and high electrode potentials. Carbon-support corrosion is another challenge at high electrode potentials and can worsen with load cycling and high-temperature operation.

Fuel cells for stationary applications will likely require more than 40,000 h of reliable operation. Stationary fuel cells with lifetimes routinely greater than 40,000 h have been demonstrated, but these fuel cells are based upon PAFC (phosphoric acid) and have made limited market penetration to date. PEM fuel cell tests for stationary applications have lasted up to 20,000 h, but market acceptance likely requires increased reliable operating duration, including over the full range of external temperatures (−35 °C to +40 °C).

U.S. DOE lifetime status and targets (with cycling and <5% rated power degradation at the end of fuel cell life) for integrated transportation PEM fuel cell power systems fueled by hydrogen are as follows: a 2005 status of ∼1,000 h, and a 2010/2015 target of 5,000 h.

The lifetime status and targets (with <10% rated power degradation at the end of fuel cell life) for integrated stationary PEM fuel cell power systems fueled by reformate are as follows: a 2003 status of 15,000 h, a 2005 status of 20,000 h, and a 2011 target of 40,000 h.

1.1.2. Japanese NEDO Fuel Cell Programs

Under METI, Japan's New Energy and Industrial Technology Development Organization (NEDO) has promoted the national development of PEMFCs. NEDO first proposed an R&D road map for the technical development of stationary and vehicular systems in 2005 and made some minor revisions to it in 2006.[7] The road map includes technical-development themes and target values for each stage of development.

NEDO also recognizes that fuel cell lifetimes and performance must be improved for vehicular fuel cell systems to be commercially viable. NEDO's road map sets the following targets for 2015: a fuel cell lifetime of >5,000 h; a vehicle efficiency of 60%, based on the lower heating value (LHV) of the fuel; an operating temperature greater than 90−100 °C; and a stack cost of ∼10,000 Yen/kW. Although NEDO does not directly promote the development of vehicular fuel cell systems, it does support developing the basic technologies needed to build fuel cells for these systems as well as studies of degradation mechanisms. After 2020, NEDO would like to see operating temperatures of ∼100−120 °C without a humidifier, to promote waste heat removal. Fuel cells must also operate at low external temperatures; NEDO's target for their widespread commercial use after 2020 is −40 °C.

NEDO's road map calls for the first-generation commercial system to be introduced in 2008 at a target cost of 1.2M Yen/kW. However, lower cost and improved durability are necessary for widespread successful commercialization. A lifetime of more than 10 years (about 90,000 h) will be needed for home-cogeneration PEMFC systems.

NEDO's status and lifetime targets for integrated family-vehicle PEM fuel cell power systems fueled by hydrogen are as follows: a 2005 status of ∼1,000 h, a 2010 target of 3,000 h, and a 2015 target of 5,000 h. NEDO's status and lifetime targets (<10% rated power degradation at the end of fuel cell life) for integrated stationary PEM fuel cell power systems for home cogeneration fueled by reformate are as follows: a 2005 status of ∼10,000 h, a 2010 target of 40,000 h, and a 2015 target of ∼90,000 h.

1.1.3. European Hydrogen and Fuel Cell Technology Platform

The European Hydrogen and Fuel Cell Technology Platform (HFP) established an Implementation Panel (IP) in 2006 to take fuel cell technology to the implementation stage.[8] This program is designed to facilitate and accelerate the development and deployment of cost-competitive, world class European hydrogen and fuel cell technologies. They expect use in transportation, stationary, and portable power applications.

The Implementation Panel developed Innovation and Development Actions (IDA) for Hydrogen Vehicles (IDA 1). The goal of this program was to improve and validate hydrogen vehicle and refueling technologies to the level required for commercialization decisions by 2015 and for a mass-market rollout by 2020. IDA 1 addresses transport applications, emphasizing road transport but also other transport applications, to meet EU goals on competitiveness and sustainable mobility. The top priority is the development of competitive hydrogen fuel cell vehicles with an emphasis on component performance and reliability, aligned with the establishment of a hydrogen refueling infrastructure and the supporting elements for market deployment and industry capacity buildup.

The specific targets for 2015 for the road propulsion fuel cell system include an efficiency of >40% on the NEDC (New European Drive Cycle), a cost of 100 Euros/kW, and lifetimes of 5000 h for cars and 10,000 h for buses.

Innovation and Development Action 3 (IDA 3) has the goal of commercially competitive fuel cells for CHP (combined heat and power) generation: >1 GW capacity in operation by 2015. PEM fuel cell systems are mainly targeted for residential units. Specific milestones have been included which show gradual increases in performance and capacities toward tangible market penetration by 2020.

The specific targets for 2009−2012 for residential systems of 1−10 kW include an electrical efficiency of 34−40%, with a total fuel efficiency of 80%, a system cost of 6,000 Euros, and a lifetime of >12,000 h.

1.2. PEM Fuel Cell Materials

To provide a context for the lifetime tests discussed below, we briefly discuss fuel cell operation and the fuel cell components of interest in durability studies. A schematic cross section of a single cell of a PEMFC showing individual components is shown in Figure 2. An individual cell consists

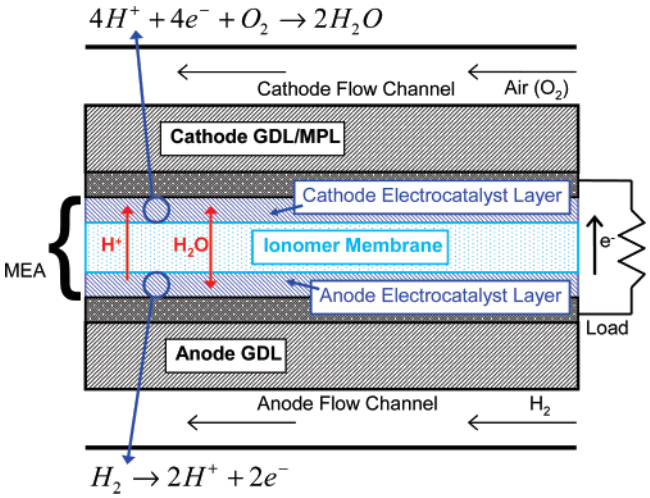

Figure 2. Schematic cross section of a typical PEM fuel cell.

of a cathode, an anode, and a separating polymer−electrolyte membrane. Each electrode has an electrocatalyst layer, and a gas diffusion layer (GDL). The catalyst layers can be attached to either the membrane or at times to the GDL material (termed the gas diffusion electrode, GDE).

Each individual cell produces a voltage of about 0.6−0.7 V; to produce a suitable voltage, individual cells are "stacked" to form a fuel cell stack. The individual cells are electrically connected in series by bipolar plates, and special end plates terminate the stacks to provide the compressive forces needed for stack structural integrity. The bipolar plates provide conducting paths for electrons between cells, distribute the reactant gases across the entire active MEA surface area (through flow channels integrated into the plates), remove waste heat (through cooling channels), and provide stack structural integrity as well as barriers to anode and cathode gases.

Directly adjacent to the bipolar plates are the GDLs, which typically consist of two layers—a macroporous substrate layer and a microporous layer (MPL). The GDLs are gas permeable and help distribute gases to the catalyst layer, conduct electrical current, and also provide a network of paths for liquid water to move from the MEA to the flow channel. The macroporous substrate layer consists of a carbon fiber matrix with a large void volume, typically 75−85%, and a primarily hydrophobic MPL consisting of carbon black mixed with fluoropolymer. The cathode GDL normally has an attached MPL; the anode GDL may or may not have a MPL. In section 5, we discuss GDLs in detail.

The electrochemical processes that drive a fuel cell occur within the cell's inner three layers, commonly known as the MEA or alternately as a catalyst-coated membrane (CCM). In the early years of PEMFC development—the mid-to-late 1960s[9,10]—researchers defined an MEA to be two gas-diffusion electrodes (GDEs) plus a proton-conducting polymer membrane, or ionomer. This form of MEA included GDL substrates with an electrocatalyst layer deposited on each GDL surface in place of what are now the MPLs. Modern PEMFC electrocatalyst layers are usually composite structures consisting of proton-conducting ionomer material and noble-metal (platinum) catalyst supported on carbon. This thin-film electrode technology was pioneered initially at Los Alamos National Laboratory in the late 1980s and early 1990s.[11−16] Since then, the meaning of "MEA" has changed from one based exclusively on the original PEM technology used by NASA and General Electric Corporation (this technology contained GDLs) to meanings which can be based on either the discrete three-layer structure (two composite electrocatalyst layers plus electrolyte without GDLs) or the five-layer structure including GDLs. Other developers still use CCM and MEA to distinguish between three-layer structures and five-layer structures.

In modern MEAs, the electrocatalysts are nanoparticles of platinum or platinum alloys deposited on high-surface-area carbon supports. The nanoparticles increase the active catalytic surface area per unit mass of platinum. However, they also pose material-stability and interaction issues. The stability of platinum, platinum alloys, and carbon particles and the interaction of the nanocatalyst particles with the carbon supports are of concern for fuel cell durability. In section 4, we discuss electrocatalysts and their supports in detail. Ionomer is also included in the electrode layer for proton transport, and it has material properties and catalyst interfaces that can degrade.

Finally, the PEM is typically a polymeric material with sulfonic-acid side chains and a fluorocarbon or hydrocarbon backbone. Nafion (Nafion is a trademark of E. I. DuPont de Nemours and Company), a perfluorinated sulfonic acid based ionomer (PFSA), has been the standard membrane material for fuel cell applications and is also the most studied fuel cell membrane material. In section 3, we discuss the degradation of polymer electrolyte membranes in detail.

1.3. Durability Tests

As research on fuel cell lifetime has increased, questions have arisen regarding the operating conditions needed to evaluate durability and how to compare data taken under different conditions. These issues have led to standard test protocols, but much of the existing durability data was taken under different operating conditions, making comparisons among different data sets difficult.

Various developers have studied degradation mechanisms and differences in the durability of various components, for both stationary and automotive applications. Most long-term stationary tests (or "life tests") are carried out at a given set point or group of set points with the voltage or, more commonly, the current density held constant for hundreds or thousands of hours per test.

For long-term tests that simulate automotive applications, the power density is usually continuously varied in some sort of cyclic form. For instance, the federal internal-combustion-engine drive cycle "US06" has been converted to an equivalent PEMFC-engine drive cycle using power-density set points taken from polarization data.[17] Durability measurements are taken using this modified US06 drive cycle to subject single cells to hours of repeated cycling.[18,19] In addition, the U.S. DOE has recently released a first version of a recommended procedure for acquiring 2,000 h of stack-test data taken with variable loads.[20] This test protocol is designed to assess the performance and durability of fuel cells for vehicular applications and to compare cell and stack performance with U.S. DOE targets. Figure 3 shows the time/current behavior of this protocol; Table 1 shows the current density/time profile. The protocol's current density is defined by the measured current at the specified voltage before the protocol is initiated (for example, C_{80} is the current density at 0.80 V). Results produced by this protocol may or may not accurately predict the lifetime of an actual fuel cell in an actual vehicle undergoing actual driving and start/stop cycles.[20] Although this protocol was not intended to be

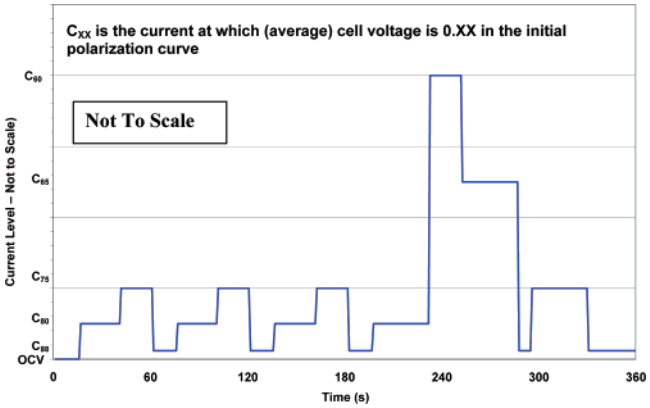

Figure 3. U.S. DOE dynamic stress test.

Table 1. Current Density vs Time for Cycle Profile

step	duration (s)	C_{XX}	step	duration (s)	C_{XX}
1	15	OCV	9	20	C_{75}
2	25	C_{80}	10	15	C_{88}
3	20	C_{75}	11	35	C_{80}
4	15	C_{88}	12	20	C_{60}
5	24	C_{80}	13	35	C_{65}
6	20	C_{75}	14	8	C_{88}
7	15	C_{88}	15	35	C_{75}
8	25	C_{80}	16	40	C_{88}

comprehensive—many issues (*e.g.*, fuel cell behavior under start/stop conditions) are not addressed—it provides insight about fuel cell durability for automotive-type transients. We expect additional issues will be addressed by future or revised protocols.

Standard durability-evaluation protocols would be of great value to the fuel cell community and are beginning to appear, although their methods and use are not yet uniform. The U.S. DOE included a set of durability protocols in their 2006 PEMFC program solicitation to industry and the national laboratories for use to evaluate newly developed components.[21] These protocols include an accelerated-test methodology based on potential cycling of electrocatalysts and a protocol to measure the corrosion of catalyst-support materials. The lack of standard durability protocols is not surprising—it was not until 2004 that a common single-cell testing protocol for BOL performance and new-component evaluation was established.[22] The USFCC (U.S. Fuel Cell Council) has a current working group to develop and standardize durability testing methods, and the U.S. DOE Office of Energy Efficiency and Renewable Energy (EERE) is developing standard automotive-stack-durability protocols through the Freedom Cooperative Automotive Research CAR (FreedomCAR) Fuel Cell Technical Team. Because so many interrelated issues are involved in the durability analysis of a PEMFC, many broad studies addressing all of these factors and operating conditions are needed.

Ideally, a component developer would like to evaluate new materials and cell designs with a minimum of long-term PEMFC testing. Conventional durability tests currently include long-term tests at most stages of development, requiring progressively longer hours per test as the cell/stack design nears completion. A final configuration of PEMFC components could be tested for a total of up to 10,000 h or more (testing of a complete fuel cell stack) before a prototype design is frozen. The prototype stack must then be validated for another ~5,000 h before being integrated with the system. In the past few years, emphasis on developing accelerated tests, preferably standardized ones, has greatly increased.

Table 2. Electrocatalyst Cycle and Metrics

cycle	step change: 30 s at 0.7 V and 30 s at 0.9 V. Single cell 25−50 cm^2
number	30,000 cycles
cycle time	60 s
temperature	80 °C
relative humidity	anode/cathode 100/100%
fuel/oxidant	hydrogen/N_2
pressure	150 kPa absolute

metric	frequency	target
catalytic activity[a]	beginning and end of life	≤60% loss of initial catalytic activity
polarization curve from 0 to ≥1.5 A/cm^2 [b]	after 0, 1K, 5K, 10K, and 30K cycles	≤30 mV loss at 0.8 A/cm^2
ECSA/cyclic voltammetry	after 1, 10, 30, 100, 300, 1000, and 3000 cycles and every 5000 cycles thereafter	≤40% loss of initial area

[a] Activity in A/mg at 150 kPa absolute backpressure at 900 mV *iR*, corrected on H_2/O_2, 100% RH, 80 °C. [b] Polarization curve per USFCC "Single Cell Test Protocol" section A6.

Table 3. Catalyst Support Cycle and Metrics

cycle	hold at 1.2 V for 24 h; run polarization curve and ECSA; repeat for total 200 h. Single cell 25−50 cm^2
total time	continuous operation for 200 h
diagnostic frequency	24 h
temperature	95 °C
relative humidity	anode/cathode 80/80%
fuel/oxidant	hydrogen/nitrogen
pressure	150 kPa absolute

metric	frequency	target
CO_2 release	on-line	<10% mass loss
catalytic activity[a]	every 24 h	≤60% loss of initial catalytic activity
polarization curve from to ≥1.5 A/cm^2 [b]	every 24 h	≤30 mV loss at 1.5 A/cm^2 or rated power
ECSA/cyclic voltammetry	every 24 h	≤40% loss of initial area

[a] Activity in A/mg at 150 kPa absolute backpressure at 900 mV *iR*, corrected on H_2/O_2, 100% RH, 80 °C. [b] Polarization curve per USFCC "Single Cell Test Protocol" section A6.

Many of the testing methods used for accelerated testing of individual components are presented in sections 2−5 in support of the individual component durability data, but they tend to not be standardized protocols. One notable attempt to standardize individual-component accelerated durability protocols has become public. The U.S. DOE and the Freedom CAR Fuel Cell Technical Team have recently established a set of durability-test protocols, which includes four tests: electrocatalyst (see Table 2), electrocatalyst supports (see Table 3), MEA chemical (see Table 4), and membrane mechanical (see Table 5).[23] Such protocols should help researchers evaluate durability and make comparisons between different materials.

2. Operational Effects on Fuel Cell Durability

Operating conditions are known to have an impact on a fuel cell's durability. In this section we focus on a number of operational effects and research done investigating their impact on fuel cell durability. These effects include exposure to impurities (on both the anode and cathode sides of the fuel cell), exposure to and start-up from subfreezing conditions, and other operating conditions. These other operating

Table 4. MEA Chemical Stability and Metrics

test condition	steady-state OCV, single cell 25−50 cm^2
total time	200 h
temperature	90 °C
relative humidity	anode/cathode 30/30%
fuel/oxidant	hydrogen/air at stoics of 10/10 at 0.2 A/cm^2 equivalent flow
pressure, inlet kPa abs (bara)	anode 250 (2.5), cathode 200 (2.0)

metric	frequency	target
F^- release or equivalent for non-fluorine membranes	at least every 24 h	no target—for monitoring
hydrogen crossover[a] (mA/cm^2)	every 24 h	≤20 mA/cm^2
OCV	continuous	≤20% loss in OCV
high-frequency resistance	every 24 h at 0.2 A/cm^2	no target—for monitoring

[a] Crossover current per USFCC "Single Cell Test Protocol" section A3-2, electrochemical hydrogen crossover method.

Table 5. Membrane Mechanical Cycle and Metrics

cycle	cycle 0% RH (2 min) to 90 °C dew point (2 min), single cell 25−50 cm^2
total time	until crossover >10 sccm or 20,000 cycles
temperature	80 °C
relative humidity	cycle from 0% RH (2 min) to 90 °C dew point (2 min)
fuel/oxidant	air/air at 2 slpm on both sides
pressure	ambient or no backpressure

metric	frequency	target
crossover[a]	every 24 h	≤10 sccm

[a] Crossover per USFCC "Single Cell Test Protocol" section A3-1, pressure test method with 3 psig N_2.

conditions include potential cycling, fuel starvation, start/stop cycling, and changes in temperature and/or relative humidity.

2.1. Impurity Effects

Impurities are the first external (operational) variable that we review in terms of their impact on fuel cell durability. Impurities present in both the hydrogen fuel stream and the air intake have been shown to negatively impact a fuel cell's performance and durability. Table 6 lists the most common impurities and their sources.

Impurities are known to affect FC performance by various mechanisms that lead to performance loss. Impurities that adsorb onto the anode or cathode electrocatalyst surface inhibit the electrode charge-transfer processes, resulting in interfacial overpotential losses. Impurities such as ammonia, which can form cations, or other cations introduced to the cell directly from salts or corrosion byproducts can cause ion exchange with protons in the ionomer. These cations lower proton conduction and can result in increased ohmic losses. Foreign substances can also change the water and/or gas transport behavior of the gas diffusion layer and thus adversely affect fuel cell performance by decreasing mass transport.

Performance losses due to impurities can be permanent and irreversible, or temporary and reversible. The performance loss of some poisoning species can be negated by simply ending introduction of the impurity or by performing a recovery procedure. Additionally, one cannot state if an effect is permanent unless rigorous recovery procedures have been attempted. Exposure to high potentials or repeated cyclic voltammetry (CV) sweeps (for catalyst poisons, such as S) and operation at high currents (for foreign cations, such as NH_4^+) should be performed to determine if the effects are permanent.

Table 6. Origin of Common Fuel and Air Impurities[45]

Hydrogen Fuel Impurities	
fuel for hydrogen	potential impurities
crude oil:	CO, NH_3, H_2S, HCN
gasolines	hydrocarbons, aldehydes
diesels	mercaptans
natural gas	CO, NH_3, H_2S, HCN, hydrocarbons, mercaptans
methanol/DME	CO, odorants, alcohols
BioMass	cations, aldehydes, alcohols, formic acid, NH_3, H_2S, HCN
water electrolysis	anions, cations
Air Impurities	
fuel combustion pollution	SO_x, NO_x, hydrocarbons, soots and particulates
ambient air, farming	NH_3
natural sources	ocean salts, dust
Others	
de-icers	NaCl, $CaCl_2$
FC system corrosion products	cations, anions

While the effects of one impurity (CO) have been thoroughly researched, there are fewer publications investigating the effect of other impurities on fuel cell performance.[24−44] Other common fuel impurities include ammonia, hydrogen sulfide, hydrogen cyanide, hydrocarbons, formaldehyde, and formic acid.[45] On the cathode side, ambient air may contain impurities such as sulfur dioxide, nitrogen oxides, and particulate matter (including salts) that can affect fuel cell performance.[45] The degradation mechanisms due to these impurities can vary, depending on the type and chemical makeup of the impurity, and the work that has been reported on the durability aspects of these impurities is reported in the following sections.

2.1.1. Fuel Impurities

For many applications, hydrogen is currently produced by reforming a hydrocarbon fuel (natural gas, methanol, propane, gasoline, and diesel), producing a hydrogen-rich gas commonly termed reformate. These processes leave impurities in the hydrogen and are dependent upon the reforming process used, the fuel itself, and post-treatment of the reformate stream. While other techniques such as electrolysis can be used to produce hydrogen, these bring about different impurity issues (such as cations) and increased production costs. For the production of hydrogen, trade-offs exist between the purity of the hydrogen (type and concentration of impurities) and cost. Therefore, the durability of fuel cells operating with hydrogen contaminants has been investigated.

The composition of reformate depends upon the reforming process and the type of fuel used. Hydrogen produced via autothermal reforming of gasoline has a typical major constituent composition[46] of 45% H_2, 20% CO_2, and 35% N_2; steam reforming of methanol gives 75% H_2 and 25% CO_2; and steam reforming of natural gas can have a composition of 80% H_2 and 20% CO_2, with smaller amounts of trace impurities. The trace impurities can have a larger impact on performance and durability than either N_2 or CO_2 even though the concentrations of these species are typically

4 orders of magnitude lower. Generally, nitrogen is considered to be simply a gas diluent; however, deviations of 10−30 mV from Nernst behavior have been measured.[47] Similar deviations from Nernst behavior have also been measured with CO_2. However, CO_2 is known to react via the reverse water-gas-shift reaction, producing CO.[48] The best-known, and well studied, example of an anode catalyst poison is carbon monoxide. Significant work on CO as a fuel cell impurity is the result of its ubiquitous presence, often at high concentrations, in the effluent from hydrocarbon reforming processes. These CO fuel cell studies have looked at many aspects of CO poisoning: examining CO performance effects in fuel cells,[24,49−63] modeling CO effects on fuel cell operation,[64−82] developing operational methods to minimize CO poisoning in fuel cells,[83−99] developing anodes more tolerant to CO,[100−106] and making fundamental electrocatalytic measurements of CO with electrocatalysts.[24,25,33,107−111] These studies have shown that CO forms a strong bond with Pt, chemisorbing on the metal surface. The chemisorbed CO blocks the adsorption of hydrogen onto active Pt sites for hydrogen electro-oxidation (HOR). This catalyst poisoning reduces electro-oxidation rates and raises electrode overpotentials, resulting in performance losses compared to CO-free tests. Fortunately, the effects of CO on fuel cell performance appear to be based upon equilibrium absorption of CO from the gas phase. As a result, the durability implications of long-term exposure to CO-containing streams have not been reviewed in detail, as they appeared to be similar to those of fuel cells without CO. This review focuses on durability of fuel cells, and we, therefore, have limited our discussion of CO as an impurity due to the reversible nature of the impurity.

Effect of Ammonia. Traces of NH_3 can be generated in the process of reforming natural gas and other hydrocarbons for H_2 production. The presence of ammonia levels as low as 13 ppm in the fuel stream has rapid deleterious effects on performance.[40] Higher concentrations (80, 200, and 500 ppm) of NH_3 have shown a marked decrease in performance in simulated reformate: cell performance decreases with exposure to NH_3 in reformate from 825 to 200 mA/cm^2 at 0.6 V.[38] Short-term exposure (<1 h) to NH_3 shows reversible effects.[40] However, the negative effects caused by long-term exposure are irreversible, meaning that further operation on neat H_2 results only in a partial recovery, as shown in Figure 4 for testing with 30 ppm NH_3. High-frequency resistance (HFR) measurements show a resistivity increase from 0.10 Ω·cm^2 before NH_3 exposure to 0.25 Ω·cm^2 after 15 h. Cyclic voltammetry (CV) of the anode, after exposure, does not indicate any noticeable NH_3 adsorption onto the catalyst layer;[43] thus, the degradation mechanism appears to be due to protonic conductivity loss. The likely culprit is that NH_3 reacts with ionomeric H^+, generating NH_4^+ and consequently lowering the protonic activity. The negative effect gradually starts at the anode catalyst layer, the first region exposed, and continues into the membrane as the ammonia diffuses deeper and deeper.

Hydrogen Sulfide. Natural gas is one of the primary sources of hydrogen, and depending on the geographic region of extraction, it may contain large amounts of H_2S (up to several vol %). Other fuels from fossil origin, such as gasoline, also have a number of sulfur-containing compounds, (*e.g.*, thiophene, thiols, and carbon sulfide). During the reforming process for H_2 enrichment, these compounds are converted to H_2S. Metals in general have a strong

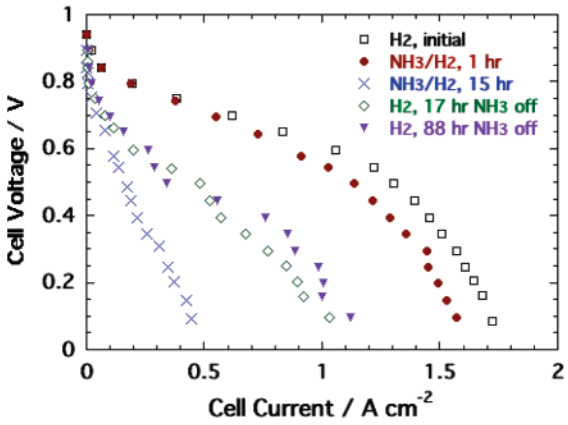

Figure 4. Polarization curves of a H_2/air fuel cell showing the effect of 30 ppm NH_3 injected into the fuel stream for a total of 15 h. After this period, the cell continued operating on neat hydrogen for an additional 88 h at a constant voltage of 0.5 V. T = 80 °C. Reprinted with permission from ref 43. Copyright 2002 The Electrochemical Society.

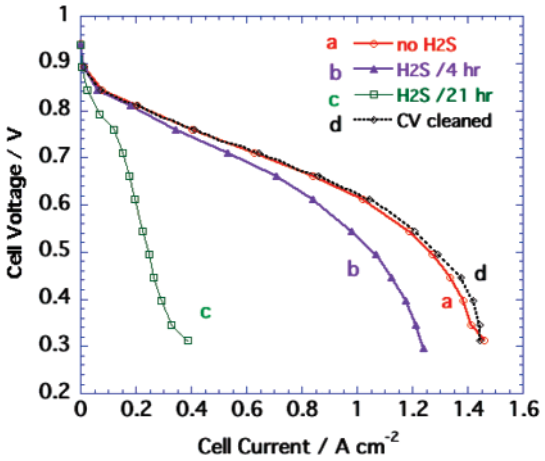

Figure 5. Polarization curves of a 5 cm^2 FC whose anode was poisoned with 1 ppm H_2S. Pt loadings were 0.2 mg Pt/cm^2 at each electrode. Curves prior to poisoning and after electrochemical cleaning are also shown. T = 80 °C. From ref 112.

chemical affinity with H_2S, and Pt catalysts are not an exception and are particularly vulnerable. The degrading effects of the presence of this impurity in the FC are significant and commensurate with H_2S concentration and time of exposure.

Figure 5 shows polarization curves for a cell exposed to 1 ppm of H_2S while running at a constant voltage of 0.5 V.[112] Performance losses are evident after just 4 h of exposure, and the cell operation becomes almost completely disabled after 21 h, as indicated by curve c. Continued operation on neat H_2 was conducted without significant recovery, indicating the irreversibility of the poisoning process by H_2S. Cyclic voltammetry performed of an anode fully poisoned by H_2S is shown in Figure 6.[113] Two major features in this CV indicate the presence of sulfur species chemisorbed onto the Pt surface. Within the potential domain of 0.1−0.4 V, in the first cycle, the typical peaks of a clean Pt catalyst corresponding to H-desorption are totally absent because the active sites are blocked by sulfur species. The second feature is seen in the potential range 0.8−1.3 V, which appears as two major merging oxidation waves. These currents correspond to the electrochemical oxidation of chemisorbed sulfur to nonpoisoning species. This result

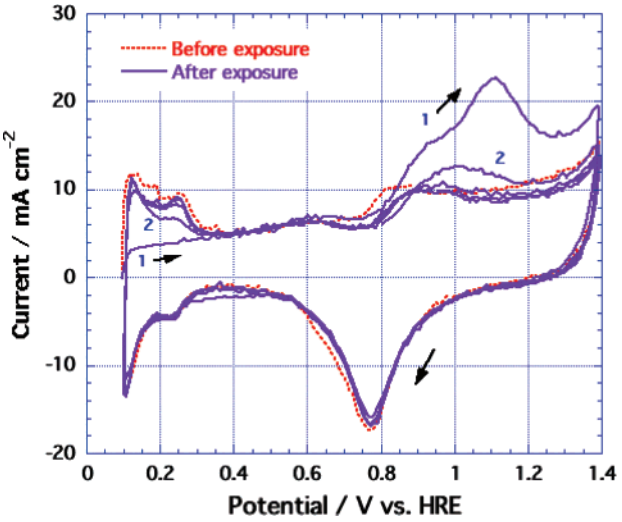

Figure 6. CV of the anode after full poisoning with H_2S. CV prior to poisoning is also shown for comparison. Scan rate = 100 mV/s. T = 80 °C. From ref 113.

Table 7. FreedomCAR Fuel Specification

component	level	LANL test
hydrogen	>99.9	95−99[a]
sulfur (as H_2S)	10 ppb	10 ppb
CO	0.1 ppm	0.1 ppm
CO_2	5 ppm	5 ppm
NH_3	1 ppm	1 ppm

[a] Includes dilution due to inert gas in stock mixtures.

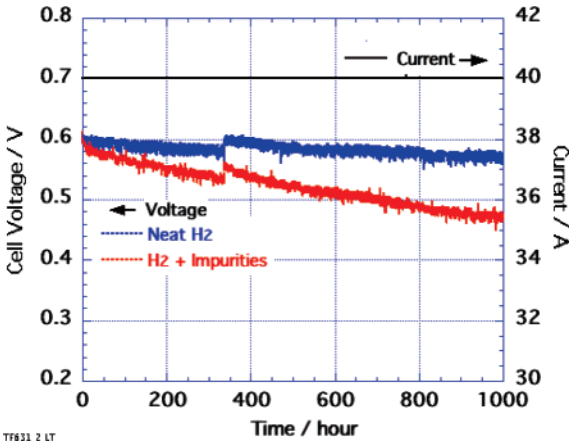

Figure 7. Voltage losses of two 50 cm^2 equivalent cells run at 0.8 A/cm^2 for 1000 h on neat hydrogen and on the mixture of Table 7. Loadings: 0.2 mg/cm^2 Pt at each electrode. Nafion membrane N112. Temperature = 80 °C. psig: 30/30. From ref 45.

explains the relative irreversibility of the Pt-catalyst poisoning. The electrochemical desorption of sulfur requires potentials unachievable in a continuously operating H_2/air fuel cell. 10 ppb of H_2S has been shown during long operating times to have a degrading effect on fuel cell performance.

Impurities and Hydrogen Fuel Quality Specifications. Recently, the U.S. FreedomCAR Fuel Cell Technology Team proposed a preliminary FC testing operation using a fuel mixture specified in Table 7. The results of a 1000 h test at constant current are presented in Figure 7. A reference cell operating on neat H_2 was also tested in parallel. At the end of the test, the losses with the mixture amounted to 100 mV. Qualitatively, the losses were ascribed to the presence of NH_3 and H_2S. First, the high-frequency resistance (HFR) of the cell increased during the operation. However, the increase in the HFR did not account for all of the observed losses. The Pt catalyst surface was partially poisoned by H_2S. After 1000 h, about 60% of the Pt surface still was sulfur-free, but the cell still experienced a significantly depressed performance. This experiment indicates that the presence of ammonia and hydrogen sulfide impurities, even at low levels, will negatively impact cell operation.

Hydrocarbon Contaminants. Hydrocarbon impurities tend to be ubiquitous from reforming reactions, with methane being the most common, as the equilibrium level of methane during reforming reactions is normally 0.1−1.0%.[114] Methane, as an impurity, is known to have no poisoning effect, as many stationary systems operate from reformed natural gas and contain methane. Other hydrocarbons, such as benzene and toluene, did not show evidence of fuel cell degradation upon exposure on the anode, although toluene hydrogenation occurs in the anode, resulting in 90% conversion of the toluene to methylcyclohexane.[39] However, benzene was noted to "smother" the cell with exposure on the cathode.[32]

2.1.2. Air Impurities

The air side of the fuel cell is exposed to air pollutants that can vary tremendously in concentration. Research has concentrated on commonly occurring air pollutants and aerosols. The work performed to date on cathode impurities includes oxides of sulfur and nitrogen, hydrocarbons, ozone, particulates, and aerosol salts.

Effects of Sulfur Dioxide Injected at the Cathode. Sulfur dioxide is a common air contaminant resulting from fossil fuel combustion and can be found in high concentrations in urban areas with heavy traffic and in close proximity to some chemical plants. The effects of SO_2 injected at the cathode are similar to those produced by the presence of H_2S in the anode.[45] Performance degradation appears to be a function of SO_2 concentration in the bulk, as the performance decrease was measured to be 53% at 2.5 ppm SO_2 as compared to a 78% decrease at 5 ppm SO_2 for the same applied dosage.[31] Performance does not improve after impurity injection is turned off; thus, is not reversible just by normal operation.[31,45] The severity of the effect is due to the strong chemisorption of SO_2 (or other S-species) onto the Pt catalyst surface. Electrochemical oxidation (during a CV) of adsorbed SO_2 shows full cell performance recovery.[31,45]

Effect of Nitrogen Dioxide. Nitrogen oxides (NO_x) are air contaminants that mostly originate in the combustion of fossil fuels. Internal combustion engine emissions are the major source of NO_x; thus, they are abundant in urban areas. NO_2 has been shown to quickly degrade fuel cell performance,[31,45] with a gradual decrease over 30 h of operation, after which degradation did not continue.[45] The rate of poisoning of PEMFCs by NO_2 does not strongly depend on NO_2 bulk concentration.[31] The degradation of performance of the fuel cell can reach 50%, while the cell performance completely recovers after applying neat air for 24 h.[31] The poisoning effects of NO_2 do not appear to be a catalyst poisoning issue, since no surface species can be detected during cyclic voltammetry;[31,45] the poisoning mechanism is still not understood.

Effect of Sodium Chloride at the Cathode. In addition to gas-phase contaminants, salts (principally from ocean mists and road deicer) may contaminate the cathode air supply.

The presence of NaCl at the electrode decreases its performance. The performance loss is mostly due to a decrease of protonic conductivity as a consequence of exchange of H^+ by Na^+ at the catalyst layer and at the membrane. Large concentrations of the salt also decreased the hydrophobicity of the gas diffusion layer, increased liquid water retention, and correspondingly decreased oxygen transport to the electrocatalyst at high current densities. Surprisingly, Cl^- does not appear to block adsorption on the catalyst surfaces, as revealed by CV measurements.[45] However, chloride has a dramatic effect on the oxygen reduction kinetics of cathode electrocatalysts.[35] Chloride has also been noted to affect GDL materials, which can lead to changes in water and gas transport.[35]

Hydrocarbon and Battlefield Contaminants. Other air impurities which could be encountered include various hydrocarbon species due to incomplete combustion of fuel or in the specialized field of military applications, which includes potential chemical warfare agents.

Benzene appears to adsorb onto catalyst sites and gradually "smothers" the cell. The phenomenon appears to be related to potential, as the effect was more marked at higher current densities, where a lower oxidizing potential was experienced, and recovery of the cell was initiated by higher cell potentials. The responses of the cell to HCN and ClCN impurities were similar and are consistent with platinum catalyst sites being preferentially occupied by the gases. The effects of sarin ($CH_3POFOCH(CH_3)_2$) and mustard ($ClCH_2CH_2SCH_2CH_2Cl$) appeared distinct from those of the two simple chemical warfare agents HCN an ClCN. The decrease in cell performance by sarin and mustard gas to a steady value was more gradual, and subsequent to the impurity, cell recovery did not occur. Sarin and mustard gas affect the fuel cell much more slowly than HCN or ClCN. It was concluded that sarin and mustard are likely to bind irreversibly with the catalytic platinum site, but the size of the agent molecules reduces the rate of this reaction and may prevent neighboring platinum sites from being rapidly poisoned.[32]

2.2. Subfreezing Effects in PEM Fuel Cells

One criterion PEM fuel cells are required to meet for automotive applications is the ability to survive at and start-up from subfreezing temperatures. As a guideline, the Department of Energy's PEM fuel cell stack technical targets for the year 2010 include survivability at −40 °C and also start-up (to 50% rated power) from −20 °C in as low as 30 s with consumption of <5 MJ of energy (including shutdown "conditioning" and subsequent start-up). While there has been significant activity in this area in the patent literature, relatively little effort appears in peer-reviewed publications. From what does appear in the open literature, there have been conflicting reports regarding the ability of PEM fuel cells to tolerate cycling through subfreezing temperatures.[115−118] In this section, we examine (a) the effect of subfreezing temperatures on PEM fuel cells and components, (b) the start-up characteristics and durability of fuel cells at subfreezing temperatures, and (c) the various mitigation strategies utilized to avoid degradation due to subfreezing temperatures.

2.2.1. Effect of Subfreezing Temperatures on PEM Fuel Cells and Components

Early literature suggested that there was little degradation from freezing fuel cells to subfreezing temperatures[117,119] for a limited number of cycles. There was no significant change in performance of fuel cells subjected for three cycles to −10 °C,[118] 10 cycles to −10 °C,[117] and one cycle to −78 °C.[117] Moreover, a 50 W stack was also subjected to operation for 9 h at −10 °C without any degradation in the power.[119] However, a recent paper suggested that there could be significant degradation in the performance of PEM fuel cells subjected to cycling from −10 °C.[115] Cho *et al*. observed a 11% drop in the current at 0.6 V after four thermal cycles of the cell from −10 °C. They also reported that their cathode electrochemical surface area (measured by CV) dropped by 25% during these cycles in addition to the membrane resistance increasing. These results were attributed to ice formation that results in increased porosity of the catalyst layer and the eventual delamination of the catalyst layer from the membrane. These results have been corroborated by another study that also observed significant degradation after 10 subfreezing starts from −10 °C.[120] Oszcipok *et al*. observed a 5.4% loss in performance (current at 450 mV and 30 °C) for each cold start cycle from −10 °C. They also observed a drop in electrochemical surface area accompanied by an increase in the membrane high-frequency resistance (HFR) during 10 start-up cycles from −10 °C. These results were attributed to the formation of ice resulting in structural changes to the catalyst and the gas diffusion layer (GDL). However, these results are in disagreement with another study that has shown little performance loss for a fuel cell subjected to 55 freeze/thaw cycles that included a gas purge in between each of the cycles.[121]

These apparent discrepancies (from no degradation to 5.4% degradation/cycle) in the various literature results can be attributed to several factors. The preparation method of the membrane electrode assembly (MEA) is critical in determining the freeze/thaw durability of the PEM fuel cell. If the electrode/electrolyte adhesion is weak, then there is a greater degradation in the performance due to ice formation resulting in delamination. This may explain some of the discrepancies in the literature results where some electrodes were sprayed on to the GDL while others were prepared directly on the membrane. Moreover, the degradation is also a function of the rate of heating/cooling in addition to the freezing temperature. This is evidenced by rapid cycling (quenching) to −80 °C leading to delamination of the electrode while normal cycling to −40 °C (even for 100 cycles) shows no such delamination in an identically prepared MEA.[116] Studies have also revealed that there is little loss in performance of even fully humidified cells using carbon cloth backing. However, the breakage of carbon fibers in carbon paper backing leads to loss in performance during freeze/thaw cycles. Therefore, in addition to the preparation method and cycling conditions, the component materials used in the fuel cell assembly will also play a vital role in determining the durability of fuel cells subjected to multiple freeze/thaw cycling.

The effect of freezing water on the properties of fuel cell components is therefore of great interest in understanding the various degradation mechanisms in play during freeze/thaw cycling of fuel cells. However, this is not well understood and there is little published literature on the effect of ice formation on the catalyst and GDLs. In contrast, there are several papers describing the effect of freezing water on the membrane (Nafion) properties.

The conductivity of Nafion is highly dependent upon the state of water in the polymer, and it has been shown to have an increased activation energy at lower temperatures, where

the water in the membrane is likely in the frozen state.[122,123] The water in Nafion has also been characterized as nonfreezing water, bound freezing water, and free water.[124] The free water behaves like bulk water and freezes at 0 °C, while the bound freezing water is water that is trapped in the channels of Nafion and has its freezing point suppressed depending on the size of the channel, which in turn depends on the degree of hydration of the polymer.[122] Finally, the chemically bound water does not freeze all the way down to −120 °C and is thought to be the source of the relatively high conductivity of Nafion even in the frozen state. A recent study has reported the detailed characterization of water in Nafion at subfreezing temperatures as a function of the initial water content per sulfonic acid group (λ).[125] This study revealed that the water in the center of the Nafion clusters tends to freeze first, leaving a more concentrated acid in the remainder (periphery) of the pore volume.

Although the state of water in Nafion is reasonably well characterized at low temperatures, there is little information on the long-term effect of freeze/thaw cycling on the membrane properties. A recent study has revealed that extensive (385 cycles) cycling between −80 °C and +40 °C can result in a change in the mechanical and chemical properties of the dry membrane, including lower oxygen permeability, higher through plane conductivity, and decreased strength.[126] The detailed characterization of the durability of Nafion and other PEMs under fuel cell conditions (humid conditions and under stress) during freeze/thaw cycling will need to be performed to better evaluate the PEM fuel cell durability.

There is only limited literature available on the durability of the catalyst layer and GDL under freeze/thaw cycling. These reveal that even a free-standing hydrated catalyst layer can be subjected to cracking and peeling while cycling (6 cycles) from −30 °C.[127] This damage was associated with a loss in the electrochemical surface area of the catalyst that can be avoided by drying the catalyst. This result can further help explain some of the discrepancies in the literature.

The water content in the catalyst layer will be determined by the extent of drying of the fuel cell before freezing, so the various literature studies may have widely different starting water contents in the catalyst layer. Furthermore, because the saturated vapor pressure curve for water is a strong function of temperature, even cells that operate at undersaturated conditions can exhibit condensation and freezing as the temperature drops after shutdown. Another factor that can affect the state of hydration of the catalyst layer in the fuel cell is the movement of liquid water toward a freezing front, commonly referred to as "frost heave"; essentially, water is drawn to a freezing front by capillary forces, which then lowers the radius of curvature further and induces further movement of water. He and Mench[128] present a one-dimensional model of this effect, and their results suggest that liquid water can be drawn from adjacent layers of the cell to form ice lenses adjacent to the catalyst layers that can block gas access to portions of the catalyst and induce delamination.

Some recent results have revealed that the GDL properties can change when subjected to freeze/thaw cycling.[129] It was observed that 50 freeze/thaw cycles from −35 °C (*ex situ*) resulted in a change in the air permeability of the GDL material. This was attributable to a weakening of the microporous layer (MPL) during the freeze cycling. This study also found that there was no change in the resistivity, contact angle, and porosity of the material during the freeze cycling. Another study of the GDL material under *in situ* conditions revealed that the external contact angle can change from 131° to 112° when subjected to 10 cold starts from −10 °C.[120] This loss in hydrophobicity of the material resulted in a loss in fuel cell performance.

These studies indicate that while there might not be catastrophic failure associated with freeze/thaw cycling of fuel cells, there may be slow changes in component properties and MEA integrity that may lead to degradation in fuel cell performance when subjected to extensive freeze/thaw cycling, associated with the loss in performance with GDL property degradation described in greater detail in section 5. These changes could include delamination, loss in catalyst electrochemical surface area, and changes in GDL pore structure and membrane physical/chemical properties. The effects of freeze/thaw cycling on the various component properties need to be evaluated in greater detail in order to better understand the degradation mechanisms that can result from freeze/thaw cycling. All these studies should take into account the initial water content in the material, the rate of heating/cooling, and the temperature of freezing.

2.2.2. Start-up Characteristics of Fuel Cells at Subfreezing Temperatures

Most literature studies have indicated that PEM fuel cells are capable of self-starting at subfreezing temperatures as low as −20 °C without any external heating.[130] This is primarily achieved either by drying out the cell during shutdown or by replacing the water with a nonfreezing solvent such as ethylene glycol.[121,130,131] There are a few reports of the inability of fuel cells to self-start from −5 °C[132] or −15 °C,[133] which may be related to the authors' failure to dry out the fuel cells to the desirable extent or, more likely, the high thermal mass of their cells.

When the fuel cell is operated at subfreezing temperatures, the water generated at the cathode will tend to form ice that can result in a loss in performance of the fuel cell. One study has revealed that this water is initially present in a supercooled state and then its temperature rises to 0 °C at the time of freezing.[134] The measured (AC impedance) charge-transfer resistance during a cold start from −10 °C has been shown to increase with time, providing further evidence for ice buildup in the catalyst layer.[120] Moreover, the water formation in the membrane during the start-up of a dried cell also results in membrane hydration, resulting in a lowering of the HFR of the cell.[120] These competing aspects have been modeled using either empirical based statistical models[135] or detailed models of the various parameters affecting the cell potential.[136] These models reveal that the fuel cell should be operated at a sufficiently high load to generate enough heat for an unassisted start. Furthermore, the cell has to heat up to above freezing temperature fast enough to avoid the ice formation from completely shutting down the electrochemical reaction at the cathode catalyst layer. To assist in this, the cathode gas flow rate can be increased (to blow ice away and to carry any excess water) and the inlet gases can be heated (to limit time below freezing temperatures). Because of the low vapor pressures of water at low temperatures, however, and the low heat capacities of the reactant gases, these approaches have limited utility in affecting the start-up profiles of full-sized stacks.[130]

In addition to the problems of self-start, there are several degradation mechanisms of concern while starting fuel cells

under subfreezing conditions.[135] These are primarily related to the ice formation in the membrane, catalyst layer, MPL, and GDL. However, given the limited literature data, it is not possible at this time to quantitatively evaluate the effects of these various degradation mechanisms.

2.2.3. Mitigation Strategies Utilized To Avoid Degradation Due to Subfreezing Temperatures

The patent literature has over 100 patents of various mitigation strategies to use while operating/storing fuel cells at subfreezing temperatures. A detailed analysis of this patent literature has been conducted by NREL and is available online.[137] In essence, these mitigation strategies fall into three categories: (a) those that keep the fuel cell warm, thus preventing ice formation, (b) those that prevent ice formation either by drying out the fuel cell or by replacing the water with a nonfreezing liquid, and, finally, (c) those that prevent ice formation during start-up by providing heat. Fuel cell stacks can be kept warm by providing insulation or by providing heat either through a battery or by operating the cell intermittently in a low power mode. The freezing water can be avoided by eliminating carrying a water tank on board and by running the fuel cell at lower inlet RHs and reclaiming the exhaust water, though it is not clear if the current class of membrane materials will operate stably under such conditions. The water inside the stack can be minimized by running the cell under dry reactant gases (H_2, air) or dry nitrogen before shutdown or by vacuum drying the fuel cell. Moreover, during start-up, extra heat can be provided from a battery, by catalytically combusting hydrogen, or by preheating the reactant gases, and the heat carrying capacity of the reactant gases is rather low. All these strategies aim to avoid/minimize the ice formation that can result in fuel cell performance loss, though they add complexity and are likely incompatible with the DOE's 5 MJ energy target.

2.3. Other Operating Conditions

Many of the mechanisms associated with PEM fuel cell degradation have to do with carefully processed materials relaxing to their equilibrium states, which unfortunately do not exhibit the same characteristics as materials immediately after processing, which can yield nonequilibrium states subject to subsequent relaxation. In many cases, operation of the fuel cell can accelerate existing decay modes or even invoke entirely new modes of degradation. A working fuel cell is exposed to a wide range of potentials, local relative humidities, and temperatures. Many of the decay mechanisms described elsewhere in this review have to do with the degradation that a cell experiences even if it remains at cell potentials between 0.6 and 1.0 V, at moderate to high relative humidities, with an operating temperature of 60−90 °C. In some cases, however, transient conditions or excursions can invoke entirely new decay mechanisms. We discuss examples of these modes in this section.

2.3.1. Load Cycling: Potential

A fuel cell, particularly one that must meet the challenging dynamic load of an automotive application, will undergo many rapid changes in load over the course of its lifetime. As the fuel cell cycles from high to low current, its cell potential will also vary, generally between 0.6 and 1.0 V. For cells operating with relatively pure hydrogen as a fuel, the anode will stay fairly close to the reversible hydrogen potential, due to the facile nature of the hydrogen oxidation reaction.[138] This implies that the cathode experiences potential swings as cell potential changes to match variable power demands. The variation of the cathode potential will change several properties of the electrode materials, notably the degree of oxide coverage of both platinum and carbon, and the hydrophobicity of the surfaces.[139−141]

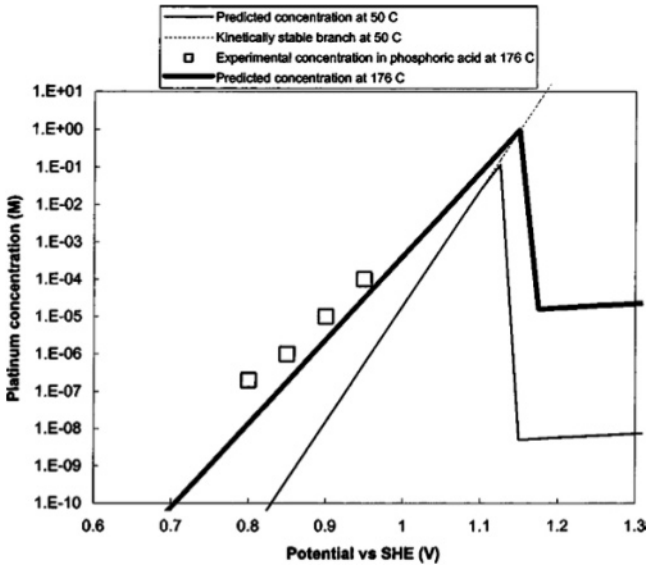

Figure 8. Equilibrium concentration of dissolved platinum vs electrode potential from a mathematical model. Reprinted with permission from ref 143. Copyright 2003 The Electrochemical Society.

A more subtle distinction has to do with the fact that the oxide can actually serve to protect the platinum surface from dissolution at higher potentials. When the cathode potential rises rapidly to higher values, the platinum can dissolve at a rapid rate until a passivating oxide layer is formed. Patterson presented data on the rapid loss of electrochemically active area with potential cycling,[142] and the phenomenon was subsequently modeled by Darling and Meyers, using simple models to describe the rates of platinum dissolution and of oxide formation and their subsequent movement through the cell.[143,144] Their model predicts that platinum is fairly stable at both low and high potentials, but there is a kinetically stable branch where platinum will dissolve rapidly when transitioning from low to high potentials. This is shown schematically in Figure 8. The general trend of platinum solubility was subsequently measured in liquid electrolytes, and the same trend was discovered, although the equilibrium concentrations differed greatly from the model behavior proposed.[145,146] These results are shown in Figure 9.[146]

Any attempt to develop stable catalysts for fuel cell applications must consider the stability of the catalysts not only under constant potential conditions but also under potential cycling. To design catalysts that are robust to this degradation mode, considerably more information is needed about the nature of the oxide, the kinetics of its formation, and its ability to protect the catalyst from dissolution over the entire range of potentials.

2.3.2. Fuel Starvation

Up to this point, we have discussed only the conditions to which a cell under normal operating conditions will be exposed. Full-sized cells, on the order of several hundred square centimeters in area, will experience different condi-

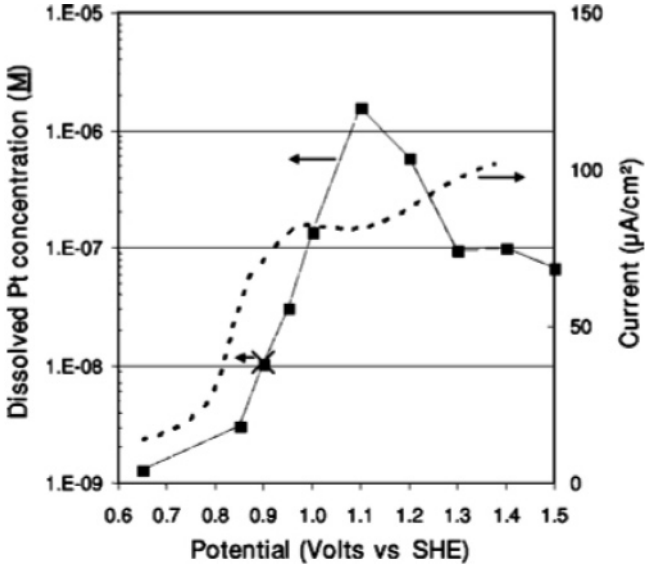

Figure 9. Measured dissolved platinum concentration in solution and initial dissolution rates in 0.57 M perchloric acid. Reprinted with permission from ref 146. Copyright 2006 The Electrochemical Society.

tions between the inlet and the outlet, and this can lead to current distributions that cannot easily be simulated in subscale testing. Furthermore, cells arranged in a stack configuration can experience different flows of fuel, air, and coolant resulting from imperfect manifolding. Therefore, adjacent cells in a stack can experience different conditions in terms of hydrogen and oxygen content, but they will be forced to carry the same current as their neighboring cells, as they are connected in series.

Several authors have noted that, in the case of gross fuel starvation, cell voltages can become negative, as the anode is elevated to positive potentials and the carbon is consumed instead of the absent fuel.[121,147,148] In the case of gross fuel starvation, for multiple cells in a stack, fuel maldistributions can lead to some cells having insufficient fuel to carry the current that is being pushed through them by adjacent cells. In the absence of a sufficient anodic current source from hydrogen, the cell potential climbs higher until oxidation occurs—in this case, the oxidation of the carbon support of the catalyst layer. A diagram illustrating the change of electrode potentials under starvation conditions is shown in Figure 10.

For reversals of this type, the anodic current is generally provided by carbon corrosion to form carbon dioxide, and results in permanent damage to the anode catalyst layer. Modeling has been conducted to describe how a poor hydrogen distribution can induce both O evolution and carbon corrosion at the cathode of the fuel cell.[149] Modeling has also predicted that O_2 crossover through the membrane controls the total amount of current that goes to carbon corrosion.[150] These issues have led to the conclusion that conventional carbon supports for Pt are unlikely to meet automotive durability targets and implementation of corrosion-resistant supports combined with controlled system strategies are required.[151]

Proper reactant distribution is critical to avoid this problem, and stack developers have accordingly sought to monitor the voltage of each cell to avoid such a problem.[152] Obviously, such an extensive monitoring system will add considerable cost and complexity to the fuel cell stack and control scheme.

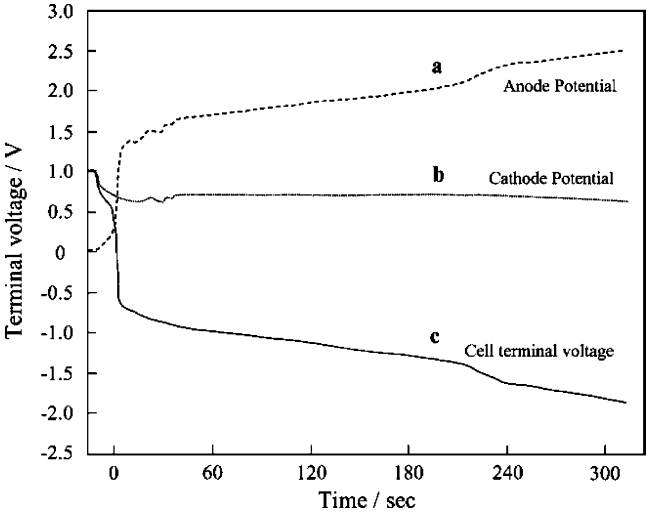

Figure 10. Electrode potentials for a cell driven to pass current after hydrogen flow is interrupted. Reproduced with permission from ref 147. Copyright 2004 Elsevier Sequoia SA.

Localized Starvation. A more subtle form of fuel starvation was proposed in a paper by Reiser *et al*.[153] They suggest that transient conditions, or *localized* fuel starvation, can induce local potentials on the air electrode significantly higher than 1 V and, thereby, induce corrosion of the carbon supports that results in permanent loss of electrochemically active area. The cell potential can remain in the range of expected conditions even as this condition persists, and this "reverse" current mechanism can induce damage to the cathode without being directly observable.

The mechanism suggests that the highly conductive bipolar plates of the fuel cell allow for sufficient redistribution of current in the plane of the current collectors that all regions of the cell experience the same potential difference. In the regions of the cell where fuel is present on the anode, the fuel cell behaves normally; the fact that the hydrogen reaction is so facile implies that the potential in the fuel-rich regions will stay close to its equilibrium voltage and is capable of delivering high currents until the hydrogen is consumed. In the regions of the cell where there is no fuel present, there is no proton or electron source at lower potentials, so the electrodes must shift to significantly higher potentials to maintain the potential difference imposed by the active part of the cell while still conserving current. Thus, a reverse current is established, and current is driven from the positive electrode to the negative electrode in the fuel-starved region, opposite the direction of normal current flow in the active portion of the cell. The only reactions that can sustain this current in the fuel-starved region are oxygen evolution and carbon corrosion on the positive electrode, and oxygen reduction from crossover on the negative electrode.

This mechanism is shown schematically in Figure 11. This problem can be induced not only by poor cell-to-cell flow distributions but also by local blockages, by differences in channel depth tolerances, and by water blockage, if water vapor condenses in the anode channels and fills the channels. A good example of this is given by Patterson and Darling.[154] This phenomenon has been visualized by neutron imaging and suggests that improper water management can cause major problems with fuel distribution and, consequently, damage to the cathode catalyst layers.[155]

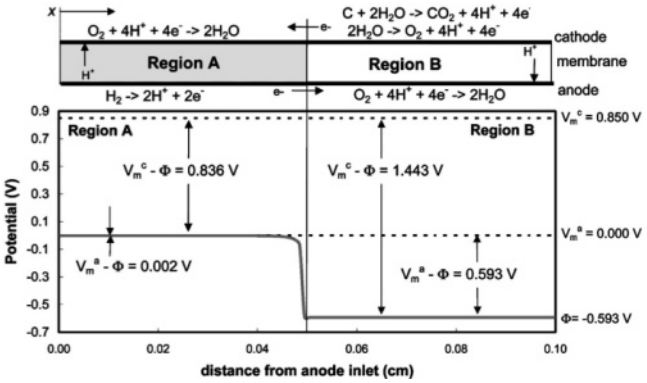

Figure 11. Schematic diagram illustrating the "reverse current" mechanism. Reprinted with permission from ref 153. Copyright 2006 The Electrochemical Society.

2.3.3. Start/Stop Cycling

While the problem of localized starvation under normal operation can perhaps be mitigated through careful control of reactants and water management (design, operating conditions, and materials choices), there is an aspect of fuel cell operation where such maldistributions must almost certainly exist, at least for a short time: namely, start-up and shutdown. Under conditions of a prolonged shutdown, unless the stack is continually provided with fuel, hydrogen crossover from the anode to the cathode will eventually empty out the anode chamber and result in an air-filled flow channel. In this case, the starting flow of fuel will induce a transient condition in which fuel exists at the inlet but the exit is still fuel-starved. As a result, starting and stopping the fuel cell can induce considerable damage to the cell. This phenomenon has been modeled and reveals that an unprotected start can induce local potentials on the cathode in excess of 1.8 V relative to a hydrogen reference electrode.[149] This modeling study suggests that potential control (voltage clipping) is by far the most effective means of minimizing this effect. A review of system-level strategies to minimize this mode of degradation has been reported by Perry *et al*.[156]

2.3.4. Temperature and Relative Humidity

Another aspect of fuel cell operation that is likely to affect the integrity of the cell is the changes in temperature and relative humidity that are associated with transitions between low and high power. In general, for cells that operate at fixed stoichiometric ratios, operation at low current implies a relatively cool and wet cell; higher currents imply a hotter, drier cell.[157] The fact that the ionomer swells with water uptake suggests that increases in water uptake as the membrane is exposed to high RH conditions can lead to compressive stresses in the membrane that then yield tensile residual stresses during drying.[158] These stresses are suggested as a significant contributor to mechanical failures of the membrane. Another recent study suggests that drying can considerably strain the membrane−electrode assembly and that mechanical failure of membranes can result from gradual reduction in ductility combined with excessive strains induced by constrained drying of the MEA.[159] Both temperature and relative humidity have been shown to affect the rate of catalyst surface area loss due to platinum particle growth.[17] These studies suggest that more needs to be learned about material properties and how they change over the course of fuel cell operation.

3. Membrane Degradation

3.1. Discussion of Polymer Electrolyte Membranes (PEMs)

The first hydrocarbon based membranes tested as electrolytes in PEMFCs for Gemini space missions, such as sulfonated phenol−formaldehyde resins, sulfonated poly(styrene−divinylbenzene) copolymers, grafted polystyrene sulfonic acid membranes (*g*-PSSA), *etc.*, were chemically weak. PEMFCs using these membranes showed poor performance and had only lifetimes of several hundred hours. Nafion, a perfluorinated sulfonic acid (PFSA) membrane, was developed in the mid-1960s by DuPont. It is based on an aliphatic perfluorocarbon sulfonic acid, and it exhibited excellent physical properties and oxidative stability in both wet and dry states. A Nafion based PEMFC was used for the NASA 30-day Biosatellite space mission.[160] Many PFSA membranes are presently commercially available from several membrane manufacturers, including DuPont, Gore, Asahi Glass, Asahi Kasei, Solvay, and 3M. The membranes are generally synthesized by copolymerization of tetrafluoroethylene and perfluorinated vinyl ether sulfonyl fluoride, followed by hydrolysis of the sulfonyl fluoride groups.[161] Proton-conducting membranes are formed from the as-synthesized material via extrusion or casting and hydrolysis steps. Early data showed that the durability of the PEMFC stack using Nafion 120 (250 μm thickness, equivalent weight = 1200) reached 60,000 h of continuous fuel cell operation at 43−82 °C.[162] However, increasing demands for maximizing performance efficiency and proton conductivity of PEMFCs by use of thinner (*ca.* $\leq$50 μm) and lower equivalent weight ($\leq$1100 EW) PEMs adversely impact the longevity of the PFSA membranes during fuel cell operation. Currently, the durability of the PFSA membranes under continuous fuel cell operation has been reported in the range of a few thousand to several tens of thousands hours, depending on operating conditions. These lower lifetimes are not just due to thinner and different membranes. Another important difference is that these fuel cells are being run under drier and more cyclic conditions. Meanwhile, random copolymer hydrocarbon based membrane materials have reemerged as viable alternatives in the past decade[163] as part of a search for membranes with better physical properties, particularly at elevated fuel cell operating temperatures, although study of their durability and degradation in operating fuel cells has just started and only a limited number of reports are found in the literature. The chemical structures of selected PFSA and hydrocarbon based copolymers in fuel cells are shown in Figure 12.

In this section, the durability of PEMs will be reviewed with emphasis on membrane degradation mechanisms. The first part outlines the membrane durability in *in situ* tests, using both accelerated and standard life tests. These tests include both chemical and physical degradation mechanisms. Next, chemical and physical degradation in membranes are treated separately. Chemical degradation of PEMs is discussed in terms of peroxide/radical and hydrolysis induced degradation. Physical degradation centered on membrane creep, microcrack formation, and morphological change is then discussed. Finally, efforts to improve PEM durability by improving chemical and physical stability are presented. Membrane durability as a function of polymer family is a common theme in our discussion.

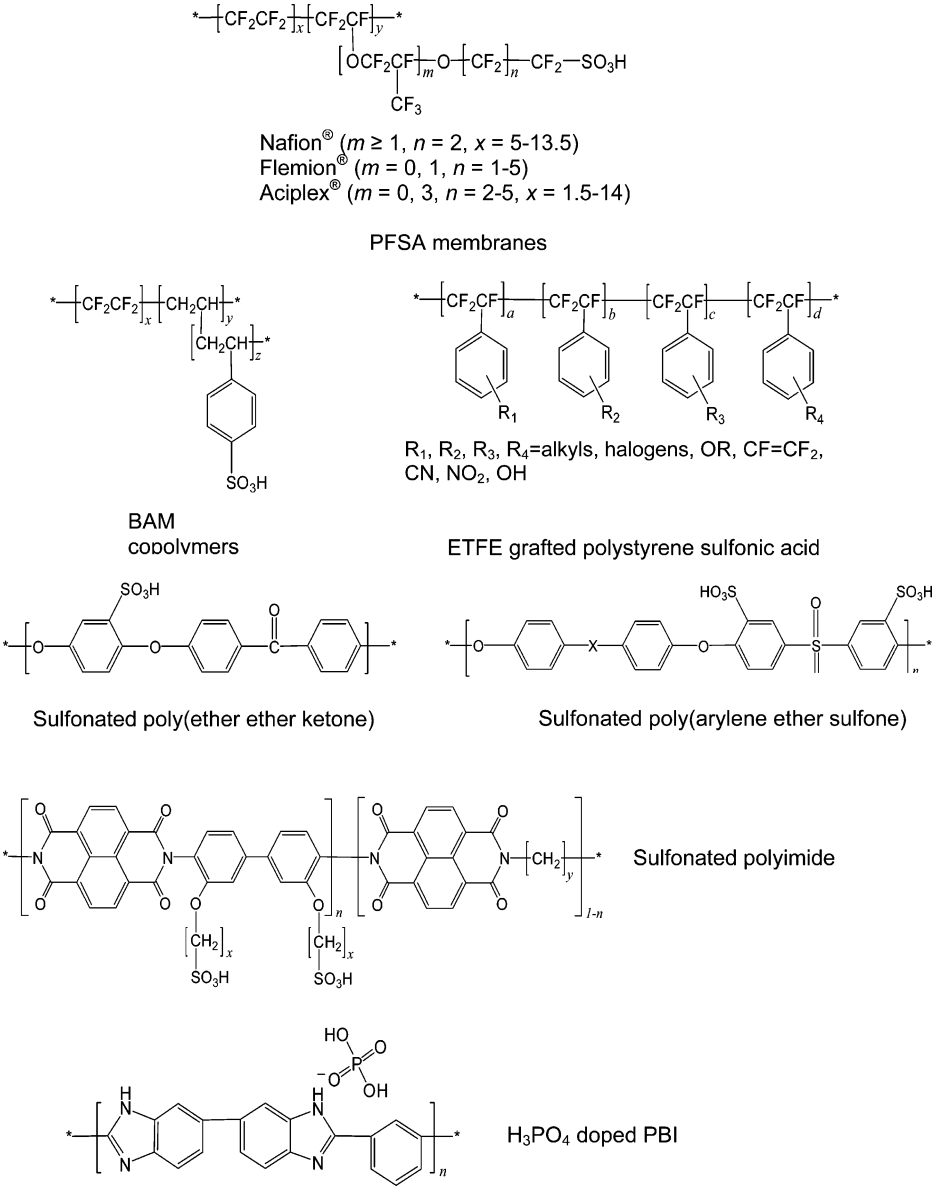

Figure 12. Chemical structures of polymer electrolyte membranes.

3.2. *In Situ* PEM Durability Evaluation

3.2.1. Life Test

In most reported fuel cell life tests, single cells or stacks using thin membranes (usually ~50 μm) were operated under steady-state conditions, because these conditions were most easily applied (although, for many applications, unsteady conditions are more appropriate). Cell temperatures typically ranged from 50 to 80 °C, and fully humidified conditions were typically applied. The operating current (or voltage) and reactant backpressures were varied with the target fuel cell applications. The life test under normal operating conditions provides the most relevant PEM lifetime data, although decoupling membrane related effects from those arising from other components can be difficult. This method is common in spite of its time-consuming nature and some difficulties in data analysis. *In situ* cell resistance measurement, ac impedance, gas permeability, postmortem analysis using optical microscopy, SEM, TEM, NMR, IR, X-ray, neutron techniques, and chemical structural analysis have been used with this method to investigate PEM failure mechanisms.

Table 8 summarizes the durability data of select membranes from fuel cell life tests. Stucki *et al*. reported that the life span of a fuel cell stack using Nafion 117 reached 15,000 h under 80 °C continuous operations.[164] Related PFSAs lifetimes were significantly reduced to a few thousand hours, when thinner membrane and backpressurized conditions were applied.[165,166]

The lifetimes of hydrocarbon based membranes measured by this method were also reported. Ballard Advanced Materials Co. has evaluated their first, second, and third generation membranes. Each ionomer is referred to as BAM1G, 2G, and 3G and has the chemical structure of sulfonated poly(phenylquinozaline)s, sulfonated poly(2,6-diphenyl-1,4-phenylene oxide)s, or poly(trifluorostyrene sulfonic acid)s, respectively.[167] BAM1G membranes survived several hundred hours in hydrogen/oxygen fuel cells at 70 °C. The degradation was most likely due to the oxidative decomposition leading to membrane embrittlement. In order to render better oxidative stability, BAM2G was modified with electron-withdrawing functionalities (fluoride, bromide, and cyanide); however, these attempts failed to achieve

Table 8. Durability of Selected Membranes under Fuel Cell Operation

PEM	IEC (mequiv/g)	application type	thickness (μm)	temp (°C)/ $P_{anode}/P_{cathode}$	humidification (% RH)	life test conditions	lifetime (h)	ref
Nafion	0.9	H_2/air	180	80		1 A/cm^2 (start-up), cont	2,300→20,000	164
	0.9	H_2/air	50	80/15 psig/15 psig	>100%	0.6 V cont	3,000	257
	0.9	H_2/air	25, 50	65/1 bar/1 bar	100%	0.8 A/cm^2, cont	>2,500	166
Flemion	1.1	H_2/O_2	50	80/0.1 MPa	100%	1 A/cm^2 cont	>4,000	187
Gore PRIMEA 56[a]		H_2/air	30	70/ambient	100%	0.8 A/cm^2 cont	>20,000	186
BAM 3G[a]	2.5	H_2/air		80/2 atm			14,000	167
BAM 3G	2.2	H_2/air		70/24 psig/24 psig		0.5 A/cm^2	4,061	168
styrene sulfonic acid/ Nafion composites		H_2/O_2	>160	80/0.2 MPa/0.2 MPa	100%	0.3 A/cm^2	>835	169
ETFE based radiation grafted membrane	1.1	H_2/O_2	78	60/ambient	>100%		<600	170
	1.5	H_2/O_2	25	80/1 bar/1 bar	anode: 100% cathode: 0%	0.5 A/cm^2	>770	175
	1.2	H_2/O_2	35	50/2 bar/3 bar	>100%	0.2 A/cm^2	~1,000	172
sulfonated poly(ether	1.5	H_2/O_2	40	50/ambient		0.05 V, cont	4,300	176
ether ketone)	-	H_2/O_2		90		0.5 mA/cm^2	> 1,000	173
	1.3	DMFC	60	120/1 bar/3 bar		discont	1,440	
sulfonated poly(arylene	1.3	DMFC	50	80/1 bar/1 bar	>100%	0.5 V, cont	>3,000	637
ether sulfone)	1.6	H_2/O_2	40−50	80/ambient	90%	0.2 A/cm^2, cont	5,000	174
sulfonated polyimide	1.2	H_2/O_2		60/2 atm		0.25 A/cm^2	>3,000	177
	1.8	H_2/O_2	50−60	80/1 bar/1 bar	90%	0.2 A/cm^2, cont	5,000	178
PEMEAs Celtec-P (PBI based)[a]		H_2/air		160/ambient	0%	0.2 A/cm^2 cont	>18,000	180
acid-doped PBI		H_2/O_2	NA	150	0%	0.5 V cont	5,000	161

[a] Stationary application.

improved longevity. Later, sulfonated polytrifluorostyrene based BAM3G membranes were claimed to exhibit considerably increased stability to main chain scission and achieved substantial longevity (several tens of thousands hours) in stack configurations as well as single cells.[167,168]

Other styrene sulfonic acid based copolymers, however, showed relatively poor durability. Yu *et al*. observed a significant oxidative degradation of the polystyrene sulfonic acid at the cathode side of the fuel cell.[169] By attaching Nafion on the cathode side of polystyrene sulfonic acid, he could obtain a >800 h lifetime. Radiation grafted polystyrene membranes showed limited life, in general. Buchi *et al*. and other groups showed a less than 1000 h lifetime which greatly decreased as cell temperature increased.[170−172] Having a similar polymer main chain structure to BAM 2G, sulfonated poly(ether ether ketone)s (SPEEKs) were reported to endure 1,000 h of operation at 90 °C and a constant current density of 0.5 mA/cm^2.[173] Later, several researchers achieved stable fuel cell performance of sulfonated polyarylenes for 3,000−5,000 h under continuous fuel cell operation at 50−80 °C.[173−176]

The durability of sulfonated polyimides was also investigated. Mercier's group operated a fuel cell using a sulfonated naphthalene dianhydride base polyimide at 60 °C and 250 mA/cm^2 for 3,000 h in hydrogen/oxygen (3 bar each).[177] Asano *et al*. reported single cell performance at a constant current density of 0.2 A/cm^2 using a hydrolytically stable polyimide lasting 5,000 h at 80 °C.[178] However, unlike most other hydrocarbon based membranes, hydrolysis is a crucial degradation mode for sulfonated polyimides, as we discuss below.

Phosphoric acid doped polybenzimidazoles (PBIs) were developed by researchers at Case Western Reserve University as high-temperature operable membranes.[179] This electrolyte system differs from the previously discussed "traditional" PEM electrolytes, as the membrane is a phosphoric acid electrolyte with a polymer matrix. These membranes were tested at elevated temperature (>150 °C) in order to achieve adequate conductivity and eliminate liquid water that would cause the phosphoric acid to leach out of the membrane during operation. In these studies, they demonstrated 200 h of hydrogen/oxygen fuel cell operation at 150 °C and at a constant cell voltage of 0.55 V. More recent results by different groups demonstrated much longer lifetimes for PBI membranes;[179−182] 5,000 h at 150 °C[181] and 6,000 h at 160 °C[183] with low decay rates in cell voltage. The likelihood of condensation in these systems upon shutdown or idling conditions makes it a challenge for them to operate under the transient conditions likely to be experienced in automotive systems, but there might be advantages to the higher temperatures for stationary applications with relatively modest load cycling requirements

3.2.2. Accelerated Life Test

Accelerated fuel cell life tests have become common, because life tests under standard conditions can often last thousands of hours. In accelerated tests, membrane degradation can occur much faster than under normal operating conditions.[121] However, the appropriateness of a given accelerated condition as a gauge of general durability is not necessarily clear. To date, four different accelerated parameters or a combination of these parameters have been employed in accelerated life testing: (1) elevated temperature, (2) reduced humidity, (3) open circuit voltage (OCV), and (4) cycling [relative humidity (RH), temperature, potential, freeze/thaw, or start/stop] conditions. Membrane degradation is often monitored by changes in gas crossover rate or fluoride-ion emission rate (FER) during the *in situ* test. Table 9 shows some reported data from the accelerated life tests.

Fuel cell tests under elevated temperatures (>100 °C, a target for automotive applications due to heat rejection issues) have been conducted in search of membranes with high-temperature stability.[121] Elevated temperature operation

Table 9. Membrane Durability Using the *in Situ* Accelerated Test

acceleration parameter	polymer	IEC (mequiv/g)	application type	membrane thickness	temp (°C)/ $P_{anode}/P_{cathode}$	accelerated conditions	degrad rate	suggested membrane failure mode after test	ref
cell temp	Nafion	0.9	H_2/air	180 μm	120/24 psig/	120 cell temp	50 h	pinhole and tearing	184
	sulfonated PEEK/PBI/PAN			100 μm	24 psig	with 50 ppm CO	390 h	tearing	
cell temp, humidity,	Nafion	0.9	H_2/O_2	25 μm	100/1.5 atm/ 1.5 atm	100 °C, 25% RH	70 h	membrane failure—increased gas crossover	185
and OCV	sulfonated polysulfone	1.5				and OCV condition	~300 h		
cell temp, humidity, and potential cycling	Nafion	0.9	H_2/O_2	50 μm	100/150	potential cycles 1 min	60 h	membrane thinning	185
	sulfonated polysulfone	1.5		60 μm	kPa	at 0.4 V and 1 min at 1V	> 350 h		
humidity	Nafion	0.9	H_2/air	50 μm	75	81% RH at 0.3 A/cm^2	1900 h	local pinhole formation	613
	sulfonated polysulfone	1.6	H_2/O_2	50 μm	80/ambient	60% RH at 0.2 A/cm^2	2350 h	oxidative degradation	174
humidity and OCV	perfluorinated ionomer	NA	H_2/air	30 μm	80/ambient	anode cathode temp = 60 °C and OCV	720 h	hydrogen peroxide decomposition	195
	Flemion	1.1	H_2/O_2	50 μm	80	low humidity and OCV	150 h (~30% loss)	carbon radical degradation	214
OCV	Nafion	0.9	H_2/O_2	50 μm	70	hydrated and OCV	24 h	hydrogen peroxide degradation	196
RH cycling	Nafion	0.9	H_2/O_2	25 μm	80	RH cycles (150% RH to 0% RH, 2 min each)	4000 cycles	fatigue, viscoelastic creep	199
	sulfonated polysulfone	1.8					300 cycles	mechanical embrittlement	
	Nafion	0.9	H_2/O_2	25 μm	100	RH cycles (0—100%)	> 200 h		185
	sulfonated polysulfone	1.5					25 h	microcrack formation	

(>100 °C) has significantly shortened PEM lifetimes (lifetimes less than a few hundred hours are typical when operated above 100 °C[184,185]). The lifetime of PFSA membranes seem particularly dependent on elevated temperature and reduced humidity. Mechanical failures such as pinhole formation and tearing were often observed from postmortem characterizations.

Low RH operation (inadequate humidification) has also led to accelerated cell failure through membrane degradation, whereas more aggressive humidification of reactant gases contributes to greatly increased membrane lifetimes.[186—192] Often, the low humidity conditions were combined with OCV testing in order to accelerate hydrogen peroxide rates as H_2O_2 generation is accelerated at OCV conditions.[185,193] As seen in Table 9, the lifetimes of PEM membranes have been most drastically reduced at low humidification and/or OCV conditions.[194—198] Although limited data are available in the open literature, humidity and start/stop cycling conditions seem to cause accelerated membrane degradation.[171,199] Hydrocarbon based membranes usually showed higher sensitivity to mechanical embrittlement or fatigue during RH cycling experiments compared to the PFSA membranes, possibly related to swelling/shrinkage issues.

The fuel cell life test under accelerated operating conditions has become popular, since it is less time-consuming but still reflects in cell degradations. The development of standard test protocols for cycling accelerated fuel cell tests is being pursued by several research groups and organizations. Although 3M Company presented an elegant experimentally based statistical MEA lifetime prediction from various acceleration factors,[200] this approach is limited to specific modes of fuel cell failure and is not much help in understanding membrane-degradation mechanisms.

3.3. Chemical Degradation

3.3.1. Peroxide/Radical Degradation

Chemical degradation of membranes during operation was recognized in the early R&D era for space missions.[160,201] LaConti *et al*. proposed a mechanism that oxygen molecules permeate through the membrane from the cathode side and are reduced at the anode Pt catalyst to form hydrogen peroxide.[202,203]

$$H_2 + Pt \rightarrow Pt{-}H \text{ (at anode)} \tag{3.1}$$

$$Pt{-}H + O_2 \text{ (diffused through PEM to anode)} \rightarrow {}^{\bullet}OOH \tag{3.2}$$

$${}^{\bullet}OOH + Pt{-}H \rightarrow H_2O_2 \tag{3.3}$$

It is known that H_2O_2 formation in oxygen reduction on polycrystalline[204,205] and single[206,207] crystalline Pt as well as Pt/C catalyst[208—210] is greatly enhanced in the anode potential region, where atomic hydrogen is adsorbed on Pt. This fact supported the mechanism proposed by LaConti *et al*. A recent rotating ring—disk electrode study suggested that H_2O_2 yield exceeds 80% at Pt/C catalysts dispersed highly on a glassy carbon disk in the anode potential range (~0 V).[210] The presence of H_2O_2 has been confirmed in exhaust gas,[196] in drain water,[195] and directly in the membrane[211] during operation of PEMFCs. However, the absolute concentration remains in doubt.

PFSA membranes are generally stable against 30% H_2O_2 even at 80 °C, in the absence of impurity metal ions (or other radical generating sources such as UV light). However, the presence of Fe^{2+} and Cu^{2+} ion greatly accelerates the membrane degradation rate.[197,212] LaConti *et al*. also postulated that the formed H_2O_2 could react with minor impurities such as Fe^{2+} and Cu^{2+}, forming hydroxyl ($^{\bullet}OH$) and hydroperoxy ($^{\bullet}OOH$) radicals that could attack the membrane.[160,202,203]

$$H_2O_2 + M^{2+}\ (\text{found in MEA}) \rightarrow M^{3+} + {}^{\bullet}OH + OH^{-} + \quad (3.4)$$

$$^{\bullet}OH + H_2O_2 \rightarrow H_2O + {}^{\bullet}OOH \quad (3.5)$$

It was reported that iron contamination from end plates accelerates the rate of membrane degradation.[213] Endoh *et al*. observed electron spin resonance (ESR) signals from deteriorated MEAs and attributed the signals to carbon radicals.[214,215] They suggested that the carbon radicals are formed from $^{\bullet}OH$ and $^{\bullet}OOH$ radicals, though they did not find direct evidence of the peroxide radicals. Pachenko *et al*. also observed an ESR signal from the electrode carbon materials during cell operation.[216]

Recent Findings in Degradation Mechanisms. As mentioned earlier, inadequate humidification greatly enhances membrane degradation during operation as well as under OCV. The reason for the enhanced degradation rate has not been fully understood so far and is the subject of much debate by many researchers. Inaba *et al*. reported that sulfate ions and ferrous ions are accumulated under low-RH operation and that they were washed out in drain water under highly humidified conditions.[188] The boiling temperature of H_2O_2 (150 °C)[217] is higher than that of water, and hence, they attributed the high degradation rate to accumulation of impurities and H_2O_2 in the membrane under low humidification. A high activity of H_2O_2 in the vapor state has also been raised as a reason for the increased membrane degradation rate.[218,219]

OCV durability tests have recently been carried out by many research groups and have proven to be valuable approaches for understanding degradation. Several groups have tested membrane durability of single-side-catalyzed MEAs without potential control, conditions meant to mimic OCV.[220−223] Most have reported that membrane degradation is more significant in the MEAs catalyzed only at the cathode side than in those catalyzed only at the anode side. This fact is inconsistent with the mechanism mentioned earlier, in which H_2O_2 is formed at the anode catalyst. Two mechanisms have been suggested: one is hydrogen peroxide formation upon reduction of adsorbed oxygen on the cathode catalyst with permeating H_2,[212] and the other is direct formation of $^{\bullet}OH$ or $^{\bullet}OOH$ radicals from oxygen-containing species on Pt (*e.g*., Pt−OH and Pt−OOH).[221,223] However, these mechanisms should be verified because the potential of the cathode (∼1 V) at OCV is more positive than the potential for hydrogen peroxide formation ($E°_{H_2O_2} = 0.695$ V) and the lifetime of the radicals is too short to attack the bulk of the electrolyte membrane.[214] Liu *et al*. observed that the interaction of permeating H_2 with an adsorbed oxide layer formed electrochemically on Pt, at +1.0 to 1.5 V in a nitrogen atmosphere, does not lead to a significant FER, and they showed that gaseous O_2 is necessary for degradation to occur.[223]

Platinum dissolution from the cathode and particle deposition inside the bulk membrane, called the Pt band, is another serious degradation phenomenon in operation,[224] under potential cycling[225] and at OCV.[194] Ohma *et al*. found that the Pt band is formed in a relatively short time (several tens to a few hundreds of hours) depending on test conditions and suggested that the Pt band formation greatly enhanced H_2O_2 formation and membrane degradation.[194] The Pt band is formed at a position where the theoretical potential profile in the membrane suddenly changes from the cathode side (∼1 V) to the anode side (∼0 V) and therefore the potential requirement for H_2O_2 formation mentioned above is satisfied. In addition, oxygen flux is greatly enhanced, especially under H_2/air conditions, because the Pt band is formed in the vicinity of the cathode catalyst layer under H_2/air conditions.[194] Ohma's mechanism helps explains the discrepancy in the results of one-sided catalyzed MEAs mentioned above, because the Pt band originates from the dissolution of the cathode catalyst. Inaba *et al*. found that FER gradually increased with time in an OCV test at 80 °C while gas crossover rate did not change appreciably for the initial 30 days.[188] They attributed this discrepancy to the growth of the Pt band.

Recently, Liu *et al*. presented a contradictory report on the effect of humidification.[223] When the humidification of hydrogen at the anode was kept at 50% RH, the lifetime of the MEA was longer when air at the cathode was humidified at 0% RH (>4,000 h) compared to the case at 50% RH (∼700 h). They attributed the shorter lifetime at low RH to more impurities with water from the gas bubbler at high RH. Alternatively, it is possible that their results reflect the difference in the rate of the Pt-band formation, because the dissolution of Pt is greatly suppressed under lower humidification.[226]

Decomposition Mechanism of PFSA Membranes. In drain water during operation of PEMFCs, fluoride ions, sulfate ions, and low-molecular weight perfluorosulfonic acid are found. Direct gas mass spectroscopy of the cathode outlet gas indicated the formation of HF, H_2O_2, CO_2, SO, SO_2, H_2SO_2, and H_2SO_3 under OCV durability tests.[196] PFSA membranes contain no α-hydrogens, which are vulnerable to radical attacks, and hence, the membranes would be stable against radical attacks[227] if they have the perfectly fluorinated structures shown in Figure 12. The susceptibility to peroxide radical attack has been attributed to a trace amount of polymer end groups with residual H-containing terminal bonds.[166] Hydroxy or hydroperoxy radicals attack the polymer at the end group sites and initiate decomposition. An example of attack on an end group such as $-CF_2X$, where X = COOH, is shown as[166,218]

$$R_f{-}CF_2COOH + {}^{\bullet}OH \rightarrow R_f{-}CF_2 + CO_2 + H_2O \quad (3.6)$$

$$R_f{-}CF_2{}^{\bullet} + {}^{\bullet}OH \rightarrow R_f{-}CF_2OH + R_f{-}COF + HF \quad (3.7)$$

$$R_f{-}COF + H_2O \rightarrow R_f{-}COOH + HF \quad (3.8)$$

Note that −COOH is regenerated in reaction 3.8. Hence, once decomposition begins at one end group, a complete PFSA unit is decomposed to HF, CO_2, and low-molecular-weight compounds by the radical depolymerization reactions (called the "unzipping" mechanism). Degradation studies using model compounds have proved that decomposition starts from $-CHF_2$ and $-CF_2COOH$ groups.[228] The decom-

Table 10. Peroxide Stability by Fenton's Test

membrane type	Fenton's reagent formulation	temp (°C)	degradation rate constant at 68 °C	ref
polysulfone sulfonic acid	3% H_2O_2/4 ppm Fe^{2+} solution	68	0.218 min^{-1}	160
sulfonated poly(benzimidazole)		68	0.211 min^{-1}	160
1% divinylbenzene cross-linked polystyrene sulfonic acid			0.125 min^{-1}	160
polyphenylene sulfonic acid			0.026 min^{-1}	160
6% divinylbenzene cross-linked polystyrene sulfonic acid			0.022 min^{-1}	160
phosphonated poly(benzimidazole)			0.016 min^{-1}	160
polytrifluorostyrene sulfonic acid and cross-linked polyphosphazene			0.008 min^{-1}	160
perfluorosulfonic acid			0.000 min^{-1}	160
divinyl benzene cross-linked polystyrene sulfonic acid	3% H_2O_2/4 ppm Fe^{2+} solution	68	>90%[a]	638
sulfonic acid and cross-linked polyphosphazene		68	<5%	638
Nafion		68	<1%	638
side-group sulfonated polyether ether ketone	3% H_2O_2/2 ppm Fe^{2+}	80	1−3%	639
poly(arylene ether) containing sulfofluorenyl group (IEC = 1.8 mequiv/g)		80	~10%[b]	236
Nafion		80	2−3%	236
sulfonated arylene ether/fluorinated alkane copolymer (IEC = 1.74 mequiv/g)	30% H_2O_2/30 ppm Fe^{2+}	25	4 h (6 h)	640
sulfonated polyimide (IEC = 1.95 mequiv/g)		25	20 h (24 h)	641
sulfonated (arylene ether)s with pendant biphenyl group		25	32 h (55 h)	237

[a] Weight loss after soaking in Fenton's reagent after 24 h. [b] Weight loss after soaking in Fenton's reagent after 1 h. [d] Time to start to break film (complete dissolution).

position rate of model compounds without −COOH end groups is 2−3 orders of magnitude lower than those of compounds with −COOH end groups.[229] Curtin *et al*. reported that these reactive end groups of Nafion could be minimized during the membrane extrusion processes by pretreating the polymer with fluorine gas.[166] After more than 50 h of exposure, they could remove 61% of the H-containing end groups, and further testing found a 56% decrease in released fluoride ions in the Fenton test, as compared with the case of an untreated polymer.

Even when the residual H-containing end groups are completely fluorinated, the degradation rate of PFSA membranes cannot be reduced to "zero", suggesting another mechanism exists for membrane degradation. Hommura *et al*. carried out durability tests of Flemion membranes and reported that the average molecular weight decreased while the number of −COOH groups increased with time when the membranes are exposed to vapor-phase H_2O_2 at 120 °C.[218] They suggested that not only the unzipping reactions but also main chain scission (which produces vulnerable −COOH groups) is involved in the mechanism for membrane decomposition. It has been suggested that the ether linkages are the weakest sites of the side chains for radical attack.[229]

Detailed degradation mechanisms of sulfonated polyaromatic ethers are under dispute. EPR[230] and DFT[231] investigations suggest that ether link cleavage can be initiated by hydroxyl and hydroperoxy radicals attack as judged by Fenton's test and the subsequent oxygen molecule addition on aromatic rings. A recent study by Jang *et al*. revealed that sulfonated poly(ether sulfone) membranes degraded mainly at the cathode side after fuel cell durability tests.[232] As partially fluorinated hydrocarbon ionomers, BAM3G membranes seem to have considerable stablity to main chain scission and have successfully achieved substantial longevity (several tens of thousands hours) in multistack configurations as well as in single cells.[167]

Fenton's Test. As it has been recognized that the formation and reactivity of free radical peroxide species are a major source of degradation of PEMs used in fuel cells, Fenton's test, using a H_2O_2 solution containing a trace amount of Fe^{2+}, has become a common *ex situ* accelerated test for membrane durability.[166,212,233] For PFSAs, this seems reasonable because membrane degradation is caused by the peroxide radical route as described earlier. It was reported that a compound, $HOOC-CF(CF_3)-O-CF_2CH_2SO_3H$, identified by ^{19}F NMR and mass spectroscopy, is commonly detected as the primary short-chain degradation product of Nafion in both PEMFC operation and the Fenton tests.[228]

PFSA membranes usually show excellent chemical stability; hence, harsh conditions are employed in the accelerated tests. For example, PFSA membranes are immersed in 30% H_2O_2 solution containing 20 ppm Fe^{2+} ions at 85 °C for 16−20 h, and their durability is evaluated as the total amount of fluoride ions emitted in the solution.[166] Sulfate ions are also detected in the solution and can be used to evaluate the decomposition of the sulfonic acid moieties.[212] Aoki *et al*. developed a novel *ex situ* method for membrane durability tests, in which mixed gases of H_2 and air were supplied at given ratios to a water suspension of Pt/C catalyst coated with Nafion.[174,234] This method has an advantage in that it can simulate the anode side (H_2-rich) and the cathode side (O_2-rich) by changing the ratio of H_2/air. They observed a larger amount of fluoride ion (0.27% of the total fluorine in the membrane) in the H_2-rich atmosphere than in the O_2-rich atmosphere (0.16%), which supported the degradation mechanism proposed by LaConti *et al*.[160] Hommura *et al*. developed another *ex situ* method exposing PFSA membranes with H_2O_2 vapor at 120 °C.[218,219]

Compared to PFSAs, hydrocarbon based membranes have been known to show much faster degradation in the Fenton's reagent. Table 10 summarizes the reported peroxide stability of various PEMs. LaConti *et al*. evaluated the relative stability of several types of PEMs by Fenton's reagent; the stability decreased in order PFSA > cross-linked sulfonated polyphosphazene = polytrifluorostyrene sulfonic acid > phosphonated poly(benzimidazole) > high cross-linked polystyrene sulfonic acid > polyphenylene sulfonic acid > low cross-linked polystyrene sulfonic acid = sulfonated poly(benzimidazole) = polysulfone sulfonic acid = polyethylene polystyrene sulfonic acid copolymer.[160] Poor peroxide stabil-

ity of thermomechanically stable sulfonated polyarylenes (and polyheterocycles) provoked further research efforts to investigate the structural effects on peroxide oxidative stability. The oxidative stability of the sulfonated PEMs increased with increasing numbers of hydrophobic groups (or fluorine containing groups) and decreasing ion exchange capacity (IEC) and water-absorbing capability.[235,236] It has also been reported that sulfonated polyarylenes with pendant sufonic acid groups are more stable to peroxide oxidation than backbone sulfonated PEMs.[223,237] However, detailed improving mechanisms are not known yet.

A significant drawback of the Fenton's test is the difficulty in evaluating its accelerating factor, *i.e.*, correlating the test results with the durability of membranes in PEMFC operation. The early statement[160] that PEMs showing degradation rates less than 0.02 after 8 h (Table 8) may be possible candidates for 3,000 h or more of H_2/air PEMFC (at 80 °C and near-ambient pressures) was not valid, since some PEMs can function for hundreds to thousands of hours in a fuel cell while it has been shown that similar membranes become brittle with partial loss of their IEC after a few hours in Fenton's reagent of 3% H_2O_2/2 ppm Fe at 68 °C. On the other hand, Nafion 112, which has a projected lifetime of 26,000 h at 80 °C and 50 kPa by Fenton's test, usually showed much shorter life in fuel cell operation. This rather poor correlation has been rationalized with the following explanations: First, the PEM degradation in fuel cells is a result of a complex combination of different degradation processes which were strongly influenced by membrane, fabrication, and operating conditions, and thus, the peroxide/radical degradation of Fenton's test cannot be offered as the only measure for membrane lifetime prediction. Second, the lifetime prediction of PEMs using excessive peroxide content in an accelerated Fenton's test is unrealistically high in normal fuel cell operating conditions. Third, the concentration of $H_2O_2^+$ in the MEAs partly depends on the gas permeability of the membranes; the gas permeation of most hydrocarbon based membranes is much lower than that of Nafion. Fourth, direct lifetime comparison across the different membrane families is almost impossible when different fuel cell operating conditions are applied. It is unclear what order of reaction in peroxide to use for Fenton's test as concentration decreases. In general, Fenton's test seems to be a good accelerated test for judging chemical degradation of PFSAs, but it is an insufficient gauge for hydrocarbon membranes and cannot account for nonchemical degradation routes. As a single test, it, at best, provides an upper bound lifetime for PFSAs. For hydrocarbon membranes, insufficient understanding is presently available to address the mechanisms of chemical failure in PEM membranes.

3.3.2. Hydrolytic Degradation

Peroxide/radical attack has been the primary chemical stability concern for fuel cell membranes (due in large part to the relatively good stability of investigated materials to other routes of chemical attack). In fact, membranes that have not shown good hydrolytic stability (or oxidative stability in the absence of peroxide/radicals), by and large, have not received significant attention by the research community. An important exception to this are sulfonated polyimides (SPIs), which have shown a high sensitivity to hydrolysis but have still received considerable research interest due to a combination of factors (good performance at short times, good mechanical properties, the effective use of similar materials in phosphoric acid based cells, *etc.*).

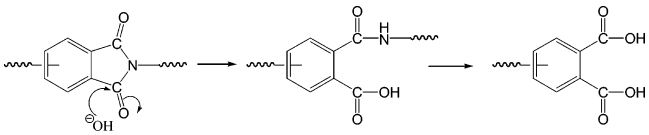

Figure 13. Hydrolytic reaction of the imide rings resulting in chain scission.

In chemical studies of hydrolytic degradation, the eluted product does not contain nonsulfonated diamine moieties, suggesting that hydrolysis took place mainly on the imide bonds neighboring sulfonated diamine residues but hardly on the bonds neighboring nonsulfonated ones.[238] Consequently, the hydrolytic stability increased, reducing the IEC in same family of SPIs. These results are consistent with non-sulfonated polyimides that show good hydrolytic stability, suggesting that the presence of acid sites is critical for hydrolytic degradation.

Genies *et al*. proposed a two-step hydrolysis mechanism based on data obtained using FT-IR and NMR techniques (Figure 13).[239] In the first step, one carbonyl group of SPIs is attacked, leading to the formation of amic acid structure. This partial hydrolysis leads to an increase of polymer chain flexibility without any decrease of the molecular weight. Following this partial hydrolysis, the second carbonyl group can also be attacked by water molecules, leading to the formation of amine and diacid terminal groups. This complete hydrolysis results in chain scission and the loss of the mechanical properties.

Hydrolytic stability strongly depends on SPI structures. While phthalic (five-membered rings) SPIs are mechanically stable polymers, sulfonation of the phthalic polyimides results in the phthalic ring becoming highly susceptible to hydrolysis. This leads to short fuel cell lifetimes of sulfonated phthalic SPIs. Naphthalenic (six-membered ring) SPIs have shown improved hydrolytic stability.[232] NMR spectroscopy using model compounds has shown that sulfonic acids containing phthalic imide aged at 80 °C lose all signs of the carbon peaks associated with the imide ring, while no structural changes of the sulfonic acid containing naphthalenic imide were observed up to 120 h.[239] Genies *et al*. synthesized naphthalenic (six-membered ring) polyimides using 4,4′-diamino-2,3′-biphenyl disulfonic acid (BDA) and 1,4,5,8-tetracarboxylic dianhydride (NDA).[239] The fuel cell life using the naphthalenic polyimides (IEC = ∼1.3 mequiv/g) was in the range of 1,200−3,000 h at 60 °C depending on flexibility in the hydrophobic part of the polymer.[177,240]

Another structural factor for the hydrolytic stability is the flexibility of the polymer. Einsla *et al*. demonstrated that copolyimide membranes utilizing a flexibile backbone structure displayed better hydrolytic stability. For example, by simply changing the sulfonated diamine from the rigid BDA to the more flexible 4,4′-diaminodiphenylether-2,2′-disulfonic acid (ODADS), the hydrolytic stability greatly improved.[241,242]

The hydrolytic stability could further increase by increasing the basicity of the diamines, since electron-donating groups decrease the electrophilicity of the imide ring, making it less susceptible to hydrolytic attack. The research group of Okamoto compared the hydrolytic stability of polyimides using a series of SPIs having basic diamines. The SPIs having 9,9′-bis(4-aminophenyl)fluorine-2,7-disulfonic acid (BAPFDS) showed higher stability than the SPI having ODADS.[243] The SPIs bearing a pendant sulfonic acid group such as 2,2′-bis(3-sulfopropoxy)benzidine (2,2′-BSPB) or 3,3′-bis(3-sul-

fopropoxy)benzidine (3,3′-BSPB) displayed much better water stability, probably due to the higher basicity of the diamine moieties attributed to the electron-donating ability of the propoxy groups.[244,245] Watanabe's group also suggested that SPIs having long aliphatic side chains have improved hydrolytic stability. Besides the electron density effect, they suggested that steric separation from the hydrophilic acidic groups could reduce the chance of water molecules attacking the imide ring.[246,247] Using SPIs containing aliphatic groups both in the main chain and in the side chains (IEC = 1.8 mequiv/g), a 5,000 h life under H_2/air fuel cell conditions was obtained.[247] The ^{1}H NMR analyses showed that the tested SPIs had only a minor change in the IEC (from 1.87 to 1.76 mequiv/g) after the testing. These lifetimes are acceptable for many applications and show the importance within the SPI family of specific chemistry on lifetime and susceptibility to hydrolysis. Finally, the hydrolytic stability of imide block copolymers was greatly increased,[129] possibly because of the nanophase morphology.

3.3.3. Efforts to Improve Chemical Properties

Membrane manufacturers have developed PFSA membranes or MEAs with improved chemical and thermal stability as well as improved water management at high temperatures. Curtin *et al*. reduced the number of H-remaining end groups by treating Nafion polymer with fluorine gas, and they improved the chemical stability against the radicals as mentioned previously.[166] Endoh *et al*. have developed a PFSA based membrane composite (NPL), which has shown good durability under high temperature and low humidity conditions.[215] The NPL membrane showed excellent stability over 1,000 h in an OCV test at 120 °C and 18% RH. The FER was about 2×10^{-8} g cm^2 h^{-1}, which was less than 1% of the FER in an OCV test using their standard MEA. They also demonstrated continuous operation using an NPL based MEA for more than 4,000 h at 120 °C, 200 kPa, 0.2 A cm^{-2}, and 50% RH.

For PEMs containing styrene sulfonic acid, the motive of backbone fluorination was no doubt to improve hydroperoxide stability. As mentioned above, sulfonated polytrifluorostyrene based BAM3G showed improved chemical stability compared to nonfluorinated aliphatic analogues. The evaluation of commercial radiation grafted membranes also indicated that a trifluorostyrene grafted ETFE based membrane (RAYMION, CEC, Japan) showed excellent stability while a styrene sulfonic acid grafted PTFE membrane (PERMION) showed rapid degradation due to the poor oxidative stability of the styrene group.[248]

The chemical stability of sulfonated polyarylene ether membranes is strongly dependent on the location of the sulfonic acid. Xing *et al*. investigated the radical stability of sulfonated polysulfones. The weight losses of sulfonated polysulfone membranes in the H_2O_2 solution at 60 °C showed that the sulfonated group attached to the meta-sulfone position had the best stability (8.5% weight loss) compared with the sulfonated group attached to the ortho-sulfone (23% weight loss) and ortho-ether positions (40% weight loss).[249] Sulfonated polyarylene ether membranes having a sulfonic acid group attached to the meta-sulfone position can be synthesized via direct copolymerization of sulfonated monomers.[163,250,251]

Another approach to improve the durability of MEAs is to introduce an additional layer for H_2O_2 decomposition or radical trap.[252] It has been reported that the durability of PEMs was improved by placing a catalyst layer based on Pt, Pd, Ir, *etc*. inside the membrane between the anode and the cathode. Tsurumaki developed radical-trap layers, which are based on rare earth metal oxides, on both sides of the membrane, and they demonstrated that the durability of the MEA in OCV tests was improved by 1 order of magnitude compared with that of their standard MEA.[253]

Chemical degradation of PEMs also could be mitigated by reducing reactant crossover. A few researchers have attempted to reduce reactant crossover by introducing cross-linking,[254] increasing crystallinity,[255] and increasing membrane thickness.[256] However, in all cases, there were trade-offs in that membrane resistance increased, which adversely impacted fuel cell performance.

3.4. Physical Degradation

3.4.1. Membrane Creep

Chemical degradation of PEMs has received considerable attention, but physical factors leading to degradation are also important. During the normal operation of a fuel cell, the MEA is put under compressive force between the bipolar plates. Under this constant compressive stress, polymer electrolyte membranes undergo time-dependent deformation (*i.e.*, creep). Polymer creep can cause permanent membrane thinning and eventually failure (pinhole formation, for example) and can be an important factor when compounded by chemical or other physical degradation routes.

Stucki *et al*. observed substantial thinning of the Nafion 117 membrane after 15,000 h of continuous 80 °C operation and suggested that the membrane dissolution process was triggered and/or enhanced by local stress on the membrane.[164] Yu *et al*. also observed membrane thinning at the H_2 inlet region followed by membrane pinholes and reactant gas crossover after a 2,520 h life test.[169] He speculated that the inadequate water content due to low humidification of the feed stream accelerated the physical degradation of the membrane. Membrane thinning may occur at a stress concentrated region to a greater degree. Borup *et al*. observed that the membrane thickness compressed at 80 °C between two flow field plates was approximately 46 μm on the flow field groove, which was about 16% thinner than that on the flow field land, probably due to elongation of the membrane in the open flow field area.[257]

The creep response of an extruded Nafion 115 membrane was reported by Satterfield *et al*.[258] In their experiments, Nafion put under tension stretched rapidly over the first several minutes and then slowed significantly. The creep rate, defined as the slope of the strain−log(time) response at times greater than 100 min, normalized by the applied stress, increased with temperature. Samples with higher water contents crept faster initially, but the rate of creep slowed at longer times, while the dry samples crept less initially but continued to creep more at longer times. Although these *ex situ* experiments are only offered in the realm of speculation, the results are generally consistent with observations regarding membrane degradation. Under normal fuel cell operating conditions (*ca.* operating temperature is ≤80 °C and hydrated conditions), Nafion creep occurs at a slow rate, so catastrophic failure can take thousands of hours until the mechanical properties yield to the cell compressive forces. On the other hand, as the α relaxation temperature (which depends on both temperature and RH) is approached, mechanical creep can proceed in a much shorter time period

Table 11. Thermal Transition Temperatures of Various Polymer Electrolyte Membranes for Fuel Cells

polymer electrolyte	thermal transition temp (°C) lower	thermal transition temp (°C) higher	melting temp (°C)	ref
Nafion	−100 to 20	100−135	230 (115)	259, 642
sulfonated polystyrene	110	110−180		267, 269, 270
sulfonated poly SEBS[a]	−55	80−99		268, 271
polystyrene PVDF block copolymer	−36 to −43	120−166		643
polystyrene grafted PTFE		116−122	325	644
polystyrene grafted FEP		144	265	272
polystyrene grafted PVDF	−30	90	160	645
sulfonated polysulfone[b]	232−282	303−3		250
sulfonated PEEK	175−200			646, 647

[a] Third temperature transition appeared at 114−175 °C, which is not well understood. [b] Higher transition temperature was observed only at IEC > 1.7 mequiv/g.

(*e.g.* failure in hundreds of hours or less under hot/dry conditions). As explained below, the transition temperatures typically decrease with increased hydration. This implies that hot/wet would be worse than hot/dry.

Kundu *et al.* compared the mechanical properties of the Nafion membrane before and after 80 °C H_2/air fuel cell life tests (72 h) and found that both the Young's modulus and yield strength of aged sample decreased by about 15% when compared with a fresh sample.[259] The reduced Young's modulus and yield strength make the membrane more susceptible to permanent deformation and eventual failure in a fuel cell during long-term operation. This combination of reduced physical properties in aged samples and thinning of membranes can result in a self-accelerated process, in which the thinnest membrane cross sections produce the highest gas crossover rates.

The creep behavior of hydrocarbon based membranes has also been investigated. Blackwell *et al.* reported the mechanical creep and recovery behavior of sulfonated SEBS block copolymers.[260] They found that low degrees of sulfonation (<6%) improved creep resistance due to hydrogen-bonding interactions between SO_3H groups and/or morphological effects. At sulfonation levels, the percent strain over time increased due to the formation of a continuous EB phase or residual water bound to the sulfonic acid group that plasticized the sPS domains.

Creep of sulfonated polyarylenes (or other heterocyclic copolymers) seems to take place much more slowly compared to that of other polymers during fuel cell operation.[261] Aged sulfonated polyarylenes or heterocyclic membranes after fuel cell life testing have shown almost no change in membrane thickness, while similar results using Nafion have shown significant thinning.[169,174,185,262] In fact, these materials have even demonstrated longer lifetimes under high-temperature (>100 °C) testing (see Table 9).[184,185] The diminished role of creep, as concerns failure in sulfonated polyarylenes, is probably due to the fact that little creep takes place at well below the relaxation transition temperature and these materials have extremely high relaxation temperatures. The rate of creep increases as the temperature is raised and goes through a maximum near the relaxation transition point. Nafion has two relaxation transitions, labeled α and β in descending order of temperature over a temperature range of −50 to 150 °C.[263] The α relaxation appears at around 100 °C and has a higher intensity. The β relaxation appears over a wide temperature range (−100 to 20 °C) depending on hydration. Although the accurate assignments of the thermal transitions and mechanical relaxations in Nafion are critical to the fundamental understanding of membrane creep behavior, the molecular/morphological origins of the relaxation transition are not clear.

Eisenberg and co-workers initially suggested that α relaxations were attributed to the glass transition temperature of the fluorocarbon matrix while β relaxations were attributed to a relaxation of the ionic domains.[263] Later, they reassigned α and β relaxation as a glass transition temperature of ionic domains and the fluorocarbon matrix, respectively.[264] Recently, Page *et al.* suggested that α relaxation was the onset of long-range (ionic) mobility of both the main and side chains via a thermally activated destabilization of the electrostatic network, while the β relaxation represents thermally activated main-chain motions that are facilitated through side-chain mobility (genuine glass transition temperature of Nafion).[265,266]

PEMs containing styrene derivatives generally have two thermal relaxation temperatures. The thermal transition at lower temperature reflects the glass transition of the non-sulfonated polymer matrix while the thermal transition at higher temperature is assigned for the glass transition of ionic domains where strong intermolecular ionic interactions between sulfonated polymer segments exist. The glass transition of ionic clusters, however, is often missing at low degrees of sulfonation due to the random nature of sulfonation or overlap with the matrix glass transition. Lightly sulfonated polystyrene has shown two thermal relaxation temperatures, consisting of the ion-rich domains (110−180 °C) and the polystyrene matrix (110 °C).[267−270] Thermal transition of sulfonated styrene-ethylene/butylene-styrene membranes showed a glass transition of the ethylene/butylene matrix near −55 °C and the glass transition of the polystyrene block near 90 °C. The glass transition temperature of the polystyrene block increased with degree of sulfonation.[271] FEP (or PTFE) grafted polystyrene sulfonic acid systems showed one glass transition temperature at 116−144 °C, probably due to overlap of the glass transitions of the matrix and styrene sulfonic acid domains. Some grafted polystyrene sulfonic acids had crystalline structure.

Polyarylenes have much higher thermal transition temperatures, which depend on the degree of sulfonation. Wang *et al.* reported that direct copolymerized sulfonated poly(arylene ether sulfone) copolymers have glass transition temperatures greater than 200 °C. Polysulfone copolymers having a higher degree sulfonation showed a secondary glass transition, probably from ionic domains above 300 °C, near their thermal degradation limits (∼350 °C).[250] Sulfonated poly ether ether ketone also showed a high glass transition temperature (190 °C). Because of the wholly aromatic rigid framework of the polymer backbone, the thermal transition

of polyarylenes was relatively small and sometimes undetected.[236,241] Table 11 summarizes the relaxation temperatures of several polymer electrolytes that have been investigated for use in fuel cells. The thermal transition temperature of polymer electrolytes has been found to decrease as membrane hydration increases. Kundu *et al*. reported that the onset of the α transition temperature in Nafion decreased from 78 to 67 °C when the membrane was hydrated.[259] Gupta *et al*. observed that the glass transition temperature of FEP grafted polystyrene sulfonic acid was decreased from 144 to 61 °C as sample drying temperature decreased and, thus, when the sample remained partially hydrated.[272] The glass transition temperature of polyarylene ethers also decreased upon hydration (*e.g*., 267 °C for dry versus 126 °C for the same sample liquid equilibrated),[273] which was attributed to plasticization by strongly bound water.

3.4.2. Microcrack Fracture

Another common PEM failure mechanism found in long-term fuel cell operation has been microcrack (craze) fracture. Microcrack fracture has usually been observed in local stress concentrated regions, such as the edge of the flow channel, where the bipolar plate land and groove meet.[259] In the edge of the flow channel, the polymer electrolyte may stretch by the pinching action of the flow field lands, particularly when a pressure differential exists across the membrane. Another common place for crack propagation is the boundary region between the reaction and nonreaction zones of the membrane. Failure near the boundary region may come from peroxide radical chemical degradation by reactant gas reached through imperfect sealing of gaskets or the formation of a "hot spot".[172] Local stresses can also be developed from the misalignment of the gas diffusion layers and catalyst layers or by differential swelling between the reaction area and nonreaction area. Microcrack fracture resulting from these stresses has been observed under accelerated RH cycling tests as well as under normal operating conditions.

General Motors researchers reported that the gas crossover rate of several PFSA membranes abruptly increased in a relatively short time (few hundred hours) after RH cycling conditions.[199,274] These results were interpreted using a membrane stress model and suggested a failure mechanism in which small flaws in the membrane grew through crack propagation due to the RH cycling life tests.[185] In these tests, similarly reduced lifetimes were noted for both RH cycling and voltage cycling. However, a lower fluoride emission rate during RH cycling suggested decreased chemical degradation but increased physical degradation, most likely due to the mechanical stress from membrane swelling/dehydration. Huang *et al*. tested the mechanical properties of Nafion under RH cycling and observed microcracks in the direction of applied tensile stress after RH cycles.[159]

Membrane failure through microcrack fracture was also observed in glassy ionomers such as sulfonated polystyrene or polyarylenes. Bellinger *et al*. investigated the fatigue properties of sulfonated polystyrene ionomers.[275] They found that the craze stability decreased with increasing ion content up to *ca*. 5 mol % and then increased after 5 mol %. The fractured surface showed a series of discontinuous crack growth bands representing crack propagation through essentially a single craze that successively develops from each crack tip position and a rough region representing the later stages of catastrophic crack propagation after a tensile fatigue test.[276] Reyna-Valencia *et al*. observed deformation of SPEEK under tensile stress and concluded that the failure mode was crazing characterized by banding perpendicular to the tensile axis and fibrillation in the plastic necking edges.[277]

Microcrack failure of sulfonated polyarylenes is considered as a predominant failure mechanism for these materials. Steck *et al*. reported that the longevity of the nonfluorinated polymers bearing differing levels of sulfonic acid functionality was limited to approximately 500 h because of the increased brittleness under normal fuel cell operating conditions.[167] This result was consistent with other data that reported a much shorter lifetime for the sulfonated poly(ether sulfone) (which contains isopropylidene links) than that expected of Nafion under RH cycling conditions (see Table 9).[185,199,274]

Membrane tear toughness (or elongation at break) and dimensional stability have been related to the microcrack failure. Huang *et al*. demonstrated that strain to failure was well correlated with the number of RH cycles in aged samples, although the yield stress and yield strain remain largely unchanged.[159] Other researchers also pointed out that microcrack resistance was correlated well with tear toughness.[278,279] For Nafion, the tear toughness (or elongation at break) along the machine direction is less than that along the transverse direction while cast ionomers had isotropic tear properties. Membrane failure in MEAs run under accelerated conditions exhibited tears along the machine direction for extruded membranes regardless of orientation to the flow fields, while cast membranes with isotropic physical properties showed more random tears.[280] It has been observed that larger dimensional change accelerates the microcrack fracture.[159,199] For example, the density of the microcracks in Nafion at the 80−120% RH cycling conditions was higher than that at the 30−80% RH cycling conditions because the changes in water content in the Nafion membrane under 80−120% RH cycling are much greater than those under 30−80% RH cycling conditions.

The most common method to evaluate the crack resistance in PEMs is stress−strain curves, even though membrane tear tests are likely more relevant to actual failure mechanisms.[278,280] Since limited data with other methods (such as tear tests) exist, we discuss the stress−strain behavior of PEMs and draw general correlations to microcrack failure.

The tensile strength and modulus of Nafion decrease as temperature and hydration increase. The Dupont product data sheet for Nafion (1100 EW) reports that tensile strength and modulus decrease from 34 to 25 MPa and 114 to 64 MPa, respectively, when temperature is increased from 23 to 100 °C in liquid water equilibrated samples.[281] The humidity dependence of the modulus of Nafion is rather complex.[282] Two temperature regions have to be discerned. At temperatures between room temperature and 50 °C, the modulus of Nafion decreases with increasing humidity. At temperatures between 50 and 100 °C, the modulus at 0% RH can be lower than that of hydrated Nafion. That is, the maximum value of the modulus at a given temperature is no longer at the dry state but is shifted to higher humidity with increasing temperature. Bauer *et al*. compare the storage modulus of Nafion at 75 °C and observed 145 and 240 MPa at 0 and 2% RH, respectively.[283] The higher modulus at 2% RH is probably due to the morphology stabilization of ionic domains with water molecules. The stabilization of ionic domains with water molecules assumed that water forms hydrogen bridge bonds and oligohydrates which act as cross-

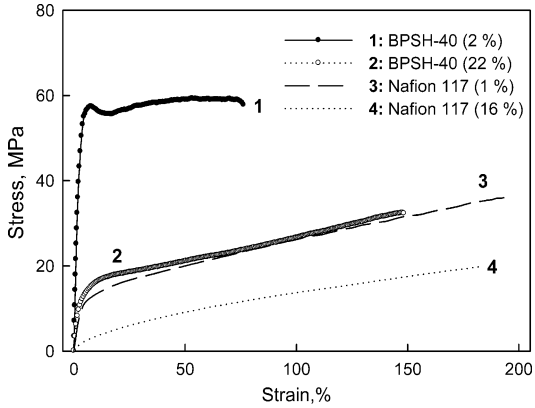

Figure 14. Stress−strain curves of sulfonated poly(arylene ether sulfone) (BPSH) and Nafion 117 at dry and humidified conditions; the numbers in parentheses represent the weight basis water content. Reprinted with permission from ref 286. Copyright 2005 Wiley-VCH Verlag GmbH & Co.

linkers linking the sulfonic acid groups and preventing them from ionic cluster disintegration. This behavior has also been observed in sorption isotherms of Nafion at elevated temperature.[284,285] Elongation at break of Nafion is relatively invariant with temperature, hydration, and strain rate. Typical values of elongation at break are 200−350%.

The dependence of mechanical properties on membrane temperature and hydration may have important implications in the long-term stability of fuel cells. Under the normal fuel cell operating temperature (≤80 °C), catastrophic failure can be delayed for thousands of hours, although the deformation of Nafion occurs in a relatively shorter time. On the other hand, as operating temperature increases, membrane failure can occur much faster due to the decreased mechanical properties even under dry conditions. Under wet conditions, the situation is even worse, since membrane creep increases.

Sulfonated SEBS copolymers have shown similar trends in mechanical behavior when compared to Nafion. Weiss *et al*. reported that sulfonated SEBS copolymers have improved mechanical properties compared to unsulfonated SEBS due to the restricted molecular mobility of the polystyrene phase due to electrostatic interactions.[268] Tensile strength, modulus, and elongation at break decreased with temperature, particularly above the α transition of the PS-rich domains. For example, the tensile strength of sulfonated SEBS (11.9% sulfonation) decreased from 27.6 to 2.62 MPa, and elongation at break decreased from 690 to 300% when temperature increased from 23 to 100 °C. Upon hydration, a slight decrease of tensile stress and elongation at break (∼20%) was observed.

Sulfonated polyarylenes (and heterocyclics) have much different mechanical behavior. These membranes exhibit nonlinear stress−strain behavior starting at extremely small strains, and conspicuous yielding and necking behavior takes place during the uniaxial loading, resembling characteristics of thermoplastic polymers under cold draw.[261] Compared to elastomeric ionomers (such as Nafion), they have relatively higher tensile strength and modulus and decreased elongation at break in both dry and wet states. Figure 14 shows a comparative example of stress−strain curves of Nafion and sulfonated polyarylenes.[286] The better mechanical strength and modulus of these thermoplastic ionomers can be an advantage under the compressive forces of operating cells. However, the mechanical properties of polyarylenes change dramatically as a function of hydration and temperature, and increased water uptake of these materials often leads to increased stress during RH cycling. Reyna-Valencia *et al*. observed that the modulus of sulfonated poly(ether ether ketone) in liquid water decreased (∼70%), compared to the case at 30% RH and at 23 °C.[277] An increase of 17 °C in temperature caused an additional drop in modulus in such a way that membranes lost 75−94% of their original stiffness depending on their degree of sulfonation. The dramatic change of the mechanical properties of sulfonated polyarylenes and dimensional changes due to water uptake upon hydration and temperature may promote crack propagation. These are likely primary reasons that membrane durability has been shown to increase with reinforcement and polyarylenes have shown relatively poor durability under RH cycling conditions (see Table 9).

3.4.3. Structural/Morphological Changes

Structural/morphological changes of PEMs may also play a role in membrane performance in fuel cells; however, due to their (often) indirect effects, these changes are not particularly easy to correlate with degradation. Still, due to their likely impact on durability, we have chosen to include morphological effects in our discussion.

Morphological changes (under different pretreatment conditions) have been inferred from changes of physical properties, and they have been measured directly by techniques such as AFM, TEM, SEM, and scattering.[265,266] These studies have focused on a number of different parameters, including thermal history, the presence of water during processing steps, the effects of ion exchange with acidic sites (different salt forms), cast versus extruded membranes, and the addition of additives.[285,287−291] These studies have shown the importance of the history of the sample in terms of its properties and (potentially) durability.

A number of studies have focused on Nafion. Studies of hydration of Nafion have shown that preboiled membranes have significantly increased water uptake, water/gas transport,[292−294] and conductivity compared to membranes dried at elevated temperature and rehydrated at room temperature. These changes in properties have been attributed to the formation and break-up of hydrated ion clusters in the membranes due to hydrothermal processes. Morphological changes in Nafion after heat treatment were first reported by Yeo and Yeager, who classified the membrane in three different forms.[295] Membranes without heat treatment were referred to as the "E-form" (expanded form), and membranes which were heat treated at 80 and 105 °C were the "N-form" (normal form) and "S-form" (shrunken form), respectively. Zawodzinski *et al*. reported that Nafion after drying at elevated temperature had decreased water uptake compared to that dried at lower temperatures.[285,296] They attributed the decreased water uptake under higher temperature drying conditions to shrunken ionic clusters. Hinatsu *et al*. reported that the water uptake of perfluorinated copolymers after immersing the membrane in water between 25 and 140 °C produced different water uptakes.[297] The water uptake of a perfluorinated membrane (N-form) increased approximately linearly with temperature up to 100 or 110 °C and then abruptly increased above this temperature. Tricoli *et al*. reported reduced conductivity (∼30%) of a Nafion membrane treated in water at 80 °C after storing the membrane at 20 °C for 2 months.[298] Sone *et al*. reported that the proton

conductivity of Nafion decreased as heat-treatment temperature increased due to structural changes.[299] Finally, researchers from GM have suggested that freeze−thaw cycling of humidified samples might also lead to morphological changes and increased conductivity.[126] Due to significant changes in water uptake and conductivity of Nafion depending on processing, a common method to prevent or minimize (significant) morphological changes during operation is to treat (acidify) Nafion membranes (or MEAs) at temperatures higher than fuel cell operation.

Beyond hydration and conductivity, other properties of Nafion have also been related to the history of the membrane. Wei *et al*. observed that a structural relaxation of dehydrated membranes occurred at 79 and 116 °C by measuring shear response forces using shear modulation force microscopy.[300] Interestingly, the two transition temperatures they found were roughly identical to the drying temperatures used to classify Nafion membranes originally suggested by Yeo and Yeager. These researchers found that the extended form morphology was recoverable under wet, elevated temperature (*e.g*., 100 °C) conditions. Cheng *et al*. reported increased crystallinity of Nafion after a 200 h DMFC life test.[301]

Pretreatment conditions have also been reported to impact the physical properties of sulfonated polyarylenes through morphological effects. Alberti *et al*. investigated the effect of pretreatment of sPEEK on proton conductivity.[302] The conductivity of a sPEEK membrane having an IEC of 1.6 mequiv/g treated in boiling water for 4 h prior to measurement showed a slight temperature dependence from 0.03 to 0.07 S/cm over the temperature range 25−150 °C, while the conductivity of a nontreated membrane changed by more than a factor of 10 over the same temperature range. Kim *et al*. observed an increased water uptake and proton conductivity for sulfonated poly(arylene ether sulfone) after elevated temperature water treatment.[291,303] They also found a temperature denoted as the hydrogel temperature where an abrupt increase of water uptake, mechanical disintegration, and conductivity reduction occurred. The hydrogel temperature of the membranes ranged from 60 to 140 °C, as the degree of sulfonation was varied from 60 to 30%.

In an operating cell, effects of constraint pressure may further impact morphological changes. Ma *et al*. found heavy conductivity anisotropy of Nafion over the in-plane and thickness direction after hot-pressing at high temperature, 150 °C, and pressure, 600 kgf/cm^2. Preliminary SAXS measurements indicated that the impeded interaggregate transport of the H^+ among the deformed ion clusters along the hot-press direction might be responsible for the anisotropic conductivity.[304] Casciola *et al*. observed an irreversible conductivity decay of Nafion 117 under controlled applied pressure on the electrodes. In their experiments, they observed conductivity decay when the membrane was forced to swell anisotropically along the plane parallel to the membrane surface, which they attributed to an anisotropic deformation of ionic pathways.[305]

While morphological changes have not been conclusively linked to loss of fuel cell performance, it is clear that morphological changes are occurring under operation, and factors such as processing history can be important in other physical and/or chemical degradation pathways.

3.4.4. Efforts To Improve Physical Properties

The thermal and mechanical properties of PFSAs are becoming more recognized as critical properties of PEMs. One approach to perfluorinated ionomers that has had (perhaps indirect) an effect on thermal and mechanical properties has been the replacement of a long side chain or Nafion with a short side chain linear perfluorosulfonic acid group. PFSAs with short side chains were first developed in the mid-1980s by Dow Chemical Corporation (so-called Dow membrane or Dow Experimental membrane). This ionomer is similar in structure to Nafion but has a shorter pendant side chain (and no branch points) which carries the functional ion-transporting group. Tant *et al*. showed that this short chain ionomer has a higher α relaxation transition, at about 165 °C, and limited dependence on EW, as measured by dynamic mechanical analysis.[306] Another important characteristic of the Dow membrane is its crystalline structure. Tant *et al*. and later Moore *et al*. reported that even a low equimolecular weight Dow membrane (909 EW) had crystalline structure, with its melting endotherm at around 150−180 °C, which may serve to improve the mechanical properties.[306,307] Other desirable properties for fuel cell applications, such as lower water−alcohol dissolution rate, gas permeability, and electro-osmotic drag, were also recognized.[307−309] Although the Dow membrane was never commercialized, other newer PFSA membranes containing short side chains are again drawing interest.[279,310] The short side chain membrane from the 3M company showed a higher α relaxation transition temperature (125 °C compared to 100 °C for Nafion) and better mechanical properties (*i.e*., ∼7% higher modulus and 9% higher break stress at ambient conditions) over a wide temperature range.[311] The relative lifetime of this membrane was about 4 times longer than that of recast Nafion at 90 °C.

The mechanical properties of PEMs can also be improved by using a reinforcing material. W. L. Gore and others have used porous polytetrafluoroethylene (PTFE) membranes or PTFE fibrils to increase the durability of Nafion in both the hydrated and dehydrated states.[312−317] Since the PTFE reinforced Nafion membranes usually have lower conductivity, relatively thin membranes have been used. Cleghorn *et al*. reported a 26,300 h single cell life test with a commercial PTFE reinforced Gore membrane.[186] The cell showed a low performance degradation rate of 4−6 mV/h at 0.8 A/cm^2 under continuous H_2/air operating conditions. Carbon nanotubes also have been recently considered for use as a reinforcing agent.[318] Particulated fillers such as metal oxide/phosphate, or silica, are also used as a reinforcing agent.[258,319−325] These reinforcements have been reported to improve membrane creep and morphological stability at elevated temperature. Adiemian *et al*. performed a durability test for silicon oxide incorporated Nafion at 130 °C. The fuel cell performance with a silicon oxide/Nafion membrane remained constant while the cell performance with unmodified Nafion fell dramatically within an hour.[326] For highly water swollen hydrocarbon based PEMs, blending with a mechanically stable framework, such as poly(vinylidene fluoride) (PVdF) or other polymers having a base group,[327,328] has also been attempted, although durability under fuel cell conditions has yet to be demonstrated.

In order to prevent microcrack propagation at the side edge of the reaction area, the peripheral region of an MEA was protected by a gasket seal,[329−331] an adhesively bonded layer,[332]or a plastic spacer.[333] These protective layers have provided increased crack resistance around the edge of the MEA active area.

4. Electrocatalyst Stability

The worldwide effort to develop fuel cells for vehicular and stationary power applications has been enabled, in no small part, by the optimization of the microstructure of the catalyst layer, which enabled drastic reductions in the amount of platinum that is required to construct a practical fuel cell. In order for the fuel cell to retain the advantages of this optimized structure, it must be resistant to changes in morphology and surface properties. In truth, however, there can be significant changes to catalyst structure and properties with operation, and electrocatalyst stability may be a determining factor in the useful lifetime of polymer membrane fuel cell (PMFC) systems. Electrode materials consist of carbon-supported nanometer sized Pt and/or Pt alloy catalysts for both anodes and cathodes. The nanometer length scale particles provide theoretical surface areas of over 100 m^2/g and fuel cell active areas of 25−40 m^2/g.

Polymer electrolye membrane fuel cell (PEMFC) performance loss under steady-state and cycling conditions has been attributed in part to a loss of electrochemically active surface area (ECSA) of the high-surface-area carbon-supported platinum electrocatalyst.[3,142,334,335] There is growing evidence that platinum dissolution plays a major role in the ECSA loss, especially of the cathode catalyst, where high potentials are encountered.[143,224,336] This dissolved platinum can then either deposit on existing platinum particles to form larger particles[224,335] or diffuse into electrochemically inaccessible portions of the membrane-electrode assembly (*i.e.*, sites not fulfilling the requirements of gas, electron, and proton access).[224] It has been speculated that platinum dissolution occurs both as a result of potential cycling, caused by varying loads on the PEMFC stack, and under constant potential high voltage conditions typical of fuel cell stack "idling" conditions.[336] The extent of dissolution is expected to be governed by a complex interplay between the electrochemical dissolution of metallic platinum, the formation of a platinum oxide, and the chemical dissolution of this oxide.[337]

4.1. Chemical State of Platinum under PEMFC Cathode Conditions

4.1.1. Thermodynamics

Potential−pH diagrams, also termed Pourbaix diagrams, indicate the thermodynamically stable phase and oxidation state of a metal as a function of electrolyte pH and electrode potential.[338] Figure 15 shows the potential−pH diagram for the platinum−water system at 25 °C as reported by B. J. Lee[339] (thick lines) and M. Pourbaix[338] (thin lines). In this diagram, the equilibria denoted by each line are shown below, and unprimed numbers designate Pourbaix's diagram,[338] and primed numbers designate Lee's diagram.[339]

$Pt + H_2O = PtO + 2H^+ + 2e^-$	$E_0 = 0.980 - 0.591pH$	(1 and 1′)
$PtO + H_2O = PtO_2 + 2H^+ + 2e^-$	$E_0 = 1.045 - 0.0591pH$	(2 and 2′)
$PtO_2 + H_2O = PtO^{3+} + 2H^+ + 2e^-$	$E_0 = 2.000 - 0.0591pH$	(3)
$Pt^{2+} + H_2O = PtO + 2H^+$	$\log(Pt^{2+}) = -7.06 - 2pH$	(4)
$Pt = Pt^{2+} + 2e^-$	$E_0 = 1.188 + 0.0295 \log(Pt^{2+})$	(5)
$Pt = Pt^{2+} + 2e^-$	$E_0 = 0.963 + 0.0295 \log(Pt^{2+})$	(5′)
$Pt^{2+} + 2H_2O = PtO_2 + 4H^+ + 2e^-$	$E_0 = 0.837 - 0.1182pH - 0.0295 \log(Pt^{2+})$	(6)
$Pt^{2+} + 2H_2O = PtO_2 + 4H^+ + 2e^-$	$E_0 = 1.062 - 0.1182pH - 0.0295 \log(Pt^{2+})$	(6′)

One of the major differences between the diagrams derived by Pourbaix and Lee is that Lee did not account for Pt(VI), whereas Pourbaix did account for the formation of this higher oxidation state. Pourbaix and Lee estimated the formation free energy of Pt^{2+} using Latimer's equations as 229 and 185 kJ mol^{-1}, respectively.[338,339] This difference in free energy led to a larger Pt^{2+} region for the Lee-derived diagram. These differences illustrate the need for additional thermodynamic data, especially for the equilibrium between solid and liquid phases, to clarify the effect of potential on the equilibrium phases of Pt in water. Despite these differences, Pourbaix and Lee agree that PtO_2 is the stable equilibrium phase in acidic solution at the open circuit potential of a hydrogen−air PEMFC.

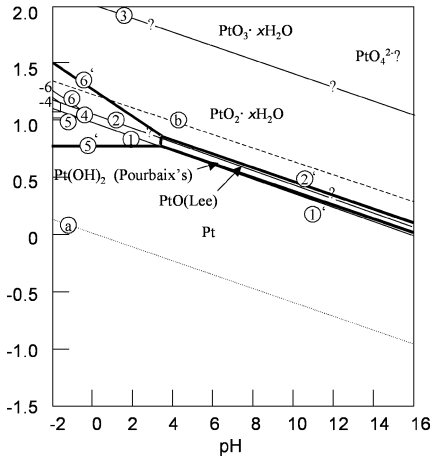

Figure 15. Regions of stability for platinum vs potential and pH.[338,339]

4.2. Spectroscopic Analysis of Pt in the Electrochemical Environment

4.2.1. Bulk Electrodes

Due to the difficulty of characterizing nanoparticles of platinum, the bulk of the literature on the electrochemical oxidation and reduction of platinum arises from studies of single crystal or polycrystalline bulk platinum using a variety of *in situ* and *ex situ* techniques. Electrochemical quartz crystal nanobalance and *in situ* X-ray studies have shown that oxidation proceeds via formation of a 0.5 Å monolayer of chemisorbed O in the 0.85−1.15 V (vs RHE) range.[139,340] In the 1.15−1.4 V potential range, e*x situ* Auger[139] and *in situ* X-ray reflectivity experiments[340] show evidence for the place exchange of O and Pt, further formation of PtO, and surface diffusion of PtO to energetically favorable sites. In addition, at >1.18 V, there is evidence for the formation of PtO_2 on Pt(111) and for the surface diffusion of PtO_2.[341] Sun *et al*. recently determined the composition of the anodically formed oxide film on bulk polycrystalline platinum using electrochemical impedance spectroscopy and X-ray photoelectron spectroscopy.[342] They concluded that the oxide film formed above 1.3 V consists of an inner PtO layer and an outer layer of PtO_2. They detected a single oxide layer at lower potentials. Based on their X-ray reflectivity data, Nagy and You concluded that reduction of oxide films formed at potentials >1.15 V roughens the Pt surface.[340]

4.2.2. Carbon-Supported Nanoparticles in Aqueous Electrolyte

Recent *in situ* X-ray absorption measurements of a carbon-supported (Vulcan XC 72) Pt nanoparticle catalyst (10 wt % Pt/C from E-Tek) in aqueous sulfuric acid or perchloric acid electrolyte have shown that OH or O, formed from the

electrochemical oxidation of Pt by water, adsorbs in different sites depending on the coverage and oxidation potential.[343] At low coverages, OH adsorbs on Pt sites at steps and edges of the 1.5−3 nm diameter Pt particles. At higher coverages, O begins to populate bridged Pt sites, and at even higher coverages, at potentials above 0.95 V in nonadsorbing perchloric acid electrolyte, O adsorbs into a subsurface site formed by the place exchange of O and Pt.

4.2.3. Carbon-Supported Platinum Nanoparticles in an MEA

As a result of the *in situ* aqueous electrolyte spectroscopic measurements of platinum summarized above, the signature voltammetric features of platinum in the 0.7−1.5 V region can be assigned to the formation and reduction of a multilayer, multivalent platinum oxide film. These same features that are observed in voltammetric scans of a carbon-supported platinum electrocatalyst in aqueous electrolyte are also observed in the voltammetry of the electrode layer in a PEMFC membrane−electrode assembly in the absence of gas-phase reactants (*i.e.*, when the anode or cathode chambers are purged with an inert gas).[344,345] The observation of increasing charge under the oxide reduction voltammetric peak in a study of a PEMFC cathode suggests that platinum is slowly oxidized at voltages relevant to fuel cell operation (*i.e.*, 0.85 and 0.95 V).[346] The surface oxygen can be formed with water as the only source of oxygen species; however, the presence of gas-phase oxygen accelerates the oxidation, with the charge equivalent of one monolayer of oxide forming after only 30 min at 0.85 V.[346] The rapid loss of PEMFC performance at high constant voltages, a current loss of one-half of its original value within 1 h, has been attributed to the blocking of platinum surface sites from participation in the oxygen reduction reaction by the formation of platinum oxide.[345] This loss, however, is completely recoverable with a short excursion of the cathode potential to 0.5 V or lower, consistent with reduction of the oxide layer formed at the higher cathode voltages.[345]

4.2.4. Pt Solubility—Equilibrium

A major factor in understanding the dissolution behavior of platinum is its solubility in aqueous electrolyte, which is governed by the chemical state of the platinum surface and of the platinum species in solution. The electrolyte components, atmosphere, solvent, pH, temperature, and potential are all major factors influencing solubility.[146,224,275,347−349,351] The solubility of bulk and powder Pt under oxidizing conditions in aqueous solutions of pH 4−10 has been determined with and without various natural ligands: Cl^-, HS^-, OH^-, NH_3, $S_2O_3^{2-}$, and $C_8H_5O_4^-$.[347,348] Wood experimentally determined the solubility of Pt at 25 °C in solutions of NaOH of variable ionic strength and found a solubility in the range of 0.014 to 0.362 mg/L.[350] The solubility was found to increase with the increase of pH in all the buffer solutions investigated, as shown in Figure 16, suggesting a basic dissolution mechanism. The nanoparticles of platinum were found to have a higher solubility than bulk platinum.[347] In the acidic region, solubility increased with the decrease of the pH, as indicated by the open circles in Figure 16. This behavior is attributed to the acidic dissolution mechanism.[351]

There have been limited studies of the effect of temperature on Pt solubility, despite its importance. The results of these studies are plotted in Figure 17 as the logarithm of Pt solubility vs inverse temperature. The solubility of Pt

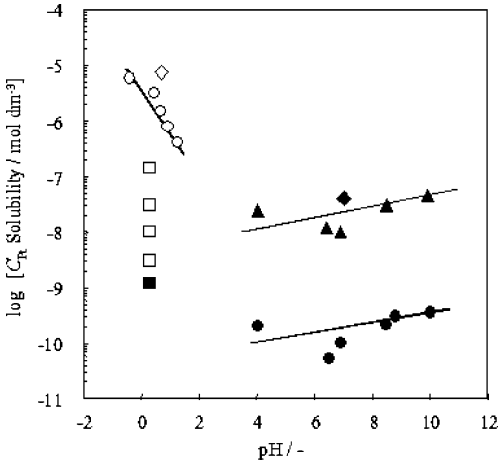

Figure 16. Logarithm of Pt solubility as a function of pH at room temperature. Open symbols, $E > 0.8$ V vs SHE; closed symbols, $E < 0.8$V vs SHE. Square, Pt/C in $HClO_4$;[146] closed circle, Pt wire in buffer solutions;[347] closed triangle, Pt powder in buffer solutions;[347] closed diamond, Pt foil in diluted water;[348] open diamond, Pt foil in 0.1 M HCl + HNO_3;[348] open circle, Pt powder in H_2SO_4.[356]

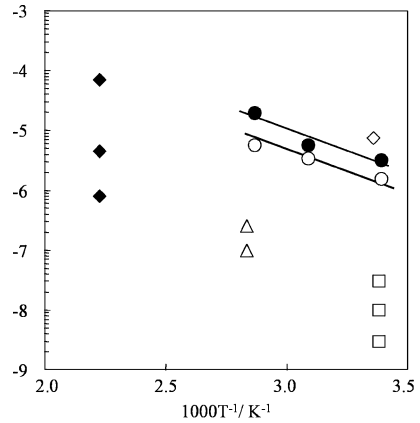

Figure 17. Logarithm of Pt solubility as a function of inverse temperature. Open square, Pt/C in $HClO_4$;[146] open triangle, in 0.5 M H_2SO_4;[224] open diamond, Pt foil in 0.1 M HCl + HNO_3;[348] closed diamond, Pt foil in 96% H_3PO_4;[349] open circle, Pt powder in 0.5 M H_2SO_4; closed circle,[356] Pt powder in 1 M H_2SO_4.[356]

increased with temperature following the Arrhenius relationship.[351] The increase of solubility with increasing temperature indicates that the dissolution reaction is endothermic.

The solubility of platinum, with relevance to the conditions of acidic fuel cells, has been measured for phosphoric, sulfuric, and perchloric acid electrolytes.[146,224,348,349] Figure 18 summarizes these results as the logarithm of Pt solubility vs potential. The solubility has been found to increase with the potential up to 1.1V vs SHE. The slope of this plot for the bulk platinum in H_3PO_4[349] and as determined by Pourbaix[338] indicates a two-electron dissolution reaction ($Pt = Pt^{2+} + 2e^-$).

However, more recent results for bulk and high-surface-area carbon-supported platinum in sulfuric and perchloric acid electrolytes showed slopes lower than expected for a two-electron process.[146,224] This suggests a dissolution mechanism involving dissolution of the oxide rather than Pt metal.

Recent density functional theory calculations suggest that a number of one-electron processes involving the electrochemical oxidation of oxides and oxyhydroxides are thermodynamically allowed.[146] The dissolved Pt species have not yet been definitively identified. Generally, a hydroxy or

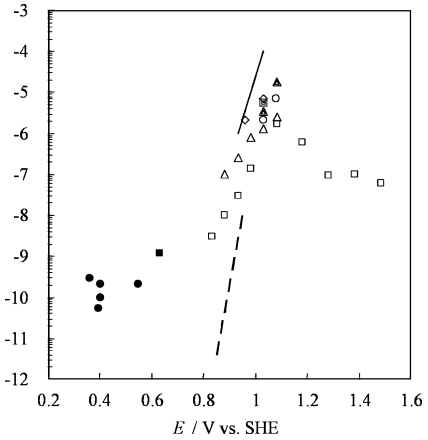

Figure 18. Logarithm of Pt solubility as a function of potential. Open square, Pt wire in 0.57 M $HClO_4$ at 23 °C;[146] open triangle, Pt/C in 0.5 M H_2SO_4 at 80 °C;[224] closed circle, Pt wire in buffer solutions;[347] open circle, Pt powder in 1 M H_2SO_4 at 22 °C;[356] open diamond, Pt powder in 1 M H_2SO_4 at 35 °C;[356] double triangle, Pt powder in 1 M H_2SO_4 at 51 °C;[356] double square, Pt powder in 1 M H_2SO_4 at 76 °C;[356] solid line, Pt foil in H_3PO_4 at 196 °C;[349] dashed line, Pourbaix.[338]

aquo complex of Pt^{2+} is considered as the dissolved species in an acidic medium as derived from the potential−pH diagrams.[146] Azaroul *et al*. suggested $PtOH^+$ is the dissolved species in aqueous solution of pH 4−10 at 25 °C and under oxidizing conditions.[347,352] Kim *et al*. determined higher valent platinum in sulfuric acid solution with the dithizone−benzene method, and a Pt(IV) complex was suggested as the dissolved species.[351]

4.3. Pt Dissolution under Nonequilibrium Conditions

4.3.1. Aqueous Electrolyte

The majority of information on the electrochemical dissolution of platinum arose from the desire to determine the cause of the evolution of the voltammetric signature of polycrystalline platinum electrodes with potential cycling (termed "electrochemical activation"). These studies included measurements of platinum dissolution during potential cycling,[353−357] square wave potential steps,[355,358−360] constant current,[353,361] and constant potential.[146,353] A ring-disk electrode study detected generation of soluble platinum species during potential cycling in sulfuric acid and perchloric acid.[354] During the cathodic-going scan, Pt(II) was detected at approximately 0.5 V and was correlated with reduction of the oxide film. Reducible species were also generated at potentials higher than 0.9 V but were not identified. Rand and Woods[357] detected both Pt(II) and Pt(IV) species in a sulfuric solution after potential cycling, and they confirmed that the charge difference between anodic and cathodic sweep corresponds with the amount of dissolved species if the upper limit of the potential cycling is chosen to avoid oxygen evolution. Ota *et al*.[361] investigated the corrosion rate of platinum in a potential range of oxygen evolution and found that in this region the corrosion rate is proportional to the oxygen evolution current. Kinoshita *et al*. measured the amount of platinum dissolved during potential cycling of a platinum sheet, high-surface-area platinum black, and carbon-supported platinum.[355] The critical upper potential limit for greatly enhanced Pt dissolution was found to be 1.0 V, in agreement with the earlier report of Rand and Woods.[357] Kinoshita *et al*.[355] also reported that the amount of platinum dissolved per cycle was independent of the upper potential limit at potentials > 1.2 V ($\approx$5 ng cm^{-2} $cycle^{-1}$). Potential cycling platinum dissolution rates calculated from data reported in the literature are summarized in Table 12. These studies show close agreement of dissolution rates per potential cycle with widely varying scan rates, indicating that the dissolution reaction is more dependent on the number of oxidation−reduction cycles rather than on the length of the cycle or time at oxidizing potentials. Potentiostatic dissolution rates of 1.4×10^{-14} and 1.7×10^{-14} g/cm^2·s were reported for 0.9 V for 10 wt % Pt/C and platinum wire, respectively, in perchloric acid electrolyte.[146]

Kinoshita *et al*.[355] examined the difference in the dissolution behavior of platinum black and carbon-supported platinum. Although they did not succeed in measuring the dissolution rates, a decrease of the surface area and an increase of the (111) face on the surface were measured. Such surface rearrangements were also observed using macroscopic single crystals.[145,359,360] An investigation to "optimize" the conditions of electrochemical dissolution of platinum in hydrochloric acid was also performed from the viewpoint of production of platinum salts.[353]

4.3.2. Phosphoric Acid Fuel Cells

Much of the speculation for the causes of platinum surface area loss is derived from the extensive literature on platinum surface area loss in phosphoric acid fuel cells (PAFCs).[362−366] These studies are relevant to the ECSA degradation observed in PEMFCs due to the similarity of electrode materials and structure; however, the platinum degradation in PAFCs is expected to be more severe due to the more corrosive conditions (*i.e.*, complexing electrolyte and higher temperatures). The platinum surface area loss in PAFCs has been attributed to dissolution of Pt at the cathode when operating at >0.8 V, redeposition of Pt to form larger particles via an electrochemical Ostwald-ripening mechanism, and loss of Pt into the electrolyte with migration toward the anode.[365] The cross-sectional distribution of platinum in a PAFC after operation showed that a large amount of platinum dissolved and migrated from the cathode into the electrolyte matrix.[363,364]

4.3.3. Polymer Electrolyte Fuel Cells

In recent years, several articles have been devoted to the study of platinum dissolution in actual PEMFC electrodes. *Ex situ* transmission electron microscopy (TEM) analysis of cathode catalyst layers after long-term steady-state and potential cycling operation has shown dramatic changes in platinum particle size and distribution.[224,225,335,367] The possible mechanisms for nanoparticle growth include local coalescence of agglomomerated particles, agglomeration of nonadjacent crystallites via Pt particle migration and subsequent ripening, and dissolution of the catalyst and subsequent reprecipitation of platinum. The particle growth rates and mechanisms may change as a function of electrode potential, cell voltage cycling conditions, current density, state of hydration of the membrane, and operating temperature. Ferreira *et al*.[224] classified coarsened platinum particles into two groups: spherical particles still in contact with the carbon support and nonspherical particles removed from the carbon support. The former results from electrochemical Ostwald ripening, and the latter results from deposition in the ionomer by dissolved hydrogen. Both processes require preceding dissolution of the platinum.

Table 12. Summary of Potential Cycling Platinum Dissolution Rates

dissolution rate ($g/cm^2 \cdot s$)	dissolution rate ($g/cm^2 \cdot cycle$)	electrode type	conditions	ref
7.5×10^{-11} (0.05−1.4 V)	4.5×10^{-9}	Pt sheet	0.05 to (1.2−1.4) V, 45 mV/s, 1 M H_2SO_4, RT	355
1.0×10^{-10}	5.5×10^{-9}	Pt wire	0.41 to 1.46 V, 40 mV/s, 1 M H_2SO_4, RT	357
3.8×10^{-11}	4.8×10^{-9}	Pt disk	0.4 to 1.4 V, 8.3 mV/s, 1 M H_2SO_4, RT	354
2.8×10^{-11}	3.3×10^{-9}	Pt disk	0.4 to 1.4 V, 8.3 mV/s, 0.1 M $HClO_4$, RT	354
1.5×10^{-7}	3.0×10^{-9}	Pt wire	0.5 to 1.5 V, 100 V/s, 1 M H_2SO_4, 40 °C	648

Guilminot *et al.*[337] reported detection of Pt^{z+} ions ($z = 2$, 4) in the membrane of a cycled MEA using ultraviolet spectroscopy; however, Pt^{z+} was also detected in the as-prepared MEA. Yasuda *et al.*[225,368,369] studied electrochemically cycled MEAs using TEM and cyclic voltammetry. The Yasuda papers presented strong evidence for platinum dissolution, diffusion of the dissolved platinum into the membrane, and reduction of the dissolved platinum as particles in the membrane near the membrane−cathode interface by dissolved hydrogen. However, neither group observed the dissolution phenomena directly, *e.g.*, the existence of particles with decreased diameter. Darling and Meyers developed mathematical models for dissolution and redeposition of platinum in PEMFCs.[143,144] They assumed that platinum dissolution is determined by potential, particle size, and coverage ratio by oxide. In their model, the oxide layer can protect the platinum from dissolution, but the kinetics of oxide formation are slow relative to the rate of dissolution, so rapid changes in potential can expose the bare platinum to corrosive potentials in the interim between the potential step and coverage of the surface with oxide. Changes of the ECSA, particle size distribution, and concentration of ionic species during potential holding or cycling were calculated. There is a growing body of literature suggesting that platinum dissolution is a major factor limiting the lifetime of polymer electrolyte fuel cells, especially under varying load conditions and at the high potentials of the cathode, though considerably more information is needed in order to fully characterize the mechanisms of oxide formation, platinum dissolution, and redeposition.

4.3.4. Alloy Effects

Platinum alloys have been used in both phosphoric acid (PAFC)[370] and PEM fuel cell systems[371] to improve the activity of the oxygen reduction reaction. UTC developed alloy catalysts for use in PAFC power plants in the 1970s and suggested in their search that, in phosphoric acid systems, the dissociation of the O−O bond was the rate-determining step. Consequently, they sought opportunities to change the spacing of Pt−Pt and thereby affect the cleavage of the O−O bond. As data from various alloys were analyzed, it was shown that the specific activity of the catalysts could be correlated with the platinum−platinum interatomic distance.[372] This analysis is shown in Figure 19.

Several platinum alloys on high-surface-area carbon in acid electrolytes show high degrees of crystallinity and enhancement of exchange current densities (~2−3×) relative to Pt/C.[47,49,50] It has been shown that the kinetics of the reaction correlate not only to Pt−Pt bond distance but also to Pt d-band vacancies in the alloy; in studies on PtCo alloys, activities were correlated to inhibition of adsorbed OH formation.[373] A structure−activity−stability study on PtCo showed ordered fct alloy phases formed at high annealing temperatures which were more stable in an electrochemical corrosive environment with double the specific activity

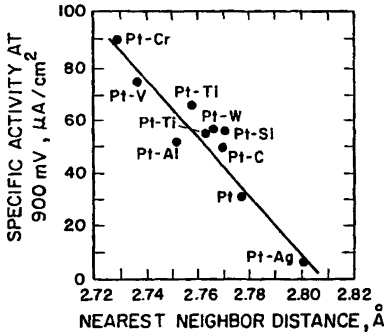

Figure 19. Correlation of specific activity to nearest-neighbor distance in platinum alloys. Reprinted with permission from ref 372. Copyright 1983 The Electrochemical Society.

compared to the conventional Pt/C catalysts.[374] Low annealing temperature produced fcc alloy phases of various stoichiometries which had about triple activities, but they were less stable.[374] Which of these effects is the primary driver of catalyst performance is still unknown. While fundamental studies of the oxygen reduction reaction continue,[52−54] the competing reaction pathways and considerable complexities of the oxide-covered alloy surfaces (not to mention the implications of ternary and quaternary alloys and beyond) require a considerable amount of experimental and theoretical effort to understand.

While alloys have been shown to enhance performance in some configurations, attention must be paid to the stability of the alloys, particularly in light of the fact that Pt−Ru catalysts, which have been used in direct methanol and reformate cells to enhance CO tolerance on the anode, have been revealed to be quite unstable under normal operation.[375] Generally, the metals which are co-alloyed with platinum would tend to be less stable as pure metals than platinum,[338] so one might naturally be concerned about introducing a less stable metal to a structure that has already been shown to degrade in the fuel cell environment.

Antolini *et al.* have written a review of the stability of Pt-alloy catalysts[376] and note discrepancies among various studies about the stability of alloys relative to platinum catalysts. They note that PtCr and PtCo tend to exhibit greater stability than PtV, PtNi, and PtFe, though there are still questions about whether the means of preparation of the catalyst matters. As previously discussed, changes in platinum crystallite morphology and carbon corrosion contribute strongly to the rates of degradation of PEM fuel cells under normal operating conditions.[4,57]

It has been shown that some platinum alloy catalysts, particularly those containing cobalt, show markedly improved stability to potential cycling relative to unalloyed platinum.[377] Yu *et al.* show significant improvements in catalyst stability with PtCo catalysts after a protocol of square-wave potential cycling between 0.87 and 1.2 V versus RHE.[377] While other studies have shown considerable loss of Co into the membrane after cycling,[378] data suggest that this is perhaps

due to imperfect formation of the alloy in the synthesis step and that leaching of the alloy after preparation can mitigate the problem.[371] TEM analysis of MEA cross sections after cycling shows clear evidence of Pt migration toward and into the PEMFC membrane for Pt/C cathodes, while PtCo/C materials show minimal deterioration.[379] However, the PtCO crystallite sizes were larger than their Pt/C counterparts; thus, the alloy produces higher mass activity and confers a higher stability to cycling and resistance to dissolution, despite a lower metal surface area compared to Pt/C. While it does appear that alloying can have a positive effect upon catalyst stability, is not clear from these studies whether the improvement in stability is due to improved thermodynamic stability or due to differences in the kinetics of platinum dissolution or in passivating oxide formation. Wikander *et al*. concluded that employing complex preparation efforts for lowering the Pt particle size below 3 nm may have limited practical value unless the particles are stabilized from electrochemical sintering.[380] If we are to design catalysts specifically to increase their stability, more information is needed about the mechanism of degradation and the role that the alloying element plays on the fundamental properties of the catalyst.

4.4. Platinum Particle Growth Analysis

The knowledge of crystallite size distribution (CSD) statistics provides important information in studying particle coarsening mechanisms. Ostwald ripening and coalescence mechanisms produce very different CSDs. Coalescence growth by aggregation of small particles maintains a log−normal distribution with an overall increase in average particle size. Ostwald ripening causes an increase in the percentage of large particles with a decrease in the relative fraction of small particles.

4.4.1. Particle Growth Analysis by XRD

The first detailed X-ray diffraction (XRD) studies on PEMFC electrodes were performed by Wilson *et al*.[4] using a Warren−Averbach Fourier transform method for determining the weighted crystallite sizes. The technique was later used by one of the coauthors (Garzon),[17,381,382] to deduce changes in the electrode crystal size distribution for fuel cells operating under cyclic and transient conditions. In the Warren−Averbach method, the peak profile is represented by a convolution of the pure peak profile and the instrumental broadening profile. The Fourier transform therefore enables the separation of instrumental broadening from the pure line profile. The experimental data are either directly Fourier transformed or least-square fitted with Poisson summation formulas (PSFs), which are then subsequently Fourier transformed. An advantage of using PSFs is the elimination of noise in the raw data, producing artifacts in the Fourier transform. Analysis of multiple peaks of different orders of (*hkl*) enables the determination of the respective size and strain coefficients. The second derivative of the size coefficient curve contains column size distribution information also.

Giorgi, Conti, and Ascerelli used a different approach for determining the growth mechanism of Pt fuel cell electrodes.[383,384] Studies of a commercially available Pt sheet were used as the reference. Pt/C catalyst powder, consisting of 20 wt % Pt supported on Vulcan carbon black, was obtained from E-TEK Inc. A three-layer structure was prepared using a spray technique. The catalyst layer was prepared by mixing Pt/C catalyst, Nafion ionomer, and glycerol. Electrodes, loaded with 2 mg/cm^2 of C, 0.11 mg/cm^2 of Pt, and 0.6 mg/cm^2 of Nafion, were then subjected to thermal treatment at 110 °C and half-cell polarization for 56 h at a current of 0.1 A. Experimental results show cathode Pt growth under these conditions, as evidenced by the CSD plots shown in Figure 20.

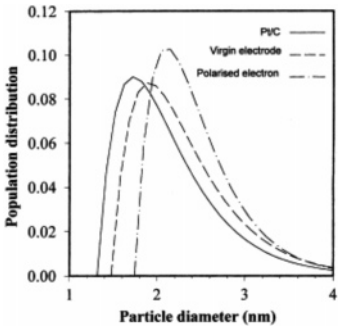

Figure 20. Particle size distribution obtained from the Pt(2 0 0) line for (—) Pt/C, (− − −) virgin electrode, and (− · −) polarized electrode. Reproduced with permission from ref 384. Copyright 2004 Elsevier Sequoia SA.

Whole Profile Analysis. Another X-ray diffraction analysis technique described by Garzon is the use of the whole-pattern or "Reitveld" (named after the inventor) method.[382] Characterization of the crystallite size, amorphous material fraction, and phase purity may be conveniently measured using X-ray scattering coupled with whole profile analysis methods. Nanometer-sized electrocatalyst produces X-ray scattering with broad often overlapping peaks. Whole profile methods allow for the precise determination of lattice parameters and accurate measurement of individual diffraction line intensities and profiles even when overlapping peaks are present. In contrast to traditional methods that simply fit diffraction peak maxima, whole profile methods model X-ray scattering data for every experimental point.

XRD analysis has been coupled with potential sweeping of an MEA to examine the causes and operating conditions leading to loss of electrocatalyst surface area.[17] During potential sweeping, the anode was exposed to hydrogen while the cathode was exposed to nitrogen. The cathode potential was swept linearly from an initial voltage (usually 0.1 V) to an upper limit voltage. After the cycling experiment was completed, postcharacterization was performed by XRD. The use of X-ray diffraction analysis to determine the degree of electrocatalyst sintering was validated by comparing the particle size with the measured electrochemically active surface area (Figure 21). A linear relationship between the platinum particle size and the measured catalytic surface area was observed, which indicated XRD postmortem measurement of platinum particle size is measuring the mechanism for platinum surface area loss; that is, growth in particle size leads to catalyst surface area loss. In studies of single cell durability testing performed by Borup *et al*., cathode catalyst particle sizes grew from about 1.9 to 3.5 nm during the drive cycle experiments over 1200 h of testing. This extent of growth was greater than that observed during steady-state testing, where the particles grew to 2.6 nm at 900 h and 3.1 nm over 3500 h. In accelerated durability cycling tests, extremely rapid cathode particle growth was observed when cells were cycled to voltages above 1 V.[17] During fuel cell cycling measurements, catalyst coarsening rates exhibited a linear increase with temperature. Low relative humidity decreased platinum particle growth but substantially in-

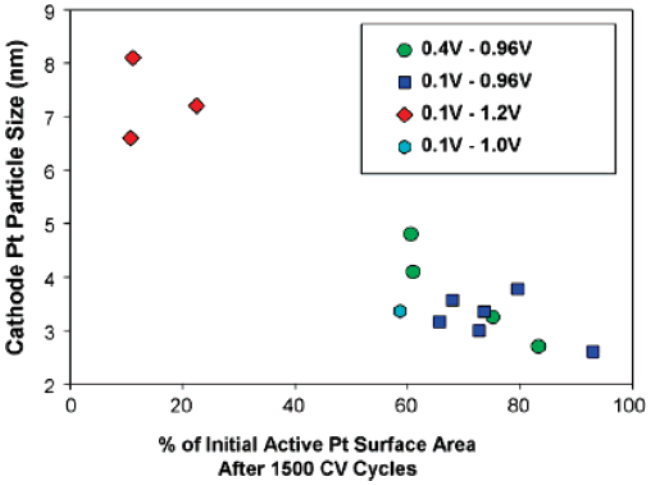

Figure 21. Particle size as determined by XRD and measured electrochemical active surface area for various potential cycling experiments. Cell 80 °C, H_2 226% RH, air 100% RH. Reproduced with permission from ref 17. Copyright 2004 Elsevier Sequoia SA.

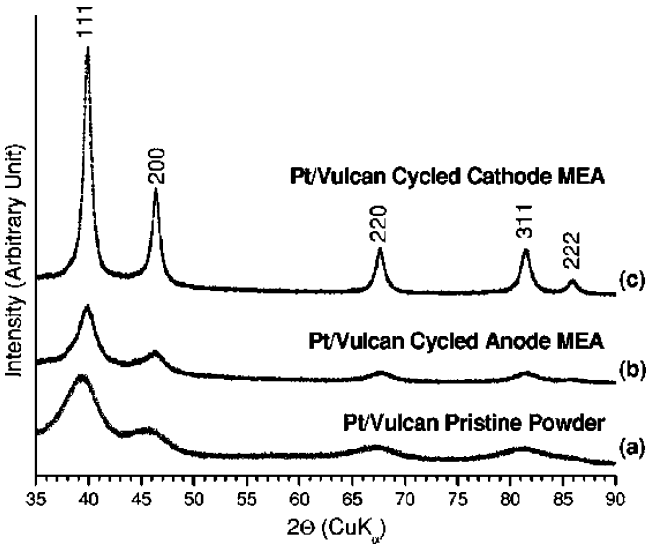

Figure 22. X-ray powder diffraction pattern of the pristine Pt/Vulcan powder sample collected at normal incidence compared to those of anode b and cathode c in the cycled Pt/Vulcan MEA sample collected at primary incidence. Reprinted with permission from ref 224. Copyright 2005 The Electrochemical Society.

creased carbon loss. The rate of carbon corrosion of the electrode catalyst layer was found to increase with increasing potential and decreasing humidity.

4.4.2. Glancing Angle X-ray Diffraction Studies

Ferreira *et al.* used a glancing angle X-ray powder diffraction technique to probe the changes in the Pt particle size of the cathode and the anode without removing them from the ionomer membrane.[224] X-ray diffraction patterns of the pristine powder and cycled 46 wt % Pt/Vulcan (anode and cathode) MEA samples were collected (see Figure 22). As the characteristic depth is greater than the thickness of MEA samples, X-ray diffraction experiments of the MEA sample at normal incidence would lead to collection of diffracted intensities of both anode and cathode. Therefore, X-ray diffraction data collection at low incident angles is required to obtain diffracted intensities from only the cathode or the anode alone. Extensive particle size growth (from 2.3 to 10.5 nm) was seen for the fuel cell cycled cathodes, in

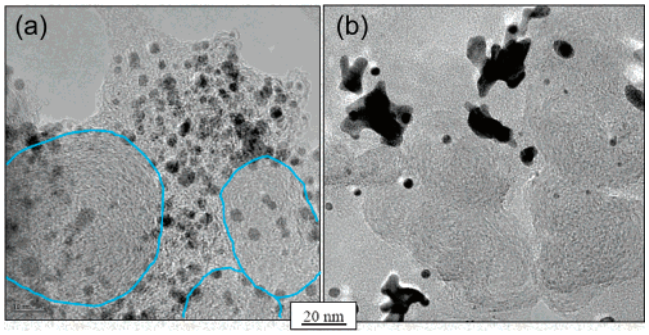

Figure 23. (a) TEM of freshly prepared MEA. (b) TEM of MEA after potential cycling at 80 °C to 1.2 V for 1500 cycles.[387]

agreement with previous work. In contrast, little growth of the fuel cell anode catalyst was observed.[224]

4.4.3. Particle Growth Analysis by TEM Imaging

Particle imaging via HR-TEM (high-resolution transmission electron microscopy) and HAADF-STEM (high angle annular dark field-scanning transmission electron microscopy) can be used for quantifying the changes in catalyst particle size, distribution, and morphology (particularly in the cathode) following electrochemical aging; in this way, particle data measured directly from the TEM/STEM images can be used to elucidate the predominant mechanism(s) of particle coarsening that contribute to reduction of the catalyst electrochemically active surface area and concomitant fuel cell performance degradation. One advantage of the use of TEM with proper sample preparation is the direct observation of the location of particle growth in the electrocatalyst layer. Samples for TEM are commonly prepared by (1) lightly dispersing the powder (as-processed or scraped from an MEA electrode) across a thin (holey/lacey) carbon film or (2) preparing an intact cross section of a three-layer MEA using diamond-knife ultramicrotomy.[385,386] Ultramicrotomy sample preparation, which makes use of *"partial"* electrode embedding, has enabled direct imaging of intact recast ionomer, carbon/Pt, and pore network surfaces within MEA porous catalyst layers via TEM. This technique has proven valuable for the imaging of catalyst particles postmortem, including the ability to determine the location inside the MEA structure where the growing particles are located.[387] An example of the value of this technique is demonstrated in Figure 23, which shows the image of a freshly prepared MEA (Figure 23a) and an MEA which underwent repeated high potential cycling to 1.2 V. In the fresh sample, Pt particles are evident in the ionomer region of the MEA; thus, the catalyst particles have separated from the carbon support material. After cycling, large particle agglomerates have formed in the ionomer region (Figure 23b).[387]

Potential cycling, such as that encountered during transient (drive cycle) operation, increases the rate of Pt particle growth in the cathode compared with steady-state operation.[381,388] At high cathode potentials (potentials between 0.9 and 1.2 V), Pt particles become unstable and the equilibrium concentration of mobile Pt species in solution will increase significantly, significantly accelerating the coarsening of Pt particles.[142,352] The effect of potential cycling on cathode Pt particle growth as analyzed by TEM is illustrated in the example shown in Figure 24, which compares the Pt size distribution in a fresh cathode with the cathode Pt size distribution following potential cycling at 0.1−1.2 V for 1500 cycles, 80 °C, and 100% RH, where the Pt size distributions

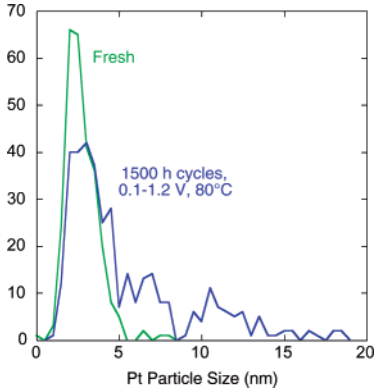

Figure 24. Pt particle size distributions comparing the Pt particles in a fresh cathode with Pt in the cathodes of MEAs subjected to 0.1−1.2 V potential cycling for 1500 h, 80 °C, and 50% RH. Modified from ref 387.

were measured directly from HR-TEM images.[387] The Pt particle size distributions become wider as a function of increasing potential, as does the nominal Pt particle size.

4.4.4. Particle Growth Mechanism

There are three primary Pt particle coarsening mechanisms that are believed to be important for PEM fuel cells: (1) Ostwald ripening occurs when small particles dissolve, diffuse, and redeposit onto larger particles, resulting in reduced Pt particle surface area via a minimization in surface energy; (2) reprecipitation occurs when Pt dissolves into the ionomer phase within the cathode and then precipitates out again as newly formed Pt particles; (3) particle coalescence occurs when Pt particles are in close proximity and sinter together to form a larger particle. It is worth noting that mechanisms (1) and (2) are quite similar: in Ostwald ripening, the nucleation site for platinum deposition is a previously existing platinum particle; in reprecipitation, the nucleation site is a particle or defect that did not previously serve as a platinum site. Each particle coarsening mechanism is characterized by distinctive elements in the evolution of the particle size distribution. For example, Ostwald ripening of the Pt particles will result in the growth of larger Pt particles at the expense of the smaller Pt particles, and the typical Gaussian particle size distribution/profile will shift to higher and wider size distributions during electrochemical aging.[383] For the case of Pt dissolution and reprecipitation, which may also be associated with Pt particle coalescence depending on the distances between new Pt particles, the mobile platinum species that dissolve into the ionomer phase will nucleate both within the ionomer phase and/or onto the carbon support surface and will result in a distribution of particle sizes depending on the localized platinum concentrations within the ionomer and on the Pt−Pt nucleating particle distances. The particle size distribution for the case of PEMFC particle growth does not shift entirely to a larger Pt size range, as would occur for complete Ostwald ripening. Instead, the size distribution gets broader due to the nucleation of small, highly separated Pt particles within the ionomer, as well as larger particles, which form due to the coarsening via coalescence of Pt particles nucleating close together. In addition, Pt^{2+} in solution in the ionomer phase may also redeposit onto existing nuclei, resulting in somewhat larger Pt particles. A change in the form/profile of the resulting Pt particle size distribution occurs when a Pt dissolution/reprecipitation mechanism is coupled with particle coalescence. This distribution is characterized by a change from a single, narrow, Gaussian Pt particle size distribution to a bimodal particle size distribution, where some fraction of small Pt particles are retained in the cathode while other Pt particles grow larger.

What Ferreira found was that, at the GDL/cathode interface, nanoscale Ostwald ripening was dominant, resulting in a larger mean particle size and a wider Gaussian size distribution, due to the limited crossover hydrogen for Pt ion deposition. Deeper in the cathode (closer to the membrane), Pt deposition in the ionomer was more likely by the crossover hydrogen reduction of the Pt ions, which resulted in a more likely "bimodal" profile. These Pt particles were all carbon-supported, and Pt atoms in the ionomer were not included in the profiles.[224]

But still, there are two concerns regarding this explanation of the different Pt size profiles with the cathode. First, some recent studies[194,225,389] showed that a Pt band could form in the membrane when flowing air at the cathode during degradation testing. The Pt band was located in a position where the hydrogen and oxygen diffusing through the membrane could react with each other and result in a sharp change in the local potential. The Pt band formation was relatively fast (a few thousand cycles or 1−2 days) under potential cycling conditions for the conventional Pt/C catalyst. Also deposited Pt atoms by hydrogen chemical reduction might be formed in the ionomer instead of on the carbon support. So these different Pt size profiles might not be caused by H_2 concentration differences per se but by differences in the potential distribution within the ionomer. Second, Pt ions in the cathode will want to diffuse into the membrane phase, so there would be a Pt ion concentration gradient in the cathode. This Pt ion transport phenomenon was not considered in Ferreira's work. With degradation, Pt mass distribution within the cathode might not be uniform, and more large Pt particles could be produced at both the carbon support and in the ionomer (if hydrogen crossover and chemical reduction of Pt ions apply) within the cathode closer to the membrane phase. So at this point in time, it is still difficult to conclude which Pt growth process is dominant. Separately counting Pt particles on or off carbon supports in TEM images could help us gain more details of Pt particle growth. Mathematical simulation including Pt ions transport could also assist in understanding cathode Pt degradations.

Pt particle size distributions measured during cycling potential (0.1−1.2 V) changed form; that is, the size distributions exhibit a greater tendency toward a bimodal form with increasing potential.[387] The size distributions for the potential cycling conditions shown in Figure 24 do not shift entirely to larger particle size ranges, as would be expected if the Pt particles were growing solely by an Ostwald ripening mechanism, where the growth of large particles occurs at the expense of small particles. Instead, the size distribution gets broader; a fraction of the very small Pt particles (<3 nm) remains after potential cycling though the total particle count decreases, and an increased number of larger Pt particles are observed and included in the distribution. These bimodal particle size distributions have been measured by both XRD and TEM after potential cycling experiments and after fuel cell testing simulating drive cycle operation.[335,382,390,391] Thus, the Pt particle growth behavior during potential cycling is best described by a combination

of Pt particle coalescence and Pt dissolution/reprecipitation within the ionomer.

4.5. Corrosion of Catalyst Support

In addition to loss of the platinum, the carbon support that anchors the platinum crystallites and provides electrical connectivity to the gas-diffusion media and bipolar plates is also subject to degradation. In phosphoric acid systems, graphitized carbons are the standard because of the need for corrosion resistance in high-temperature acid environments,[370] but PEM fuel cells have not employed fully graphitized carbons in the catalyst layers, due in large part to the belief that the extra cost could be avoided. However, as durability targets are scrutinized, it is important to consider the importance of carbon stability, and graphitized carbons are being considered for use in PEMFCs to give required corrosion stability.[392] The corrosion reaction of carbon material in aqueous acid electrolytes including proton exchange membranes is generalized[393] as

$$C + 2H_2O \rightarrow CO_2 + 4H^+ + 4e^- \qquad E^\circ = 0.207\ V$$

This reaction is thermodynamically allowable at the potentials at which the fuel cell cathode operates, but it is believed to be almost negligibly slow in that potential range because of the lower temperatures of PEM cells compared with phosphoric acid. However, even if it proceeds very slowly, it can affect the long-term durability of PEMFCs. Electrochemical corrosion of carbon materials as catalyst supports of PEMFCs will cause electrical isolation of the catalyst particles as they are separated from the support or lead to aggregation of catalyst particles, both of which result in a decrease in the electrochemical active surface area of the catalyst and an increase in the hydrophilicity of the surface, which can, in turn, result in a decrease in gas permeability as the pores become more likely to be filled with liquid water films that can hinder gas transport. In this section, carbon corrosion in PEMFCs, PAFCs, and aqueous solutions will be reviewed.

4.5.1. Carbon Corrosion in PEMFCs

In the past few years, several articles have been devoted to the study of carbon corrosion in actual gas diffusion electrodes of PEMFCs.[199,394] Roen *et al.*[394] detected CO_2 in the cathode exhaust gas during potential cycling while feeding humidified helium. Besides enhancement of CO_2 evolution at potentials higher than 0.9 V, there was also a peak at about 0.6 V during anodic sweeps when only platinum catalyst existed. The intensity of this peak increased with the amount of platinum catalyst. It was proposed that CO adsorbed on platinum during this portion of the sweep, below 0.6 V, and it was subsequently oxidized. The degree of enhancement of this reaction at potentials higher than 0.9 V also depended on the amount of platinum, but no mechanism was suggested. Mathias *et al.*[199] reported the dependence of carbon corrosion current on the potential, material, temperature, and time. The potential dependence displayed Tafel behavior, and the temperature dependence followed Arrhenius behavior. However, as described later, there is a linear relation between the corrosion current and time in the log−log plots, and two constants (initial value and time-decay exponent) depend on the material. In relation to the transient condition of the cell operation, a mechanism named the "reverse-current mechanism", which creates a potential high enough for oxygen evolution accompanied by carbon corrosion, has been proposed.[135,138,154,395] This mechanism occurs under conditions in which hydrogen-rich regions and hydrogen-starved regions coexist in the anode chamber of a single cell, resulting in local corrosion in the region of the cathode corresponding to the fuel-starved region of the anode.[135,138,395] Such a situation may occur at start-up of the system or during shutdown of the anode chamber, thereby causing degradation of the cathode.[154] It is supposed that oxygen crossover from the cathode chamber through the electrolyte membrane can be supplied at a sufficient rate to support the reverse-current mechanism.

4.5.2. Carbon Corrosion in PAFCs

Carbon corrosion in PAFCs has been investigated extensively for years, using both actual PAFC electrodes[396−402] and model electrodes in phosphoric acid.[403−412] It is worth noting that, in PEMFCs, the material and structure of the gas diffusion electrode are similar to those used in PAFC cells. However, the choice of catalyst support in PAFCs has traditionally been graphitized versions of carbon. The degree of corrosion in phosphoric acid has been evaluated by corrosion current,[403,404,407−410,412] weight loss,[397,407,408] and CO_2 generation.[403,404] Changes of the shape of cyclic voltammograms measured in aqueous acid solution were also used to measure the changes of the surface functional groups.[140,405,406,411] While cyclic voltammetry detects only electroactive oxides such as the quinone/hydroquinone couple, it is frequently used as an index of the degree of surface oxidation of the carbon material. A classification of surface functional groups on carbon material has been attempted by XPS,[397,413] but quantitative determination of their amount and changes seems to be difficult. Effects of platinum catalyst on carbon corrosion[409,411] were observed. While Kinoshita *et al.*[140] did not observe differences in the saturated density of the electroactive surface oxide after oxidation at 1.2 V between electrodes with and without platinum, Passalacqua *et al.*[409] showed an increase of the corrosion current at 0.6−1.0 V under a nitrogen atmosphere with platinum loading, and Pyun *et al.*[411] showed a depression of the surface oxide formation during corrosion at 0.7 V under oxygen atmosphere in the presence of platinum. The mechanism was not resolved in this study, but the authors speculated that participation of adsorbed oxygen atoms on the surface of platinum played a role in controlling what happens on the carbon surface. They also showed that oxygen appeared to have an effect not just upon surface oxide coverage but also on carbon corrosion. In this case, surface oxide formation was depressed under an oxygen atmosphere. It was estimated that surface oxides on carbon were further oxidized to CO_2 more easily in an oxygen atmosphere, which resulted in a smaller amount of surface oxide. If this mechanism is accurate, net carbon corrosion rates are accelerated by the presence of gas-phase oxygen.

As carbon corrodes, changes in catalyst layer morphology occur. Changes in the shapes of carbon black particles have been observed by TEM.[396] After an operation at 853 mV, the cores of primary particles of carbon black, which are less crystallized than the outer shells, corroded preferentially and became hollow. This phenomenon is important but may not be common with the case of PEMFCs, because the electrolyte might not penetrate into the microstructure as thoroughly in PEM as it does in a liquid-electrolyte cell. It is therefore possible that the inner region of the carbon

particles does not corrode in PEMFCs. Also in the case of PAFC, a mechanism of local cathode corrosion similar to the PEMFC reverse-current mechanism has been proposed.[400,401] Another major difference between carbon corrosion in PAFC and PEMFCs is that the water is present as liquid in PEMFC and acts as the oxidant during the corrosion reaction. It is worth noting, however, that carbon corrodes at potentials as low as 0.9 V in phosphoric acid at elevated temperature even for a cell that has uniform hydrogen coverage on the anode. The rate of carbon corrosion decreases linearly with time in the log−log plots, both in PEM[199] and in phosphoric acid cells.[404,409,410] However, there seems to be no theoretical basis for such a rate law. Although formation of passivating films on the carbon surface has been proposed as a mechanism,[402,410] it is hard to expect endless growth of such films. The reported periods of these experiments are on the order of 24 h, so there is still the possibility of approaching a steady state over longer time periods.

4.5.3. Carbon Corrosion in Aqueous Solutions

Fundamental studies have been carried out on carbon corrosion in aqueous acid (or neutral) solutions from the viewpoint of a PEMFC degradation mechanism.[414−419] Note that aquesous based studies allow for liquid water to act as the oxidant during the corrosion reaction, which is fundamentally different from carbon corrosion in PAFCs. In addition, studies on the corrosion or surface oxidation of graphite,[91−100] glasslike carbon,[420−426] and carbon fibers[427−429] are also informative. CO_2 evolution from electrodes made by platinum catalyzed active carbon powder in a deaerated sulfuric acid solution was studied by differential electrochemical mass spectroscopy (DEMS).[414,418] Similar to the CO_2 generation from a PEMFC cathode,[394] peaks during an anodic sweep appeared to be enhanced in the presence of platinum catalyst. This implies that carbon corrosion is enhanced by the platinum catalyst under open-circuit conditions. Generation of CO was also detected above 0.9 V, but the amount was minor. Proposed mechanisms are as follows: some surface species, such as absorbed CO, are generated at relatively low potential (~0.3 V). These species can move to the platinum catalyst by surface diffusion and are consequently further oxidized to CO_2. Changes of surface species of carbon black powder without platinum during constant potential holds in sulfuric acid solution were investigated using TG-MS, XPS, and cyclic voltammetry.[415] In this study, while potential holds below 1.0 V at room temperature did not change surface oxide, the authors found an increase of electroactive oxide at holds above 0.8 V at 65 °C. TG-MS showed that retention at 0.8 and 1.0 V enhances carboxylic acid and/or lactones, and retention at 1.2 V enhances weak acids such as phenols instead. It is worth noting that the aim of this particular study was characterization of the surface oxide, not the overall corrosion rate. The surface oxide determines hydrophobicity, which in turn affects the effective gas permeability of the electrode. If, however, the changes to hydrophobicity of the carbon support occur only at the carbon | ionomer interface, these changes might not influence the rates of gas transport through the gas diffusion electrode. Therefore, further investigations to connect the electrochemical surface oxidation of the carbon support with the hindrance of gas diffusion might be required.

Some fundamental studies on carbon oxidation have been performed using a highly oriented pyrolytic graphite (HOPG) plate[416,417] because of its suitability for observation by scanning probe microscopy techniques such as AFM. In these studies, enhancement of carbon corrosion by platinum was visualized, suggesting the effects of platinum catalyst only influence the portion of carbon in contact with platinum. In addition to the electrochemical corrosion pathway, chemical corrosion by hydrogen peroxide,[417] which is generated by oxygen reduction below 0.682 V, should also be considered, as has been suggested experimentally.[414] Morphological changes of HOPG surfaces were observed by AFM[430,431] and STM.[432,433] In these observations, bubble-like blisters caused by gas evolution were formed. Although this strange phenomenon is partly due to extremely high potentials (*e.g.*, 2.0 V) and the fragile features of HOPG, the manner of the corrosion in these experiments is worthy of further study, for blister formation should follow the penetration of electrolyte beneath the surface, and it is likely that the investigation of the details of this process may reveal common mechanisms of graphite degradation. On the other hand, the morphological change of glasslike carbon is quite different.[422,425,426] A porous layer is formed on the surface during oxidation at 2.2 V in sulfuric acid solution with a constant thickness growth rate.

The wettability and gas diffusivity of the electrode change with surface oxidation of carbon supports. However, it is difficult to evaluate them quantitatively. In the case of PAFCs, the wettability of the electrode by electrolyte was evaluated by the absorbed amount of the electrolyte in the porous electrode.[397,398] However, in some cases, the amount of absorption exceeded the total pore volume in the initial electrode, which meant that large pores were created by carbon corrosion during degradation, and absorption is no longer a simple index of the wettability.

Supported platinum-on-carbon catalysts remain the state of the art for fuel cells under development today, but considerably more information is needed about the controlling factors of reactivity and stability as new catalyst/support structures are considered. Of course, alternatives to supported platinum are under evaluation, but they present theoretical and practical challenges of their own.

4.5.4. Novel Support Materials

A substantial body of work has been generated on the development of carbon supports, ranging from the traditional blacks to various forms, treatments, surface modifications, and preparation protocols, many with durability ramifications. However, in this section, we review novel alternatives to carbon supports within the context of the durability issue. For these purposes, forms of carbon other than the conventional graphites and blacks are discussed here, such as diamond structures or nanotubes.

Nanotubes. Carbon nanotubes (CNTs) and nanofibers are essentially nanoscale cylinders of rolled up graphene sheets. If the cylinder wall is only one sheet thick, it is a single-wall nanotube (SWNT). More layers form a multiwall nanotube (MWNT), and a nonhollow cylinder is a nanofiber. As discussed in a review of nanotubes for catalysis applications,[434] the orientation of the graphene sheets and pretreatments can influence the nature of the surface and, consequently, the interaction with catalysts. A review of the synthesis and catalyzation of nanotubes specifically for fuel cell supports is provided by Lee *et al*.[435] Extensive electrochemical experimentation has been performed on nanotubes[436−453] and specific variations such as nitrogen containing nanotubes,[442,445] nanofibers of various types,[436,446,448,451−453]

single-wall nanotubes,[437,440,443,449] multiwall nanotubes,[437−439,441,444,447,449,450,454−456] nanocoils,[457,458] nanohorns,[459] nanourchins,[460] and cup-stacked nanotubes.[461]

Probably because of the relatively simple experimental apparatus required, most of the electrocatalysis support work focuses on anode catalysts for methanol oxidation[436−439,441,445−449,451,452,455,456,462−471] or ethanol oxidation.[462,472] Additional anode experimentation considered the effects of CO/H_2 on performance.[441] The use of nanotube supports with cathodes or actual fuel cell devices has also been extensively investigated,[440,443,444,451−455,459,463,464,473,474] although not to the same degree as the case of anodes, probably because the experimentation is more involved.

While a performance advantage is claimed in nearly every instance where a nanotube supported catalyst is compared to another support, nanotube durability advantages are rarely mentioned. However, Wang *et al*. show that MWNTs experience less oxidation at 0.9 V and less Pt surface area loss than XC-72 in durability testing.[79] Similarily, MWNTs are also shown to be more oxidation resistant than carbon black at 1.2 V.[447]

While a small body of evidence suggests that nanotubes and similar structures are more oxidation resistant than carbon blacks and decrease catalyst surface area loss, the improvement may not be sufficient to provide the needed benefits for commercialization, especially in light of the appreciable costs of such materials at this point. Extensive durability testing and substantial cost reductions are needed for nanotube electrocatalyst supports.

Oxides. Various metal oxides have appreciable electronic conductivities at low temperatures (numerous additional oxides are electronically conductive at high temperature), primarily due to mixed valence stoichiometries that introduce charge carriers into the structure. One such commercial conductive oxide for electrochemical applications is Ebonex, a mixed valence TiO_x material. However, lower performance is obtained using Pt catalyzed Ebonex supports compared to graphite, allegedly due to support interactions,[465] even though the Pt particles are considerably larger than those on the graphite. Further, in another study, Ebonex and niobium doped titania supports both lose electronic conductivity upon electrochemical oxidation, but the Ebonex loss is irreversible.[475] Ioroi *et al*. compared Pt catalyzed Ti_4O_7 supports with XC-72 carbon in fuel cell testing,[476] specifically in response to the carbon corrosion problem. They found the Ti_4O_7 support to be more stable than the XC-72 when polarized over 0.9 V, but fuel cell performances were not as high, once again due to larger Pt particle sizes on the oxide compared to the carbon. Kuroki *et al*. investigated indium and tin oxides as well as titania.[477] While the titania did provide the smallest Pt particle sizes (9 nm), smaller particles and, possibly, higher oxide conductivities are still needed. While the difficulties with Pt particle size compared to carbon may be primarily due to the lower oxide support surface areas, the stability advantages of the Ti_4O_7 possibly warrant further investigations.

Silicon. Numerous groups are developing silicon based fuel cells that can be manufactured using electronics fabrication techniques. Correspondingly, the systems tend to be for low power or micropower applications. A silicon substrate can be micromachined using photolithography or other techniques to form flow channels and other fuel cell features. Although most efforts use conventional supports and MEAs, high surface area silicon structures can be formed that serve as catalyst supports. For example, silicon pillars that are 6 μm high by 0.2 μm × 0.6 μm are electrochemically coated with Pt or Pt−Ru to form a methanol oxidation electrode,[478] or similar microcolumn structures can be used.[479] Alternatively, to attain sufficient catalyst surface areas, a porous silicon structure can be formed.[466,480,481] In one case, the silicon is anodized to generate a porous SiO_2 support.[480] Catalyst surface area can also be increased by coating a Pt black layer onto the silicon structure.[482] The durability of the silicon substrates and supports was not considered. Regardless, silicon based fuel cells are unlikely to find application at larger scales where cost is a major concern.

Conducting Polymer. An enormous body of literature has been generated on electronically conducting polymers for a multitude of electronic and electrochemical applications, but fuel cell efforts have been modest. Indeed, most of the literature for fuel cells focuses on anode reactions;[467,468,470,471,483] thus, it is suspected that stability may be an issue, particularly at the cathode. On the other hand, the polymeric material increases Pt dispersion and utilization,[467] which may also conceivably improve catalyst stability, albeit the support itself is suspect. Going one step further than electronically conducting polymers, Lefebvre *et al*. investigated a poly(3,4-ethylenedioxythiophene)/poly(styrene-4-sulfonate) (PEDOT/PSS) and PEDOT/polyvinylsulfate (PVS) composite support that also provides ionic conductivity.[469] Anode performances were inferior to those of Pt/carbon, and the cathode performances were comparable, though there may be a number of stability issues.

Conductive Diamond. Boron-doped diamond (for electronic conductivity) is a corrosion resistant and electrochemically stable material compared to carbon,[484] which prompts its investigation as a catalyst support. However, diamond may not be any better than carbon in limiting the mobility or dissolution of platinum nanoparticles, unless the particles are quite large or they are entrapped in some manner,[484−486] for example, Pt deposition onto a diamond film in conjunction with diamond deposition to entrap the Pt. Very high stabilities are attained in corrosion tests, but the Pt utilization may be low for fuel cell applications. Other work is oriented toward the deposition techniques and support materials. Pulsed galvanic deposition is used to attain 10−50 m^2/g Pt dispersions.[487] Electrodeposition is preferred over chemical/thermal deposition,[488] and electrodeposition occurs preferentially at boron rich areas.[489] Spontaneous deposition of Pt onto boron-doped diamond is achieved by supporting the diamond on a sacrificial Si underlayer.[490] High surface areas are achieved using porous honeycomb diamond,[491] although Pt particle sizes are still quite large. Doped diamond has also been investigated as a support for direct methanol oxidation catalysts,[492,493] and boron-doped diamond is superior to glassy carbon as a composite $Pt-RuO_x/C$ support.[493]

In summary, boron-doped diamond is an excellent support from a corrosion point of view, but its applicability may be limited due to difficulties attaining the Pt utilization and roughness factors required by commercial fuel cell applications.

Nonconductive Whiskers. A unique class of catalyst supports are nanostructured whisker-like materials developed by 3M.[494,495] While superficially not unlike other nanofiber supports, these oriented, crystalline organic whisker structures are nonconductive. Electronic conduction is provided by the Pt catalyst sputter-coated onto the high surface area whiskers. Thus, the whiskers serve as a scaffold that provides structure

and surface area to the overlying Pt deposition. The whiskers are initially formed vertically oriented as a film overlying a release substrate by the thermal sublimation and subsequent annealing of a red organic pigment, *N*,*N*-di(3,5-xylyl)-perylene-3,4:9,10-bis(dicarboximide) (called perylene red). The crystalline whisker structures have lengths of about 500−1000 nm, cross-sectional diameters of about 50 nm, and an areal number density of 3−5 billion cm^{-2}. Pt is applied by sputter deposition, and the resulting films of catalyzed whiskers are transferred from the release substrate to the surfaces of a polymer electrolyte membrane to form an MEA.[496]

The Pt deposition particles tend to be somewhat larger than those on typical support materials, probably to improve electronic conductivity and electroactivity. The combination of this near bulklike Pt activity and extremely high surface utilizations compensates for their lower active areas when compared to highly dispersed catalysts. Thus, equal or better fuel cell performances can be attained using platinum loadings similar to those of highly dispersed catalysts on conventional supports. Since the whisker material is unaffected by the fuel cell environment, catalyst durability is expected to be high, as surface area loss resulting in rearrangement or Pt dissolution is expected to be mitigated by the more stable, near bulklike catalyst layers. In one durability investigation, the stabilities of Pt−Fe and Pt−Ni alloy catalysts on perylene whiskers are reported by Bonakdarpour *et al.*,[497] though no comparisons with alloys on conventional supports are provided to establish if there are indeed advantages with these catalyst structures. Such catalyst structures may be more prone to contaminants due to the lower active areas, and they are also reportedly prone to flooding (not published). This whisker technology is utilized in 3M MEAs being developed and reported.[498]

4.6. Novel Materials: Nonprecious Catalysts for PEMFC Cathodes

In spite of a substantial reduction in platinum catalyst loading in the past 15 years, from approximately 2 mg cm^{-2} of the MEA surface area to below 0.5 mg cm^{-2} without significant impact on cell performance and lifetime,[371] electrocatalyst cost still represents a grand challenge for polymer electrolyte fuel cells and the hydrogen economy in general. The average monthly price of platinum has more than tripled between March 1999 and March 2007, from $370 to $1220 per troy ounce,[499] to a large degree offsetting the benefits of the catalyst loading reduction. In the 2007 U.S. DOE Multi-Year Research, Development and Demonstration Plan, the technical target for the cost of electrocatalysts is based on platinum costs of $450/troy ounce = $15/g (in 2002 dollars).[6]

Further reductions in platinum loading in the PEMFC cathode run the risk of lowering performance and magnifying the performance losses associated with catalyst morphology changes, thus suggesting that the approach of overcoming high catalyst costs with lower loadings carries considerable risk. This approach may be limited by the decrease in the electrocatalytic activity of platinum (and Pt-alloy catalysts) with decreasing size of nanoparticles.[500] Catalysts made of carbon-supported Pt, 2−3 nm in average particle size, offer the highest oxygen reduction reaction (ORR) activity per unit mass and are likely to remain standard for platinum based cathode materials. Among other approaches to limiting precious-metal catalyst cost, the core−shell concept,[501] *i.e.* a shell of precious metal, usually Pt or Pt-alloy surrounding a metal-free core, appears to be attractive. However, these catalysts are at a relatively early stage of development; as such, nanoparticle stability, surface segregation, and corrosion of nonprecious catalyst component(s) must be addressed before core−shell catalysts can become of greater practical value to polymer electrolyte fuel cells.

Another approach that is receiving considerable attention is the replacement of platinum with non-platinum catalysts. These catalysts are typically based on Pd[502−504] or Ru.[504−508] Although platinum is avoided, the result is the replacement of one precious metal with another, by and large, less active than platinum. Unfortunately, several precious metals of potential interest as PEMFC electrocatalysts have suffered similar or even greater increases in price than platinum has. A most recent example involves ruthenium, the price of which has risen by almost an order of magnitude in 2006−2007, reaching nearly $900 per troy ounce in early 2007, although the price has come down significantly during 2007 to approximately $350 per troy ounce.[499]

As present methods of limiting or eliminating platinum from the PEMFC cathode prove challenging, nonprecious catalysts for the oxygen reduction reaction (ORR) are becoming more attractive to the PEMFC technology. While many nonprecious metal catalysts exhibit both good oxygen reduction activity and respectable performance durability in alkaline and neutral media, virtually all precious-metal-free catalysts developed over the past several decades suffer from low activity and poor stability in the acidic environment of the PEMFC cathode. As a result, most of the effort invested to date in the development of nonprecious cathode catalysts has focused on stabilizing ORR active sites, typically via the use of high-temperature treatment (pyrolysis) of the catalyst precursor. The performance that would be needed for a cost-free non-Pt catalyst has been defined quantitatively by General Motors.[371] In addition to performance requirements, the effect of the chemical instability of materials being developed (*e.g.*, Fe macrocycles) is important, as the effect of leaching of Fe into an MEA environment is another potential degradation mechanism. Below, we will briefly review the most common non-noble metal catalyst developments.

4.6.1. Carbides, Oxides, Oxynitrides, and Carbonitrides

Tungsten carbide has a platinum-like electronic structure[509−512] and exhibits platinum-like behavior for hydrogen chemisorption.[513] For this reason, tungsten carbide and its alloys have been studied as fuel cell anode catalysts.[514−523] Other transition metal carbides (titanium, zirconium, tantalum, molybdenum, etc.) have also been considered to be candidates for efficient catalysts for redox-type reactions, owing to their high chemical and thermal stability.[524] The electrochemical behavior of transition metal carbides (tungsten carbide and its alloys,[525−531] tantalum carbide,[530−532] titanium carbide,[530,533−539] molybdenum carbide)[531] has been reported by several research groups. These results showed that tungsten and other carbides were unstable at high potentials in acid solution. Therefore, there are limited applications of tungsten and other carbides as oxygen reduction catalysts in acid solution.[540,541] Various carbides, oxides, borides, and nitrides have been examined as stable catalyst supports substituting for carbon in phosphoric acid fuel cells.[542] However, the deterioration of cell performance of a Pt-activated support electrode was unacceptably high.

Table 13. Solubility of Group 4 and 5 Metal Oxides and Oxynitrides

catalyst	temp/°C	solubility/mol·dm^{-3} (in 0.1 M H_2SO_4)
ZrO_2 (thin film)	70	3.5×10^{-6}
ZrON (thin film)	70	4.5×10^{-8}
TaON (thin film)	70	2.0×10^{-7}
TaON (powder)	50	3.3×10^{-7}
TiO_2 (plate)	50	3.5×10^{-7}

Lee *et al*. showed that tantalum addition to tungsten carbide increased stability in an oxygen containing atmosphere.[543−545] Tungsten and tantalum form complex hydroxide films, which have high corrosion resistance.[546] As a result, thin hydroxide films of W and Ta form to protect WC, and the catalytic activity remains and with increased stability.

Some complex oxides are stable in acid solution. Sodium tungsten bronzes had excellent stability in acid solution, and Šepa *et al*. found that sodium tungsten bronze had a high catalytic activity for oxygen reduction compared to platinum.[547] After his work, tungsten bronzes were examined for electrochemical oxidation of hydrogen and CO[548,549] and oxygen reduction.[549−551] However, catalytic activity was found to be due to traces of platinum[551−554] while pure sodium tungsten bronzes exhibited low ORR activity.[554]

Group 4 and 5 transition metals are well-known as valve metals, indicating that they have a high corrosion resistance in acid solutions. Ota and co-workers found that group 4 and 5 metal compounds such as oxides,[555,556] oxynitrides,[556−558] and carbonitrides,[559] which were prepared by RF magnetron sputtering, had catalytic ORR activity. The catalytic activity of ZrOxNy, TaOxNy, TiOxNy, and TaCxNy for ORR increased with the increasing substrate temperature during sputtering. Table 13 shows the solubility of group 4 and 5 metal oxides and oxynitrides measured by Ota *et al*. in 0.1 M H_2SO_4.[555,557,558,560] These solubilities are much less than that of Pt in 0.1 mol dm^{-3} H_2SO_4 at 23 °C under atmospheric conditions, *i.e.*, 3.0×10^{-6} mol dm^{-3}.[351]

Cyclic voltammograms of these compounds reached steady-state immediately, with the anodic charge corresponding to the cathodic one. This implies that there is not a one-sided reaction, *i.e.*, there is no continuous anodic dissolution. In addition, no specific oxidation or reduction current peak in the CVs was observed. Therefore, group 4 and 5 metal compounds prepared by RF magnetron sputtering have high chemical stability in acidic media. Kim *et al*. showed that titanium oxides prepared by heat treatment of titanium plate under nitrogen gas including a trace of oxygen had some catalytic activity for ORR and the activity depended on the heat treatment temperature.[351] The solubility in 0.1 M sulfuric acid at 50 °C was 3.5×10^{-7} mol dm^{-3} (Table 13) and was independent of the heat treatment temperature.[351] Ishihara *et al*. reported that tantalum oxynitride powder prepared by nitriding of tantalum oxide had some catalytic activity for ORR.[561,562] In recent years, they showed that the electrophoretic method and heat treatment were useful to increase the reproducibility.[560] The solubility in 0.1 M sulfuric acid at 50 °C was 1.0×10^{-7} mol dm^{-3} (Table 13).

Azuma *et al*. have studied the electrochemical properties of transition metal nitrides prepared by reactive RF sputtering such as ZrN,[563,564] NbN,[564,565] CoN,[566] TiN, and VN.[564] Electrochemical reduction of oxygen was carried out on an amorphous cobalt−nitride thin film electrode prepared by reactive RF sputtering.[566] However, their results were obtained in neutral solution. Zhong *et al*. showed molybdenum nitride (Mo_2N) supported on carbon powder had some catalytic activity for ORR, and the catalysts were stable for 60 h of cell operation.[567]

4.6.2. Catalysts Derived from Macrocycles, Porphyrins, and Composites

A major contribution to the progress in nonprecious metal catalysis in the past decade can be credited to Dodelet and co-workers. Over the years, the focus of the group's research expanded from strictly porphyrin-type materials,[568,569] through macrocycles and noncyclic materials studied together,[570−573] to catalysts synthesized exclusively from noncyclic precursors.[574−579] Catalysts fabricated from macrocycles represent the oldest and arguably the most widely studied category of nonprecious catalysts for oxygen reduction. Initial studies in this area involved macrocycle complexes of transition metals, *e.g.*, cobalt phthalocyanine,[580−582] which were not subjected to high-temperature treatment. However, a vast majority of the later research was devoted to heat-treated catalysts.[583−585]

Recently, there have been a growing number of studies indicating that transition metals may not be required for the reduction of oxygen on carbonaceous materials, once such materials are properly activated, usually via incorporation of ORR-active nitrogen sites. Matter *et al*.[586−589] published a series of papers on the preparation and oxygen reduction activity of catalysts. Although catalysts prepared with iron were the most ORR active, the metal-free catalysts also showed oxygen reduction activity. When addressing the superior activity of Fe-containing catalyst, the authors suggested that, rather than being directly part of the active sites, metal particles might be acting as catalysts for active-site formation during the high-temperature pyrolysis.

Although a vast majority of nonprecious metal catalysts for oxygen reduction in acidic media require heat treatment to prevent fast catalyst corrosion, attempts have been made to synthesize such catalysts without resorting to the destructive high-temperature processing step. Generally, such catalysts rely on protection of the ORR active catalytic site, metal or metal oxide, by some kind of a polymeric matrix, which results in a composite-like structure of the catalyst, either polyaniline,[590] or, more commonly, polypyrrole.[153−157]

A CoPPy composite catalyst supported on Vulcan XC-72 was synthesized and extensively tested by Bashyam *et al*.[591−593] In this case, the heat treatment was found to be of little value, leading to a decrease rather than an increase in the ORR catalytic activity of the catalyst. XAFS study revealed that, depending on the method of catalyst fabrication, the ORR active site was likely to be either "mononuclear" or cobalt-oxide-like. These two mutually exclusive active sites were shown to have similar ORR activity and stability over fairly long operating times of the fuel cell.

Although information on the long-term performance of these types of nonprecious oxygen reduction catalysts, especially under fuel cell operating conditions, is relatively scarce, published data unambiguously point to poor stability as a major problem of such materials. Regardless of which precursor is used, most Co and Fe based catalysts obtained via the pyrolysis process gradually lose their activity under the operating conditions of the PEMFC cathode.[594−599] The rate of activity loss typically depends on the pyrolysis temperature, with catalysts exposed to higher temperatures exhibiting better long-term stability. Dodelet *et al*. demonstrated improved stability of catalysts derived from heat-

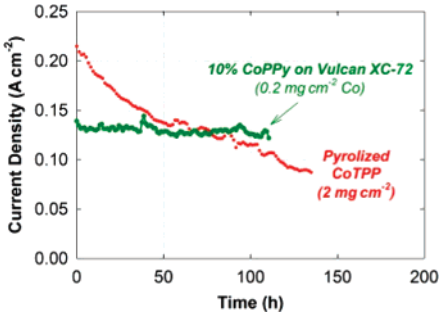

Figure 25. Life test of a hydrogen/air fuel cell operating with a CoPPy catalyst cathode. Life test data for a cell with a pyrolized cobalt tetraphenyl porphyrin cathode are shown for comparison. Cell voltage, 0.40 V; cell temperature, 80 °C.[592]

treating at 900 °C compared to 500 °C or 700 °C.[569] In turn, improved stability of heat-treated cobalt tetraphenylporphyrin (CoPPY) catalysts at 900 °C and 1000 °C was obtained at an expense of activity, which was significantly better for catalysts pyrolized at lower temperatures.[568] In general, even well-performing pyrolized macrocycle catalysts incurred ~50% performance loss in the first 100 h of operation.[593,594,597] Much better long-term stability was demonstrated in a hydrogen−air fuel cell with a CoPPy composite supported on Vulcan XC-72 as shown in Figure 25.[592,593] Unlike a heat-treated cobalt−porphyrin catalyst, the CoPPy composite showed virtually no performance loss during a 100-h life test, outperforming the pyrolized porphyrin catalyst after ~80 h of operation.

The latter case of good catalyst stability notwithstanding, the ORR activity and long-term performance durability of virtually all nonprecious catalysts developed to date are insufficient to make them practical for polymer electrolyte fuel cells. However, the progress recently achieved in the performance of different nonprecious catalysts improves the odds for the development of nonprecious catalysts for the fuel cell cathode in the foreseeable future.

5. Gas Diffusion Layer (GDL)

Many PEMFC researchers have noted that the way the GDL interacts with water changes during lifetime tests. The changes seem to occur at the microstructural level (micrometer to submicrometer) but can be seen macroscopically. Water sprayed on the surface of a fresh GDL bounces off as spherical beads, but water sprayed on the surface of a lifetime-tested GDL adheres to the surface. Evidently, the PEMFC operating environment gradually changes the GDL from hydrophobic to hydrophilic, which can degrade fuel cell operation. For example, gas convection and diffusion are hindered through a GDL after lifetime testing.[287,600−608] Moreover, liquid water saturates the catalyst−ionomer phase in the catalyst layer, restricting gas flow to the active platinum sites in the layer.[15,118,290,609,610] Maintaining the hydrophobic character of the GDL and MPL pores—known as a "GDL hydrophobicity gradient"—is important to maintaining mass transport in the fuel cell during lifetime tests.[611]

The GDL typically consists of two layers bonded together: a macroporous layer made of conductive carbon fibers and a microporous layer (MPL) made of carbon particles and a Teflon binder.[612,613] The MPL enhances electronic contact to and water removal from the catalyst layer.

Our understanding of how a GDL degrades during operation and the effects of its degradation on fuel cell performance is based on only a few recent studies.[604,607,614−619] Unfortunately, there is a large gap in the literature between studies of the GDL's physical properties and studies that relate these properties to PEMFC-durability data.

5.1. Modeling of Transport Processes

The gas diffusion media is the component most responsible for optimal water management in the PEMFC. Without good water management, the fuel cell performance is decreased due to transport losses of the reactants. Transport processes in a fuel cell involve the movement of various species through and between the cell's adjacent layers, each of which consists of different combinations of phases.

The low temperatures at which PEM fuel cells operate imply that the product water is formed as a liquid. This liquid water can collect in the pores of the catalyst layer. The liquid water must be removed to maintain clear gas pathways to the active sites of the catalysts. As a result, gas phase and a liquid phase often compete to occupy the same pores of the catalyst layers and the gas-diffusion media of typical fuel cells.[620] Liquid water in the pores of the gas-diffusion media can also affect the fuel cell's mass transport.

The first fuel cell models to employ porous-electrode theory assumed a constant level of liquid-water content throughout the thickness of the gas-diffusion layer,[621] or they assumed the liquid-water content was zero.[138] Later work modeled the effects of liquid water in the pores of the gas-diffusion layer.[622] For example, Springer *et al*. modeled the effective path lengths of the diffusing gas molecules as functions of water content and monotonically increasing functions of current density. The path length calculated from these functions was assumed to be constant throughout the gas diffusion layer.[623] The modeling showed that the water content in the gas-diffusion layer largely controls the rates of gas-phase mass transport to the catalyst surface. It also showed that the water content is a function not only of operating conditions but also of position within the catalyst layer. Models were developed to examine water content with varying degrees of input from experimental results, but the models consistently show that the water content in the pores strongly depends on the rate of water generation, which critically affects fuel cell performance.[602,624]

5.2. Saturation and GDL Surface Properties

Weber *et al*. describe four separate phases in the catalyst layer: the solid phase, the ionomer phase, the gas phase, and the liquid phase. This last phase is the liquid water in the pores of the catalyst layer.[603] Their model allows for water content that can vary with the capillary pressure in the pores of the catalyst layer and the adjacent gas-diffusion layer; liquid water's permeability and the effective gas diffusivities are strong functions of the water content in the pores. Low water content suggests only limited liquid-phase transport occurs through the GDL; high water content implies that liquid can move relatively easily but gases cannot. The relationship between water content and capillary pressure depends on the physical properties of the porous media, such as the composite contact angle of the pores and the pore-size distribution. Models have been developed to describe the dependence of water content on capillary pressure[625] and how the buildup of liquid droplets in the flow channels depends on the wettability of the GDL surface.[626] These models suggest that changes to surface properties have profound effects on mass transport in fuel cells.

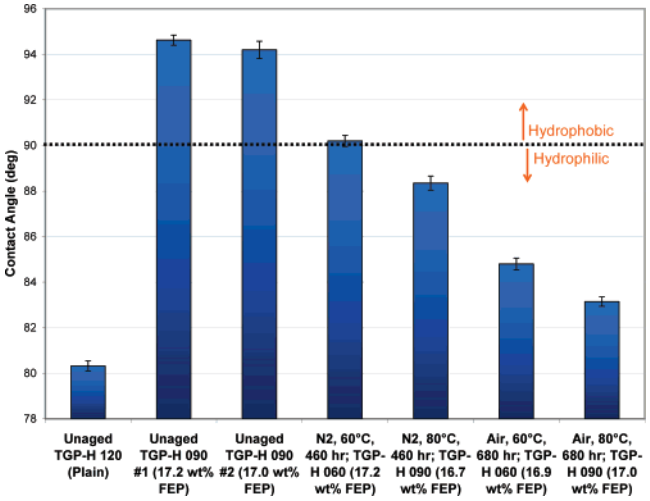

Figure 26. Contact angle measurements of GDL materials before and after aging in various environments. Image is from ref 629.

At present, no models precisely describe how the properties of porous-media surfaces in a fuel cell change as the operating conditions change. However, existing models that predict fuel cell performance for a given set of porous-media surface properties suggest that changing these properties dramatically affects fuel cell performance, especially in ranges of operating conditions for which mass-transport rates are important. Changing the pore size or the surface properties can change the water content in the pores, making the fuel cell prone to either dry out or flooding. Changes in wettability have been observed for carbon supports after prolonged exposure to the fuel cell operating environment,[627] but there is still no mechanistic model that predicts the rates of surface-property changes in the PEM fuel cell environment or correlates those changes with reduced fuel cell performance—except for rerunning the beginning-of-life models using different sets of structural and surface properties.

5.3. Degradation of Mass Transport with Operation

5.3.1. GDL Hydrophobicity Loss

As the GDL's hydrophobicity decreases, so does its mass transport.[5,628] After prolonged exposure to the strong oxidative conditions at the cathode of an operating PEMFC, carbon atoms on the GDL surfaces oxidize to form carboxyl groups or phenols, which are hydrophilic. As a result, the GDL carbon surface becomes more hydrophilic, causing a gradual increase in cathode water uptake during lifetime tests. To study the loss of hydrophobicity of the GDL or the MPL, Wood *et al*. have performed accelerated lifetime tests of GDL materials.[629] These tests aged GDL materials in liquid water, and varied oxygen concentrations and temperature during the aging process. The researchers showed that hydrophobicity decreases with time and increases with temperature and that adding O_2 molecules to the aging process reduced the hydrophobicity more than did elevated temperature alone. The contact-angle measurements of these GDL materials are shown in Figure 26.

Lee and Mérida measured some properties of a GDL after compressing it for 300 h at constant temperature in an *ex situ* test, but they did not measure permeabilities with simultaneous liquid- and vapor-phase transport.[129] During their experiment, the dry-gas-phase permeabilities remained roughly constant, but these experiments did not expose the sample to the high liquid-water intrusion pressures that likely exist in actual cells.

Reviewing durability data from 2003, Wilkinson and St.-Pierre showed that fuel cell performance degrades after MEAs are aged by soaking in deionized water. The fact that performance at low current densities shows only minimal changes after aging suggests that the primary losses are due to reduced mass transport[5] and not due to changing catalyst kinetics. The researchers noted that mass-transport losses can be linked to changes in GDL substrate hydrophobicity and that the sections of the GDL exposed to the channels of the bipolar plate are considerably more hydrophilic after 11,000 h of operation than the adjacent areas beneath the ribs of the current collector. Although focused on catalyst and membrane degradation under high relative-humidity conditions, a durability study conducted at Los Alamos National Laboratory showed that appreciable mass-transport losses occurred after 1,000 h of lifetime testing under constant-current conditions.[335] Moreover, severe mass-transport losses were observed by Liu *et al*. in fuel cell tests under both cyclic- and constant-current conditions. The cyclic tests were aggressive, and hydrogen crossover effectively ended them within 1,000 h, but the test at a constant current density of 1.06 A/cm^2 revealed severe mass-transport losses (>300 mV).[630] Another durability study performed at Ballard indicates that prolonged operation with high water content accelerates degradation, perhaps by forcing water into pores that would otherwise remain open for gas transport.[121] Intermittent interruption of the load—and thus water production (for 30 s during every 30 min of operation)—allowed the cathode mass transport to remain stabilized over considerably longer times.

Few of these studies have quantitatively correlated performance loss with changes in surface properties and the resulting changes in transport properties. One exception is a study by Schulze *et al*. that correlates fuel cell performance changes with the decomposition of PTFE binder in the porous materials.[141] The researchers note that the degradation of PTFE induces performance losses roughly twice as large as those associated with the loss of platinum surface area after 1,000 h of fuel cell operation.

Current understanding suggests that changes to the microstructure and surface characteristics of gas-diffusion media can cause changes in the water-content levels and transport properties of those media. Some durability studies have confirmed this idea, but there is still little information about the rate at which wettability changes or which key properties that determine a composite contact angle are most susceptible to degradation. Thorough studies of how liquid water enters pores whose hydrophobicity has been degraded to various degrees will be necessary to design GDL materials that adequately resist this type of degradation.

5.3.2. GDL Carbon Corrosion and Loss

It has recently been reported that carbon supports degrade during start-up and shutdown,[153] when large fluctuations in potential occur, or during fuel starvation.[121,147,148] In these situations, the cathode or anode potential drastically increases, causing carbon corrosion. Although the Teflon used in GDLs is stable against chemical corrosion and large fluctuations in potential or temperature, the carbon in the GDL/MPL is not and can be oxidized at high potentials. Kuriki *et al*. used mass-spectrometric cyclic voltammetry

(MSCV) to analyze fuel cell exhaust, which presumably contains gaseous products of carbon degradation. They concluded that carbon was directly oxidized to carbon dioxide above 0.8 V.[631] These corrosion mechanisms pertain to carbon used as an electrocatalyst support, but the carbon powder in the MPL can also be corroded in the environment of an operating fuel cell. One way to reduce carbon loss in the MPL would be to use corrosion-resistant carbons, graphitized to a higher degree than the carbon black. Porosimetry measurements can indicate that carbon is lost from the MPL during fuel cell operation.[629] The mercury and water porosimetry measurements have shown that the GDL pore structure changes during lifetime tests. Large-pore (30−60 μm diameter) volume has decreased, while small-pore volume increases. The loss in large-pore volume is likely due to irreversible compression due to the fuel cell compression.[143]

Delamination of the MPL from the GDL substrate has not been widely reported but may occur during freeze−thaw cycles, as occurs with catalyst-layer delamination from the membrane.[627,632] Cappadonia *et al*. reported that water in a Nafion membrane partially freezes around −20 °C, but unfrozen water remains in the membrane even at much lower temperature.[122] A different situation occurs in the GDL/MPL, where the pore diameters are on the order of a micron or larger and the water is not subject to the sulfonic acid of the ionomer. The volume expansion caused by ice formation can produce large isotropic stresses that can damage the structure of the catalyst layer, the MPL, or the GDL.

5.3.3. Mechanical Degradation of GDLs

There are only a few literature papers which examine mechanical degradation and review the effect of compression of gas-diffusion layers on the performance of PEM fuel cells.[129,633−636] SGL Carbon presented a relationship between in-plane resistance and compression stress of GDLs.[635] Lee and Mérida characterized some GDL properties after 300 h of compression at constant temperature in an *ex situ* test and found the dry gas-phase permeabilities remained roughly constant.[129]

A study on the effect of fuel cell compression by adjusting the bolt torque for different GDL materials found an optimal bolt torque for GDL materials with MPLs.[633] The researchers explained this optimum in terms of changes in the GDL's porosity and electrical-contact resistance. For GDLs without an MPL, less torque gives the highest power, with an indication that higher torque may damage the GDL.

6. Summary

This review article discusses one of the major remaining barriers to commercialization of fuel cells, namely durability. The correlation of durability with cost cannot be overlooked in developing fuel cell systems, as the two are interrelated in materials. In this review, we present some of the targets for PEM fuel cell systems as set by the U.S. DOE (Department of Energy) and Japanese NEDO (New Energy & Industrial Technology Development Organization). We discuss durability testing and effects that operating conditions have on fuel cell durability. Then we cover the internal component durability of fuel cells, considering the polymer−electrolyte membrane, the electrocatalyst and electrocatalyst support, and the gas diffusion media. As PEM fuel cell technology has advanced in terms of performance and cost, more emphasis has recently been put on durability, which is hopefully one of the final steps on the road to commercialization.

7. Acknowledgments

On August 27−30 of 2006, 56 researchers from National Laboratories and Universities from the United States and Japan involved with hydrogen and PEM fuel cells conducted a workshop in Santa Fe, New Mexico. The topic of the workshop was specifically to discuss PEM Fuel Cell Degradation. This review discusses the Scientific Aspects of Polymer Electrolyte Fuel Cell Durability and is written by the contributors at this workshop. The contributing authors all participated in the workshop and the preparation of this journal article. Much of the effort to compile the manuscript was funded by the U.S. DOE Office of Hydrogen, Fuel Cells and Infrastructure Technologies and by Japan's New Energy and Industrial Technology Development Organization.

8. References

(1) Perry, M. L.; Fuller, T. F. *J. Electrochem. Soc.* **2002**, *149*, S59.
(2) Chalk, S. G.; Miller, J. F. *J. Power Sources* **2006**, *159*, 73.
(3) Fowler, M.; Mann, R. F.; Amphlett, J. C.; Peppley, B. A.; Roberge, P. R. In *Handbook of Fuel Cells, Fundamentals, Technology and Applications*; Vielstich, W., Gasteiger, H. A., Lamm, A., Eds.; 2003; Vol. 3, p 663.
(4) Wilson, M. S.; Garzon, F. H.; Sickafus, K. E.; Gottesfeld, S. *J. Electrochem. Soc.* **1993**, *140*, 2872.
(5) Wilkinson, D. P.; St.-Pierre, J. In *Handbook of Fuel Cells: Fundamentals, Technology, and Applications*; Vielstich, W., Lamm, A., Gasteiger, H. A., Eds.; 2003; Vol. 3, p 611.
(6) U.S. DOE, http://www1.eere.energy.gov/hydrogenandfuelcells/mypp/, 2007.
(7) NEDO homepage: http://www.nedo.go.jp/nenryo/gijutsu/index.html, 2007.
(8) European Technology Platform for Hydrogen and Fuel Cells (HFP), www.HFPeurope.org, 2007.
(9) Appleby, A. J.; Foulkes, F. R. *Fuel Cell Handbook*; Van Nostrand Rheinhold: New York, NY, 1989.
(10) Crowe, B. J. NASA Report SP-5115; 1973.
(11) Raistrick, L. D. *Electrochem. Soc. Proc. Ser.* **1986**, *PV 86−13*, 172.
(12) Ticianelli, E.; Derouin, C.; Redondo, A.; Srinivasan, S. *J. Electrochem. Soc.* **1988**, *135*, 2209.
(13) Ticianelli, E.; Derouin, C.; Srinivasan, S. *J. Electroanal. Chem.* **1988**, 251.
(14) Wilson, M. S.; Gottesfeld, S. *J. Appl. Electrochem.* **1992**, 22.
(15) Wilson, M. S.; Gottesfeld, S. *J. Electrochem. Soc.* **1992**, *139*, L28.
(16) Uchida, M.; Aoyama, Y.; Eda, N.; Ohta, A. *J. Electrochem. Soc.* **1995**, *142*, 463.
(17) Borup, R. L.; Davey, J. R.; Garzon, F. H.; Wood, D. L.; Inbody, M. A. *J. Power Sources* **2006**, *163*, 76.
(18) Borup, R.; Inbody, M.; Guidry, D.; Pacheco, S.; Tafoya, J. *Fuel Cell Semin. Abstr.* **2003**, 134.
(19) Wood, D. L.; Xie, J.; Pacheco, S. D.; Davey, J. R.; Borup, R. L.; Garzon, F. H.; Atanassov, P. *Fuel Cell Semin. Abstr.* **2004**.
(20) U.S. DOE, *Durability test Protocol for PEM Fuel Cells*, 2005.
(21) U.S. DOE, *Solicitation announcement DE-PS36-06GO96018*, 2006.
(22) Lane, D.; Teather, E.; Rockward, T. Q.; Uribe, F. A.; McNeil, D.; Bailey, R.; Pien, M. *Fuel Cell Semin. Abstr.* **2004**, 303.
(23) U.S. DOE, *Cell Component Accelerated Stress Test Protocols for PEM Fuel Cells*, 2007.
(24) Ciureanu, M.; Wang, H *J. Electrochem. Soc.* **1999**, *146*, 4031.
(25) Garcia, G.; Silva-Chong, J. A.; Guillen-Villafuerte, O.; Rodriguez, J. L.; Gonzalez, E. R.; Pastor, E. *Catal. Today* **2006**, *116*, 415.
(26) Hayter, P.; Mitchell, P.; Dams, R.; Dudfield, C.; Gladding, N. *ETSUF/02/00126/REP, Prep. Dept. of Trade and Industry*, 1997.
(27) JARI. *Japan Automobile Research Institute*, 2004, http://www.hnei.hawaii.edu/JARI.pdf.
(28) Mikkola, M.; Rockward, T.; Stenersen, E.; Uribe, F. *205th Meeting of the Electrochemical Society*, 2004.
(29) Mikkola, M. S.; Rockward, T.; Uribe, F. A.; Pivovar, B. S. *Fuel Cells Fund. Sys.* **2007**, *07*, 153.
(30) Mohtadi, R.; Lee, W. K.; Cowan, S.; Van Zee, J. W.; Murthy, M. *Electrochem. Solid-State Lett.* **2003**, *6*, A272.
(31) Mohtadi, R.; Lee, W. K.; Van Zee, J. W. *J. Power Sources* **2004**, *138*, 216.

(32) Moore, J. M.; Adcock, P. L.; Lakeman, J. B.; Mepsted, G. O. *J. Power Sources* **2000**, *85*, 254.
(33) Mukerjee, S.; Urian, R. C. *Electrochim. Acta* **2002**, *47*, 3219.
(34) Myers, D.; Ahluwalia, R.; Kumar, R. *Annual DOE Fuel Cell Program Review*, 2006.
(35) Myers, D.; Wang, X.; Papadias, D.; Ahluwalia, R.; Wang, X.; Kuma, R. *2nd Annual MEA Manufacturing Conference*, 2006.
(36) Pino, L.; Recupero, V.; Lagana, M.; Minutoli, M. *Abstr. Fuel Cell Semin.* **1998**, *10*, 671.
(37) Rockward, T.; Uribe, F. *Electrochem. Soc. Meeting Abstracts*, 2005.
(38) Soto, H. J., Univ. of South Carolina, 2005, Avail. UMI, Order No. DA3173194, 107.
(39) Thampan, T.; Rocheleau, R.; Bethune, K.; Wheeler, D. *Mater. Res. Soc. Symp. Proc.* **2006**, *Volume Date 2005*, 21.
(40) Uribe, F.; Zawodzinski, T., Jr. *200th Meeting Electrochem. Soc.* **2001**, Abstract 339.
(41) Uribe, F.; Valerio, J.; Rockward, T.; Stenersen, E. *205th Meeting Electrochem. Soc.* **2004**, Abstract 332.
(42) Uribe, F.; Rockward, T. LANL Provisional Patent Application #97B96, 2005.
(43) Uribe, F. A.; Gottesfeld, S.; Zawodzinski, T. A., Jr. *J. Electrochem. Soc.* **2002**, *149*, A293.
(44) Veldhuis, J.; deBruijn, F.; Mallant, R. *Abstr. Fuel Cell Semin.* **1998**, *47*, 598.
(45) Garzon, F.; Brosha, E.; Pivovar, B.; Rockward, T.; Springer, T.; Uribe, F.; Urdampilleta, I.; Valerio, J. *2006 Annual DOE Fuel Cell Program Review*, 2006.
(46) Semmelsberger, T. A. Ph.D. Thesis, Case Western Reserve University, 2005.
(47) Gu, T.; Lee, W.-k.; Van Zee, J. W.; Murthy, M. *Proc. Electrochem. Soc.* **2002**, *Proton Conducting Membrane Fuel Cells III*, 287.
(48) Gu, T.; Lee, W.-k.; Van Zee, J. W. *Appl. Catal., B* **2005**, *56*, 43.
(49) Amphlett, J.; Baumert, R. M.; Mann, R. F.; Peppley, B. A.; Roberge, P. R.; Rodrigues, A. *Abstr. Am. Chem. Soc.* **1993**, *206*.
(50) Benesch, R.; Jacksier, T. *J. Am. Chem. Soc.* **2005**, *127*, 14607.
(51) Bhatia, K.; Wang, C. Y. *Electrochim. Acta* **2004**, *49*, 2333.
(52) Ciureanu, M.; Wang, H. *J. New Mater. Electrochem. Syst.* **2000**, *3*, 107.
(53) Jiang, R.; Kunz, H. R.; Fenton, J. M. *205th Meeting Electrochem. Soc.*, 2004, p 674.
(54) Krishnan, P.; Park, J. S.; Kim, C. S. *J. Power Sources* **2006**, *159*, 817.
(55) Lee, W.; Van Zee, J. W.; Murthy, M. *Fuel Cells* **2003**, *3*, 52.
(56) Murthy, M.; Esayian, W.; Hobson, A.; MacKenzie, S.; Woo-kum, L.; Glandt, J.; Van Zee, J. W. *4th Int. Sym. on New Mater. for Electrochemical Systems* **2001**, 281.
(57) Qi, Z.; He, C. Z.; Kaufman, A. *J. Power Sources* **2002**, *111*, 239.
(58) Qi, Z.; Kaufman, A. *J. Power Sources* **2003**, *113*, 115.
(59) Si, Y.; Jiang, R. C.; Lin, J. C.; Kunz, H. R.; Fenton, J. M. *J. Electrochem. Soc.* **2004**, *151*, A1820.
(60) Sung, L.; Yan, Y. Y.; Chu, H. S.; Shyu, R. J. *Fuel Cell Sci., Eng. Technol.* **2004**, 621.
(61) Thampan, T.; Rocheleau, R.; Bethune, K.; Wheeler, D. *MRS Meeting, The Hydrogen Cycle-Generation, Storage and Fuel Cells. Sym.*, 2005.
(62) Yongchao, S.; Ruichun, J.; Jung-Chou, L.; Kunz, H. R.; Fenton, J. M. *J. Electrochem. Soc.* **2004**, *151*, A1820.
(63) Zhang, J.; Thampan, T.; Datta, R. *J. Electrochem. Soc.* **2002**, *149*, A765.
(64) Baschuk, J.; Rowe, A. M.; Li, X. G. *Am. Soc. Mech. Eng.* **2002**, *1*, 55.
(65) Baschuk, J.; Rowe, A. M.; Li, X. G. *Trans. ASME J. Energy Resources Technol.* **2003**, *125*, 94.
(66) Baschuk, J.; Xianguo, L. *Int. J. Global Energy Issues* **2003**, *20*, 245.
(67) Baschuk, J. J.; Li, X. G. *Int. J. Energy Res.* **2003**, *27*, 1095.
(68) Chu, H.; Wang, C. P.; Liao, W. C.; Yan, W. M. *J. Power Sources* **2006**, *159*, 1071.
(69) Janssen, G.; De Heer, M. P.; Papageorgopoulos, D. C. *Fuel Cells* **2004**, *4*, 169.
(70) Korsgaard, A. R.; Nielsen, M. P.; Bang, M.; Kaer, S. K. *Proc. of 4th Int. ASME Conf. on Fuel Cell Science FUELCELL2006*, 2006.
(71) Liu, P.; Logadottir, A.; Norskov, J. K. *Electrochim. Acta* **2003**, *48*, 3731.
(72) Murthy, M.; Moore, D. *206th Meeting of the Electrochem. Soc.*, 2004, p 1886.
(73) Rodrigues, A.; Amphlett, J. C.; Mann, R. F.; Peppley, B. A.; Roberge, P. R. *Proc. 32nd Intersociety Energy Conversion Eng. Conf.* **1997**, *2*, 768.
(74) Springer, T. E.; Rockward, T.; Zawodzinski, T. A.; Gottesfeld, S. *J. Electrochem. Soc.* **2001**, *148*, A11.
(75) Thirumalai, D.; Zawodzinski, T. A.; Springer, T. E.; Gottesfeld, S. *Abstr. Electrochem. Soc.* **1997**.
(76) Wang, C.; Chu, H. S. *J. Power Sources* **2006**, *159*, 1025.
(77) Wang, C.-P.; Chu, H.-S. *Proc. of 4th Int. ASME Conference on Fuel Cell Science FUELCELL2006*, 2006.
(78) Yan, Q.; Liu, Q.; Wu, J. *206th Meeting Electrochem. Soc. Abstracts* **2004**, 1964.
(79) Yan, W.; Chu, H. S.; Wang, C. P.; Liao, W. C. *J. Power Sources* **2006**, *159*, 1071.
(80) Zhang, J.; Fehribach, J. D.; Datta, R. *Proc.—Electrochem. Soc.* **2005**, *P2003−30*, 134.
(81) Zhou, T.; Liu, H. *Fuel Cell Sci., Eng. Technol.* **2003**.
(82) Chu, H. S.; Wang, C. P. *J. Power Sources* **2006**, *159*, 1025.
(83) Adams, W.; Blair, J.; Bullock, K. R.; Gardner, C. L. *J. Power Sources* **2005**, *145*, 55.
(84) Adcock, P. A.; Pacheco, S.; Brosha, E.; Zawodzinski, T. A.; Uribe, F. A. *Proc.—Electrochem. Soc.* **2005**, *P2002−31*, 159.
(85) Carrette, L.; Friedrich, K. A.; Huber, M.; Stimming, U. *Phys. Chem. Chem. Phys.* **2001**, *3*, 320.
(86) Divisek, J.; Oetjen, H. F.; Peinecke, V.; Schmidt, V. M.; Stimming, U. *Electrochim. Acta* **1998**, *43*, 3811.
(87) Rohland, B.; Plzak, V. *J. Power Sources* **1999**, *84*, 183.
(88) Wan, C.-H.; Zhuang, Q.-H. *Electrochim. Acta* **2007**, *52*, 4111.
(89) Gottesfeld, S.; Pafford, J. *J. Electrochem. Soc.* **1988**, *135*, 2651.
(90) Allan, D. E.; Wilkinson, D. P.; Chow, C. Y. F.; Johannes, E. P.; Roberts, J. A.; St-Pierre, J.; Longley, C. J.; Chan, J. K. K. PCT Int. Appl. WO9934465, 1999.
(91) Knights, S. D.; Lauritzen, M. V.; Vohra, R.; Wilkinson, D. P. Eur. Pat. Appl. EP 1017121, 2000.
(92) Roberts, J.; Van der Geest, M.; St-Pierre, J.; Wilkinson, D. P.; Lee, A.; Moroz, S. U.S. Patent 6,329,089, 2001.
(93) St-Pierre, J.; Wilkinson, D. P.; Campbell, S. A. U.S. Patent Appl. Publ. 2003010629, 2003.
(94) Wilkinson, D. P.; Knights, S. D.; Lauritzen, M. V. PCT Int. Appl. EP0736921, 2000.
(95) Wilkinson, D. P.; Thompsett, D. *Proc. of the Int. Sym. on New Materials for Fuel Cell and Modern Battery Systems*, **1997**, 266.
(96) Wilkinson, D. P.; Voss, H. H.; Dudley, J.; Lamont, G. J.; Basura, V. PCT Int. Appl. WO9508850, 1995.
(97) Wilkinson, D. P.; Voss, H. H.; Dudley, J.; Lamont, G. J.; Basura, V. PCT Int. Appl. WO 9508851, 1995.
(98) Wilkinson, D. P.; Voss, H. H.; Dudley, J.; Lamont, G. J.; Basura, V. U.S. Patent 5,482,680, 1996.
(99) Wilkinson, D. P.; Voss, H. H.; Prater, K. B.; Hards, G. A.; Ralph, T. R.; Thompsett, D. Eur. Patent EP0736921, 1996.
(100) Crabb, E.; Marshall, R.; Thompsett, D. *J. Electrochem. Soc.* **2000**, *147*, 4440.
(101) Holleck, G.; Pasquariello, D. M.; Clauson, S. L. *Second Int. Sym. on Proton Conducting Membrane Fuel, Cells II* **1998**, 150.
(102) Isono, T. S.; Kaneko, M.; Akiyama, Y.; Miyake, Y.; Yonezu, I. *J. Power Sources* **2000**, *86*, 269.
(103) Mukerjee, S.; Lee, S. J.; Ticianelli, E. A.; McBreen, J.; Grgur, B. N.; Markovic, N. M.; Ross, P. N.; Giallombardo, J. R.; De Castro, E. S. *Electrochem. Solid-State Lett.* **1999**, *2*, 12.
(104) Papageorgopoulos, D.; Keijzer, M.; de Bruijn, F. A. *Electrochim. Acta* **2002**, *48*, 197.
(105) Santiago, E.; Giz, M. J.; Ticianelli, E. A. *J. Solid State Electrochem.* **2003**, *7*, 607.
(106) Stevens, D.; Rouleau, J. M.; Mar, R. E.; Atanasoski, R. T.; Schmoeckel, A. K.; Debe, M. K.; Dahn, J. R. *ECS Trans.* **2006**, *3*, 355.
(107) Gasteiger, H.; Markovic, N. M.; Ross, P. N. *J. Phys. Chem.* **1995**, *99*, 16757.
(108) Lee, S.; Mukerjee, S.; Ticianelli, E. A.; McBreen, J. *Electrochim. Acta* **1999**, *44*, 3283.
(109) Rheaume, J.; Muller, B.; Schulze, M. *J. Power Sources* **1998**, *76*, 60.
(110) Roth, C.; Benker, N.; Buhrmester, T.; Mazurek, M.; Loster, M.; Fuess, H.; Koningsberger, D. C.; Ramaker, D. E. *J. Am. Chem. Soc.* **2005**, *127*, 14607.
(111) Strmcnik, D.; Gaberscek, A.; Hocevar, S.; Jamnik, J. *Solid State Ionics, Diffus. React.* **2005**, *176*, 1759.
(112) Garzon, F.; Brosha, E.; Pivovar, B.; Rockward, T.; Valerio, J.; Uribe, F. *U.S. DOE Hydrogen Program Review* **2005**.
(113) Uribe, F. *U.S. DOE Hydrogen Program Review* **2004**.
(114) Krumpelt, M.; Krause, T. R.; Carter, J. D.; Kopasz, J. P.; Ahmed, S. *Catal. Today* **2002**, *77*, 3.
(115) Cho, E.; Ko, J.-J.; Ha, H. Y.; Hong, S.-A.; Lee, K.-Y.; Lim, T.-W.; Oh, I.-H. *J. Electrochem. Soc.* **2003**, *150*, A1667.
(116) Mukundan, R.; Kim, Y. S.; Garzon, F.; Pivovar, B. *ECS Trans.* **2005**, *1*, 403.
(117) Simpson, S. F.; Salinas, C. E.; Cisar, A. J.; Murphy, O. J. *First Int. Sym. on Proton Conducting Membrane Fuel Cells, Electrochem. Soc.*, 1995, p 182.
(118) Wilson, M. S.; Valerio, J. A.; Gottesfeld, S. *Electrochim. Acta* **1995**, *40*, 355.

(119) Deryu, C.; Jiang, R.; Gardner, K.; Jacobs, R.; Schmidt, J.; Quakenbush, T.; Stephens, J. *J. Power Sources* **2001**, *96*, 174.
(120) Oszcipok, M.; Riemann, D.; Kronenwett, U.; Kreideweis, M.; Zedda, A. *J. Power Sources* **2005**, *145*, 407.
(121) Knights, S. D.; Colbow, K. M.; St-Pierre, J.; Wilkinson, D. P. *J. Power Sources* **2004**, *127*, 127.
(122) Cappadonia, M.; Erning, J. W.; Stimming, U. *J. Electroanal. Chem.* **1994**, *376*, 189.
(123) Siu, A.; Schmeisser, J.; Holdcroft, S. *J. Phys. Chem. B* **2006**, *110*, 6072.
(124) Yoshida, H.; Miura, Y. *J. Membr. Sci.* **1992**, *68*, 1.
(125) Thompson, E. L.; Capehart, T. W.; Fuller, T. J.; Jorne, J. *J. Electrochem. Soc.* **2006**, *153*, A2351.
(126) McDonald, R. C.; Mittelsteadt, C. K.; Thompson, E. L. *Fuel Cells* **2004**, *4*, 208.
(127) Guo, Q. H.; Qi, Z. G. *J. Power Sources* **2006**, *160*, 1269.
(128) He, S.; Mench, M. *J. Electrochem. Soc.* **2006**, *153*, A1724.
(129) Lee, C.; Merida, W. *J. Power Sources* **2007**, *164*, 141.
(130) *Fuel Cell Operations at SubFreezing Temperatures Workshop*, http://www1.eere.energy.gov/hydrogenandfuelcells/fc_freeze_workshop.html, 2005.
(131) Cho, E.; Ko, J.-J.; Ha, H. Y.; Hong, S.-A.; Lee, K.-Y.; Lim, T.-W.; Oh, I.-H. *J. Electrochem. Soc.* **2004**, *151*, A661.
(132) Hishinuma, Y.; Chikahisa, T.; Kagami, F.; Ogawa, T. *JSME Int. J. Ser. B, Fluids Thermal Eng.* **2004**, *47*, 235.
(133) Qiangu, Y.; Toghiani, H.; Young-Whan, L.; Kaiwen, L.; Causey, H. *J. Power Sources* **2006**, *160*, 1242.
(134) Ishikawa, Y.; Morita, T.; Nakata, K.; Yoshida, K.; Shiozawa, M. *J. Power Sources* **2007**, *163*, 708.
(135) Oszcipok, M.; Zedda, M.; Riemann, D.; Geckeler, D. *J. Power Sources* **2006**, *154*, 404.
(136) Ahluwalia, R. K.; Wang, X. *J. Power Sources* **2006**, *162*, 502.
(137) Pesaran, A. A.; Kim, G.-H.; Gonder, J. D. http://www.nrel.gov/hydrogen/pdfs/pem_fc_freeze_milestone.pdf, 2006.
(138) Fuller, T. F.; Newman, J. *J. Electrochem. Soc.* **1993**, *140*, 1218.
(139) Jerkiewicz, G.; Vatankhah, G.; Lessard, J.; Soriaga, M. P.; Park, Y. S. *Electrochim. Acta* **2004**, *49*, 1451.
(140) Kinoshita, K.; Bett, J. A. S. *Carbon* **1974**, *12*, 525.
(141) Schulze, M.; Wagner, N.; Kaz, T.; Friedrich, K. A. *Electrochim. Acta* **2007**, *52*, 2328.
(142) Patterson, T. 2002 AIChE Spring National Meeting, 2002; p 313.
(143) Darling, R. M.; Meyers, J. P. *J. Electrochem. Soc.* **2003**, *150*, A1523.
(144) Darling, R. M.; Meyers, J. P. *J. Electrochem. Soc.* **2005**, *152*, A242.
(145) Komanicky, V.; Chang, K. C.; Menzel, A.; Markovic, N. M.; You, H.; Wang, X.; Myers, D. *J. Electrochem. Soc.* **2006**, *153*, B446.
(146) Wang, X., X.; Kumar, R.; Myers, D. J. *Electrochem. Solid-State Lett.* **2006**, *9*, A225.
(147) Taniguchi, A.; Akita, T.; Yasuda, K.; Miyazaki, M. *J. Power Sources* **2004**, *130*, 42.
(148) Wilkinson, D. P. In *202nd Meeting of Electrochemical Society*, Salt Lake City, Utah, 2002.
(149) Meyers, J. P.; Darling, R. M. *J. Electrochem. Soc.* **2006**, *153*, A1432.
(150) Gu, W.; Makharia, R.; Yu, P. T.; Gasteiger, H. A. *Prepr. Symp.—Am. Chem. Soc., Div. Fuel Chem.* **2006**, *52*, 692.
(151) Makharia, R.; Kocha, S. S.; Yu, P. T.; Sweikart, M. A.; Gu, W.; Wagner, F. T.; Gasteiger, H. A. *ECS Trans.* **2006**, *1*, 3.
(152) Barton, H. R. U.S. Patent 6,724,194, 2004.
(153) Reiser, C. A.; Bregoli, L.; Patterson, T. W.; Yi, J. S.; Yang, J. D.; Perry, M. L.; Jarvi, T. D. *Electrochem. Solid-State Lett.* **2005**, *8*, A273.
(154) Patterson, T. W.; Darling, R. M. *Electrochem. Solid-State Lett.* **2006**, *9*, A183.
(155) Pekula, N.; Heller, K.; Chuang, P. A.; Turhan, A.; Mench, M. M.; Brenizer, J. S.; Unlu, K. *Nucl. Instrum. Methods Phys. Res. Sect. a-Accelerators Spectrometers Detectors Associated Equipment* **2005**, *542*, 134.
(156) Perry, M. L.; Patterson, T. W.; Reiser, C. *ECS Trans.* **2006**, *3*, 783.
(157) Yan, X. Q.; Hou, M.; Sun, L. Y.; Cheng, H. B.; Hong, Y. L.; Liang, D.; Shen, Q.; Ming, P. W.; Yi, B. L. *J. Power Sources* **2007**, *163*, 966.
(158) Kusoglu, A.; Karlsson, A. M.; Santare, M. H.; Cleghorn, S.; Johnson, W. B. *J. Power Sources* **2006**, *161*, 987.
(159) Huang, X. Y.; Solasi, R.; Zou, Y.; Feshler, M.; Reifsnider, K.; Condit, D.; Burlatsky, S.; Madden, T. *J. Polym. Sci., Part B: Polym. Phys.* **2006**, *44*, 2346.
(160) LaConti, A. B.; Hamdan, M.; McDonald, R. C. In *Handbook of Fuel Cells-Fundamentals, Technology and Application*; Vielstich, W., Gasteiger, H. A., Lamm, A., Eds.; John Wiley & Sons: New York, 2003; Vol. 3.
(161) Banerjee, S.; Curtin, D. E. *J. Fluorine Chem.* **2004**, *125*, 1211.
(162) Steck, A. *Proc. 1st Int. Sym. New Materials for Fuel Cell Systems*, 1995; Savagodo, O., Roberge, P. R., Veziroglu, T. N., Eds.; p 74.
(163) Hickner, M. A.; Ghassemi, H.; Kim, Y. S.; Einsla, B. R.; McGrath, J. E. *Chem. Rev.* **2004**, *104*, 4587.
(164) Stucki, S.; Scherer, G. G.; Schlagowski, S.; Fischer, E. *J. Appl. Electrochem.* **1998**, *28*, 1041.
(165) Borup, R. *DOE Hydrogen Program Review*, 2004.
(166) Curtin, D. E.; Lousenberg, R. D.; Henry, T. J.; Tangeman, P. C.; Tisack, M. E. *J. Power Sources* **2004**, *131*, 41.
(167) Steck, A. E.; Stone, C. Proceedings of the 2nd International Symposium on New Materials for Fuel Cell and Modern Battery Systems, Montreal, 1997; p 792.
(168) Wei, J.; Stone, C.; Steck, A. E. U.S. Patent 5,422,411, 1995.
(169) Yu, J.; Yi, B.; Xing, D.; Liu, F.; Shao, Z.; Fu, Y.; Zhang, H. *Phys. Chem. Chem. Phys.* **2003**, *5*, 611.
(170) Buchi, F. N.; Gupta, B.; Haas, O.; Scherer, G. G. *Electrochim. Acta* **1995**, *40*, 345.
(171) Gubler, L.; Kuhn, H.; Schmidt, T. J.; Scherer, G. G.; Brack, H. P.; Simbeck, K. *Fuel Cells* **2004**, *4*, 196.
(172) Wang, H.; Capuano, G. A. *J. Electrochem. Soc.* **1998**, *145*, 780.
(173) Rozière, J.; Jones, D. J. *Annu. Rev. Mater. Res.* **2003**, *33*, 503.
(174) Aoki, M.; Chikashige, Y.; Miyatake, K.; Uchida, H.; Watanabe, M. *Electrochem. Commun.* **2006**, *8*, 1412.
(175) Gubler, L.; Prost, N.; Gursel, S. A.; Scherer, G. G. *Solid State Ionics* **2005**, *176*, 2849.
(176) Soczka-guth, T.; Baurmeister, J.; Frank, G.; Kanuf, R. US, 2002; Vol. 6,355,149.
(177) Faure, S.; Cornet, N.; Gebel, G.; Mercier, R.; Pineri, M.; Sillion, B. 2nd International Symposium on New Materials for Fuel Cell and Modern Battery Systems, 1997; p 818.
(178) Asano, N.; Aoki, M.; Suzuki, S.; Miyatake, K.; Uchida, H.; Watanabe, M. *J. Am. Chem. Soc.* **2006**, *128*, 1762.
(179) Wang, J.-T.; Savinell, R. F.; Wainright, J.; Litt, M.; Yu, H. *Electrochim. Acta* **1996**, *41*, 193.
(180) Frank, G. In *Proc. 2nd European PEFC Forum*, 2003.
(181) Li, Q.; He, R.; Jensen, J. O. *Fuel Cells* **2004**, *4*, 147.
(182) Xiao, L. X.; Zhang, H. F.; Scanlon, E.; Ramanathan, L. S.; Choe, E. W.; Rogers, D.; Apple, T.; Benicewicz, B. C. *Chem. Mater.* **2005**, *17*, 5328.
(183) Schmidt, T. J. 208th Meeting Electrochem. Soc., Los Angeles, 2005; p 2197.
(184) Lakshmanan, B.; Huang, W.; Olmeijer, D.; Weidner, J. W. *Electrochem. Solid-State Lett.* **2003**, *6*, A282.
(185) Protsailo, L. 2006 DOE Hydrogen Program Review, Arlington, VA, 2006.
(186) Cleghorn, S. J. C.; Mayfield, D. K.; Moore, D. A.; Moore, J. C.; Rusch, G.; Sherman, T. W.; Sisofo, N. T.; Beuscher, U. *J. Power Sources* **2006**, *158*, 446.
(187) Endoh, E.; Terazono, S.; Widjaja, H. In *Electrochem. Soc. Abstracts*, Salt Lake City, UT, 2002.
(188) Inaba, M.; Yamada, H.; Umebayashi, R.; Sugishita, M.; Tasaka, A. *Electrochemistry* **2007**, *75*, 207.
(189) Luo, Z.; Li, D.; Tang, H.; Pan, M.; Ruan, R. *Int. J. Hydrogen Energy* **2006**, *31*, 1831.
(190) Oomori, Y.; Yamazaki, O.; Tabata, T. In *11th FCDIC Fuel Cell Symp.*; FCDIC: Tokyo, 2003.
(191) Yoshioka, S.; Yoshimura, A.; Fukumoto, H.; Horii, O.; Yoshiyasu, H. *Fuel Cell Bull.* **2005**, *3*, 11.
(192) Yu, J.; Matsuura, T.; Yoshikawa, Y.; Islam, M. N.; Hori, M. *Phys. Chem. Chem. Phys.* **2005**, *7*, 373.
(193) Yan, Q.; Wu, J. *207th Meeting Electrochem. Soc.*, 2005; MA2005-01, abstract # 1514.
(194) Ohma, A.; Suga, S.; Yamamoto, S.; Shinohara, K. *ECS Trans.* **2006**, *3*, 519.
(195) Inaba, M.; Kinumoto, T.; Kiriake, M.; Umebayashi, R.; Tasaka, A.; Ogumi, Z. *Electrochim. Acta* **2006**, *51*, 5746.
(196) Teranishi, K.; Kawata, K.; Tsushima, S.; Hirai, S. *Electrochem. Solid-State Lett.* **2006**, *9*, A475.
(197) Qiao, J.; Saito, M.; Hayamizu, K.; Okada, T. *J. Electrochem. Soc.* **2006**, *153*, A967.
(198) Mittal, V. O.; Kunz, H. R.; Fenton, J. M. *J. Electrochem. Soc.* **2006**, *153*, A1755.
(199) Mathias, M. F.; Makharia, R.; Gasteiger, H. A.; Conley, J. J.; Fuller, T. J.; Gittleman, C. J.; Kocha, S. S.; Miller, D. P.; Mittelsteadt, C. K.; Xie, T.; Yan, S. G.; Yu, P. T. *Interface* **2005**, *14*, 24.
(200) Hicks, M. 2006 DOE Hydrogen Program Review, Washington DC, 2006.
(201) LaConti, A. B.; Liu, H.; Mittelsteadt, C.; McDonald, R. C. *ECS Trans.* **2006**, *1*, 199.
(202) LaConti, A. B. In *ACS Polymer Division Topical Workshop on Perfluorinated Ionomer Membranes*, Lake Buena Vista, FL, 1982.
(203) LaConti, A. B.; Fragala, A. R.; Boyack, J. R. In *Proceeding of the Symposium on Electrode Materials and Process for Energy Conversion and Storage*; McIntyre, J. D. E., Will, S. S., F. G., Eds.; The Electrochemical Society, Inc.: Princeton, NJ, 1977.

(204) Damjanovic, A. *Modern Aspects of Electrochemistry*; Plenum: New York, 1969; Vol. 5.
(205) Tarasevich, M. R.; Sadkowski, A.; Yeager, E. *Comprehensive Treatise of Electrochemistry*; Plenum: New York, 1983; Vol. 7.
(206) Markovic, N. M.; Gasteiger, H. A.; Ross, P. N. *J. Phys. Chem.* **1995**, *99*, 3411.
(207) Markovic, N. M.; Ross, P. N. *Surf. Sci. Rep.* **2002**, *45*, 117.
(208) Antoine, O.; Durand, R. *J. Appl. Electrochem.* **2000**, *30*, 839.
(209) Paulus, U. A.; Schmidt, T. J.; Gasteiger, H. A.; Behm, R. J. *J. Electroanal. Chem.* **2001**, *495*, 134.
(210) Inaba, M.; Yamada, H.; Tokunaga, J.; Matsuzawa, K.; Hatanaka, A.; Tasaka, A. *ECS Trans.* **2006**, *1*, 315.
(211) Liu, W.; Zuckerbrod, D. *J. Electrochem. Soc.* **2005**, *152*, A1165.
(212) Kinumoto, T.; Inaba, M.; Nakayama, Y.; Ogata, K.; Umebayashi, R.; Tasaka, A.; Iriyama, Y.; Abe, T.; Ogumi, Z. *J. Power Sources* **2006**, *158*, 1222.
(213) Pozio, A.; Silva, R. F.; Francisco, M. D.; Giorgi, L. *Electrochim. Acta* **2003**, *48*, 1543.
(214) Endoh, E.; Terazono, S.; Widjaja, H.; Takimoto, Y. *Electrochem. Solid-State Lett.* **2004**, *7*, A209.
(215) Endoh, E. *ECS Trans.* **2006**, *3*, 9.
(216) Panchenko, A.; Dilger, H.; Moeller, H.; Sixt, T.; Roduner, E. *J. Power Sources* **2004**, *127*, 325.
(217) Scatchard, G.; Kavanagh, G. M.; Ticknor, L. B. *J. Am. Chem. Soc.* **1952**, *74*, 3715.
(218) Hommura, S.; Kawahara, K.; Shimohira, T. *Polym. Prepr., Jpn.* **2005**, *54*, 4517.
(219) Hommura, S.; Kawahara, K.; Shimohira, T. In *Extended Abstracts of The 207th Electrochemical Society Meeting*, Quebec, Canada, 2005.
(220) Miyatake, K.; Chikashige, Y.; Watanabe, M. *Macromolecules* **2003**, *36*, 9691.
(221) Mittal, V. O.; Kunz, H. R.; Fenton, J. M. *ECS Trans.* **2006**, *1*, 275.
(222) Mittal, V. O.; Kunz, H. R.; Fenton, J. M. *Electrochem. Solid-State Lett.* **2006**, *9*, A299.
(223) Liu, H.; Gasteiger, H. A.; Laconti, A.; Zhang, J. *ECS Trans.* **2006**, *1*, 283.
(224) Ferreira, P. J.; la O', G. J.; Shao-Horn, Y.; Morgan, D.; Makharia, R.; Kocha, S.; Gasteiger, H. A. *J. Electrochem. Soc.* **2005**, *152*, A2256.
(225) Yasuda, K.; Taniguchi, A.; Akita, T.; Ioroi, T.; Siroma, Z. *Phys. Chem. Chem. Phys.* **2006**, *8*, 746.
(226) Ohyagi, S.; Sasaki, T.; Matsuda, T.; Iseki, Y.; Nakajima, H.; Morikawa, S.; Shintaku, M.; Kaito, C. *The 47th Battery Symposium in Japan*, Tokyo, 2006.
(227) Mitov, S.; Panchenko, A.; Roduner, E. *Chem. Phys. Lett.* **2005**, 485.
(228) Healy, J.; Hayden, C.; Xie, T.; Olson, K.; Waldo, R.; Brundage, M.; Gasteiger, H. A. *Fuel Cells* **2005**, *5*, 302.
(229) Schiraldi, D. A.; Zhou, C.; Zawodzinski, T. A. In *Extended Abstracts of The 210th Electrochemical Society Meeting*, Cancun, Mexico, 2006.
(230) Hübner, G.; Roduner, E. *J. Mater. Chem.* **1999**, *9*, 409.
(231) Panchenko, A. *J. Membr. Sci.* **2006**, *278*, 269.
(232) Jang, W. B.; Lee, C.; Sundar, S.; Shul, Y. G.; Han, H. *Polym. Degrad. Stab.* **2005**, *90*, 431.
(233) Schumb, W. C.; Satterfield, C. N.; Wentworth, R. L. *Hydrogen Peroxide, American Chemical Society Monograph Series*; Reinhold Pub. Co.: New York, 1955.
(234) Aoki, A.; Uchida, H.; Watanabe, M. *Electrochem. Commun.* **2005**, *7*, 1434.
(235) Miyatake, K.; Zhou, H.; Matsuo, T.; Uchida, H.; Watanabe, M. *Macromolecules* **2004**, *37*, 4961.
(236) Chikashige, Y.; Chikyu, Y.; Miyatake, K.; Watanabe, M. *Macromolecules* **2005**, *38*, 7121.
(237) Wang, L.; Meng, Y. Z.; Wang, S. J.; Li, X. H.; Xiao, M. *J. Polym. Sci., Part A: Polym. Chem.* **2005**, *43*, 6411.
(238) Gebel, G.; Meyer, G.; Perrot, C.; Gonon, L.; Moriat, S.; Gardette, J. L. *Polymer* **2006**, *47*, 5003.
(239) Genies, C.; Mercier, R.; Sillion, B.; Cornet, N.; Gebel, G.; Pineri, M. *Polymer* **2001**, *42*, 359.
(240) Perrot, C.; Meyer, G.; Gonon, L.; Gebel, G. *Fuel Cells* **2006**, *6*, 10.
(241) Einsla, B. R.; Hong, Y. T.; Kim, Y. S.; Wang, F.; Gunduz, N.; McGrath, J. E. *J. Polym. Sci., Part A: Polym. Chem.* **2004**, *42*, 862.
(242) Einsla, B. R.; Kim, Y. S.; Hickner, M. A.; Hong, Y. T.; Hill, M. L.; Pivovar, B. S.; McGrath, J. E. *J. Membr. Sci.* **2005**, *255*, 141.
(243) Guo, X.; Fang, J.; Watari, T.; Tanaka, K.; Kita, H.; Okamoto, K. I. *Macromolecules* **2002**, *35*, 6707.
(244) Yin, Y.; Fang, J.; Cui, Y.; Tanaka, K.; Kita, H.; Okamoto, K. *Polymer* **2003**, *44*, 4509.
(245) Yin, Y.; Yamada, O.; Suto, Y.; Mishima, T.; Tanaka, K.; Kita, H.; Okamoto, K. *J. Polym. Sci., Part A: Polym. Chem.* **2005**, *43*, 1545.
(246) Yasuda, T.; Li, Y.; Miyatake, K.; Hirai, M.; Nanasawa, M.; Watanabe, M. *J. Polym. Sci., Part A: Polym. Chem.* **2006**, *44*, 3995.
(247) Asano, N.; Miyatake, K.; Watanabe, M. *Chem. Mater.* **2004**, *16*, 2841.
(248) Gubler, L. G.; S. A.; Scherer, G. G. *Fuel Cells* **2005**, *5*, 317.
(249) Xing, D.; Kerres, J. *Polym. Adv. Technol.* **2006**, *17*, 591.
(250) Wang, F.; Hickner, M.; Kim, Y. S.; Zawodzinski, T. A.; McGrath, J. E. *J. Membr. Sci.* **2002**, *15*, 231.
(251) Wang, F.; Hickner, M.; Ji, Q.; Harrison, W.; Mecham, J.; Zawodzinski, T. A.; McGrath, J. E. *Macromol. Symp.* **2001**, *175*, 387.
(252) Burlastsky, S. F.; Hertzberg, J. B.; Copollini, N. E.; Condit, D. A.; Jarvi, T. D.; Leistra, J. A.; Perry, M. L.; Madden, T. H. U.S. Patent Application U.S.A., 2004.
(253) Tsurumaki, S. *Annual Review of NEDO R&D for Fuel Cells and Hydrogen Technology*; NEDO: Tokyo, 2006.
(254) Chen, J.; Asano, M.; Yamaki, T.; Yoshida, M. *J. Appl. Polym. Sci.* **2006**, *100*, 4565.
(255) Lin, J.-C.; Fenton, J. M.; Kunz, H. R.; Cutlip, M. B. *Electrochem. Soc. Meeting Abstr.* **2000**, *2000*−*2*, Abstract 238.
(256) Buchi, F. N.; Gupta B.; Hass, O.; Sherer, G. G. *J. Electrochem. Soc.* **1995**, *142*, 3044.
(257) Borup, R.; Davy, J.; Wood, D.; Garzon, F.; Inbody, M.; Guidry, D. *DOE Hydrogen Program Review*, 2005.
(258) Statterfield, M. B.; Majsztrik, P. W.; Ota, H.; Benziger, J. B.; Bocarsly, A. B. *J. Polym. Sci., Part B: Polym. Phys.* **2006**, *44*, 2327.
(259) Kundu, S.; Simon, L. C.; Fowler, M.; Grot, S. *Polymer* **2005**, *46*, 11707.
(260) Blackwell, R. I.; Mauritz, K. A. *Polym. Adv. Technol.* **2005**, *16*, 212.
(261) Liu, D.; Kyriakides, S.; Case, S. W.; Lesco, J. J.; Li, Y.; McGrath, J. *J. Polym. Sci., Part B: Polym. Phys.* **2006**, *44*, 1453.
(262) Aoki, M.; Asano, N.; Miyatake, K.; Uchida, H.; Watanabe, M. *J. Electrochem. Soc.* **2006**, *153*, A1154.
(263) Yeo, S. C.; Eisenberg, A. *J. Appl. Polym. Sci.* **1977**, *21*, 875.
(264) Kyu, T.; Eisenberg, A. In *Perfluoroinated Ionomer Membranes*; Eisenberg, H. L. Y., Ed.; American Chemical Society: Lake Buena Vista, FL, 1982; Vol. 180.
(265) Page, K. A.; Cable, K. M.; Moore, R. B. *Macromolecules* **2005**, *38*, 6472.
(266) Page, K. A.; Landis, F. A.; Phillips, A. K.; Moore, R. B. *Macromolecules* **2006**, *39*, 3939.
(267) Weiss, R. A.; Fitzgerald, J. J.; Kim, D. *Macromolecules* **1991**, *24*, 1071.
(268) Weiss, R. A.; Sen, A.; Pottick, L. A.; Willis, C. L. *Polymer* **1991**, *32*, 2785.
(269) Rigdahl, M.; Eisenberg, A. *J. Polym. Sci., Polym. Phys. Ed.* **1981**, *19*, 1641.
(270) Yang, S.; Sun, K.; William, M. *J. Polym. Sci., Part B* **1990**, *28*, 1685.
(271) Mauritz, K. A.; Blackwell, R. I.; Beyer, F. L. *Polymer* **2004**, *45*, 3001.
(272) Gupta, B.; Haas, O.; Scherer, G. G. *J. Appl. Polym. Sci.* **1994**, *54*, 469.
(273) Kim, Y. S.; Dong, L.; Hickner, M. A.; Glass, T. E.; Webb, V.; McGrath, J. E. *Macromolecules* **2003**, *36*, 6281.
(274) Lai, Y. H.; Gittleman, C. S.; Mittelsteadt, C. K.; Dillard, D. A. 3rd Int. Conf. on Fuel Cell Science, Engineering, and Technology, Ypsilanti, MI, 2005; p 161.
(275) Bellinger, M. A.; Sauer, J. A.; Hara, M. *Polymer* **1997**, *38*, 309.
(276) Hara, M.; Jar, P. Y.; Sauer, J. A. *Macromolecules* **1988**, *21*, 3183.
(277) Reyna-Valencia, A.; Kaliguine, S.; Bousmina, M. *J. Appl. Polym. Sci.* **2005**, *98*, 2380.
(278) Budinski, M.; Gittleman, C.; Yeh-Hung, L.; Litteer, B.; Miller, D. *AIChE* **2004**.
(279) Hamrock, S. J.; Yandrasits, M. A. *J. Macromol. Sci., Part C: Polym. Rev.* **2006**, *46*, 219.
(280) Yandrasits, M. In *2nd International Conference on polymer Batteries and Fuel Cells*, Las Vegas, NV, 2005.
(281) DuPont *Fuel Cells Data Sheet*, 2007, http://www.dupont.com/fuelcells/pdf/dfc101.pdf.
(282) Uan-Zo-Li, J. T. M.Sc. Thesis, Virgnia Tech. Materials Science and Engineering, 2001.
(283) Bauer, F.; Denneier, S.; Willert-Porada, M. *J. Polym. Sci., Part B: Polym. Phys.* **2005**, *43*, 786.
(284) Laporta, M.; Pegoraro, M.; Zanderighi, L. *Phys. Chem. Chem. Phys.* **1999**, *1*, 4619.
(285) Zawodzinski, T. A.; Derouin, C.; Radzinski, S.; Sherman, R. J.; Smith, V. T.; Springer, T. E.; Gottesfeld, S. *J. Electrochem. Soc.* **1993**, *140*, 1041.
(286) Harrison, W. L.; Hickner, M. A.; Kim, Y. S.; McGrath, J. E. *Fuel Cells* **2005**, *5*, 201.
(287) Lin, G.; He, W.; Nguyen, T. V. *J. Electrochem. Soc.* **2004**, *151*, A1999.
(288) Rollet, A. L. G.; Simonin, J. P.; Turg, P. *J. Polym. Sci., Part B: Polym. Phys.* **2001**, *39*, 548.
(289) Kim, M. H.; Glinka, C. J.; Grot, S. A.; Grot, W. G. *Macromolecules* **2006**, *39*, 4775.

(290) Lee, K.; Ishihara, A.; Mitsushima, S.; Kamiya, N.; Ota, K. *J. Electrochem. Soc.* **2004**, *151*, A639.
(291) Kim, Y. S.; Dong, L.; Hickner, M. A.; Pivovar, B. S.; McGrath, J. E. *Polymer* **2003**, *44*, 5729.
(292) Okuyama, K.; Nishikawa, F. *Nippon Kagaku Kaishi* **1994**, *12*, 1091.
(293) Broka, K.; Ekdunge, P. *J. Appl. Electrochem.* **1997**, *27*, 117.
(294) Lee, K.; Ishihara, A.; Mitsushima, S.; Kamiya, N.; Ota, K. *Fuel Cell Sci., Eng., Technol.* **2003**, 241.
(295) Yeo, R. S.; Yeager, H. L. In *Modern Aspects of Electrochemistry, No. 16*; Conway, B. E., Bockris, R. E. W., O'M., J., Eds.; Plenum Press: New York, 1985.
(296) Zawodzinski, T. A.; Springer, T. E.; Davey, J.; Jestel, R.; Lopez, C.; Valerio, J.; Gottesfeld, S. *J. Electrochem. Soc.* **1993**, *140*, 1981.
(297) Hinatsu, J. T.; Mizuhata, M.; Takenaka, H. *J. Electrochem. Soc.* **1994**, *141*, 1493.
(298) Tricoli, V.; Carretta, N.; Bartolozzi, M. *J. Electrochem. Soc.* **2000**, *147*, 1286.
(299) Sone, Y.; Ekdunge, P.; Simonsson, D. *J. Electrochem. Soc.* **1996**, *143*, 1254.
(300) Wei, J. H.; He, M. Y.; Overney, R. M. *J. Membr. Sci.* **2006**, *279*, 608.
(301) Cheng, X.; Peng, C.; You, M.; Liu, L.; Zhang, Y.; Fan, Q. *Electrochim. Acta* **2006**, *51*, 4620.
(302) Alberti, G.; Casciola, M.; Massinelli, L.; Bauer, B. *J. Membr. Sci.* **2001**, *185*, 73.
(303) Kim, Y. S.; Wang, F.; Hickner, M.; McCartney, S.; Hong, Y. T.; Harrison, W.; Zawodzinski, T. A.; McGrath, J. E. *J. Polym. Sci., Part B: Polym. Phys.* **2003**, *41*, 2816.
(304) Ma, S.; Siroma, Z.; Tanaka, H. *J. Electrochem. Soc.* **2006**, *153*, A2274.
(305) Casciola, M.; Alberti, G.; Sganappa, M.; Narducci, R. *J. Power Sources* **2006**, *162*, 141.
(306) Tant, M. R.; Darst, K. P.; Lee, K. D.; Martin, C. W. *ACS Symp. Ser.* **1989**, *395*, 370.
(307) Moore, R. B.; Martin, C. R. *Macromolecules* **1989**, 3594.
(308) Ridge, S. J.; White, R. E.; Tsou, Y.; Beaver, R. N.; Eisman, G. A. *J. Electrochem. Soc.* **1989**, *136*, 1902.
(309) Ren, X. M.; Gottesfeld, S. *J. Electrochem. Soc.* **2001**, *148*, A87.
(310) Ghielmi, A.; Vaccarono, P.; Troglia, C.; Arcella, V. *J. Power Sources* **2005**, *145*, 108.
(311) Rivard, L.; Pierpont, D.; Freemyer, H.; Thaler, A.; Hamrock, S. 2003 Fuel Cell Seminar, Miami Beach, 2003; p 73.
(312) Bahar, B.; Hobson, A. R.; Kolde, J. A. U.S. Patent 5,599,614, 1997.
(313) Bahar, B.; Hobson, A. R.; Kolde, J. A.; Zuckerbrod, D. U.S. Patent 5,547,551, 1996.
(314) Liu, F. Q.; Yi, B. L.; Xing, D. M.; Yu, J. R.; Zhang, H. M. *J. Membr. Sci.* **2003**, *212*, 213.
(315) Nakao, M.; Yoshitake, M. In *Handbook of Fuel Cells: fundamentals, Technology and Applications*; Vielstiern, W., Lamm, H. A. g. A., Eds.; John Wiley & Sons: West Sussex, U.K., 2003; Vol. 3.
(316) Nouel, K. M.; Fedkiw, P. S. *Electrochim. Acta* **1998**, *43*, 2381.
(317) Yu, T. L.; Lin, H. L.; Shen, K. S.; Huang, L. N.; Chang, Y. C.; Jung, G. B.; Huang, J. C. *J. Polym. Res.* **2004**, *11*, 217.
(318) Yong-Hao, L.; Baolian, Y.; Zhi-Gang, S.; Xing, D.; Zhang, H. *Electrochem. Solid-State Lett.* **2006**, *9*, A356.
(319) Hill, M. L.; Kim, Y. S.; Einsla, B. R.; McGrath, J. E. *J. Membr. Sci.* **2006**, *283*, 102.
(320) Woo, M. H.; Kwon, O.; Choi, S. H.; Hong, M. Z.; Ha, H. W.; Kim, K. *Electrochim. Acta* **2006**, *51*, 6051.
(321) Yang, C.; Costamaqna, P.; Srinivasan, S.; Benziger, J.; Bocarsly, A. B. *J. Power Sources* **2001**, *103*, 1.
(322) Yang, C.; Srinivasan, S.; Bocarsly, A. B.; Tulyani, S.; Benziger, J. B. *J. Membr. Sci.* **2004**, *237*, 145.
(323) Kim, Y. S.; Wang, F.; Hickner, M.; Zawodzinski, T. A.; McGrath, J. E. *J. Membr. Sci.* **2003**, *212*, 263.
(324) Deng, Q.; Moore, R. B.; Mauritz, K. A. *J. Appl. Polym. Sci.* **1998**, *68*, 747.
(325) Chalkova, E.; Fedkin, M. V.; Wesolowski, D. J.; Lovov, S. N. *J. Electrochem. Soc.* **2005**, *152*, A1742.
(326) Adiemian, K. T.; Lee, S. J.; Srinivasan, S.; Benziger, J.; Bocarsly, A. B. *J. Electrochem. Soc.* **2002**, *149*, A256.
(327) Kerres, J. A. *Fuel Cells* **2005**, *5*, 230.
(328) Fu, Y. Z.; Manthiram, A.; Guiver, M. D. *Electrochem. Commun.* **2006**, *8*, 1386.
(329) Barton, R. H.; Gibb, P. R.; Ronne, J. A.; Voss, H. H. U.S. Patent 6,057,054, 2000.
(330) Bonk, S. P.; Krasij, M.; Reiser, C. A. U.S. Patent 6,399,234, 2002.
(331) Steck, A. E.; Wei, J. U.S. Patent 5,464,700, 1995.
(332) Schmid, O.; Einhart, J. U.S. Patent 6,080,503, 2000.
(333) Kelland, J. W.; Braun, S. G. U.S. Patent 5,187,025, 1992.
(334) Antolini, E. *J. Mater. Sci.* **2003**, *38*, 2995.
(335) Xie, J.; Wood, D. L.; More, K. L.; Atanassov, P.; Borup, R. L. *J. Electrochem. Soc.* **2005**, *152*, A1011.
(336) Mathias, M.; Gasteiger, H.; Makharia, R.; Kocha, S.; Fuller, T.; Pisco, J. *Abstr. Pap. Am. Chem. Soc.* **2004**, *228*, 002.
(337) Guilminot, E.; Corcella, A.; Charlot, F.; Maillard, F.; Chatenet, M. *J. Electrochem. Soc.* **2007**, *154*, B96.
(338) Pourbaix, M. *Atlas of electrochemical equilibria*, 1966.
(339) Lee, J. B. *Corrosion* **1981**, *37*, 467.
(340) Nagy, Z.; You, H. *Electrochim. Acta* **2002**, *47*, 3037.
(341) You, H.; Chu, Y. S.; Lister, T. E.; Nagy, Z.; Ankudiniv, A. L.; Rehr, J. J. *Physica B* **2000**, *283*, 212.
(342) Sun, A.; Franc, J.; Macdonald, D. D. *J. Electrochem. Soc.* **2006**, *153*, B260.
(343) Teliska, A.; O'Grady, W. E.; Ramaker, D. E. *J. Phys. Chem.* B **2005**, *109*, 8076.
(344) Paik, C. H.; Jarvi, T. D.; O'Grady, W. E. *Electrochem. Solid-State Lett.* **2004**, *7*, A82.
(345) Uribe, F. A.; Zawodzinski, T. A. *Electrochim. Acta* **2002**, *47*, 3799.
(346) Paik, C. H.; Saloka, G. S.; Graham, G. W. *Electrochem. Solid-State Lett.* **2007**, *10*, B39.
(347) Azaroul, M.; Romand, B.; Freyssinet, P.; Disnar, J. R. *Geochim. Cosmochim. Acta* **2001**, *65*, 4453.
(348) Bowles, F. W.; Gize, A. P.; Vaughan, D. J.; Norris, S. J. *Chronique de la Recherche Miniere* **1995**, *529*, 65.
(349) Bindra, P.; Clouser, S. J.; Yeager, E. *J. Electrochem. Soc.* **1979**, *126*, 1631.
(350) Wood, S. A. *Geochim. Cosmochim. Acta* **1991**, *55*, 1759.
(351) Kim, J.-H.; Ishihara, A.; Mitsushima, S.; Kamiya, N.; Ota, K. *Electrochim. Acta* **2007**, *52*, 2492.
(352) Azaroul, M.; Romand, B.; Freyssinet, P.; Disnar, J. R. *Geochim. Cosmochim. Acta* **2003**, *67*, 2511.
(353) Benke, G.; Gnot, W. *Hydrometallurgy* **2002**, *64*, 205.
(354) Johnson, D. C.; Napp, D. T.; Bruckenstein, S. *Electrochim. Acta* **1970**, *15*, 1493.
(355) Kinoshita, K.; Lundquist, J. T.; Stonehart, P. *J. Electroanal. Chem.* **1973**, *48*, 157.
(356) Mitsushima, S.; Koizumi, Y.; Ota, K.-I.; Kamiya, N. *Electrochem. Commun.* **2007**, *75*.
(357) Rand, D. A. J.; Woods, R. *J. Electroanal. Chem.* **1972**, *35*, 209.
(358) Arvia, A. J.; Canullo, J. C.; Custidiano, E.; Perdriel, C. L.; Triaca, W. E. *Electrochim. Acta* **1986**, *31*, 1359.
(359) Canullo, J. C.; Triaca, W. E.; Arvia, A. J. *J. Electroanal. Chem.* **1986**, *200*, 397.
(360) Egli, W. A.; Visintin, A.; Triaca, W. E.; Arvia, A. J. *Appl. Surf. Sci.* **1993**, *68*, 583.
(361) Ota, K. I.; Nishigori, S.; Kamiya, N. *J. Electroanal. Chem.* **1988**, *257*, 205.
(362) Aragane, J.; Murahashi, T. *Nippon Kagaku Kaishi* **1988**, 1670.
(363) Aragane, J.; Murahashi, T.; Odaka, T. *J. Electrochem. Soc.* **1988**, *135*, 844.
(364) Aragane, J.; Urushibata, H.; Murahashi, T. *J. Appl. Electrochem.* **1996**, *26*, 147.
(365) Honji, A.; Mori, T.; Tamura, K.; Hishinuma, Y. *J. Electrochem. Soc.* **1988**, *135*, 355.
(366) Tseung, A. C. C.; Dhara, S. C. *Electrochim. Acta* **1975**, *20*, 681.
(367) Schulze, M.; Schneider, A.; Gulzow, E. *J. Power Sources* **2004**, *127*, 213.
(368) Akita, T.; Taniguchi, A.; Maekawa, J.; Siroma, Z.; Tanaka, K.; Kohyama, M.; Yasuda, K. *J. Power Sources* **2006**, *159*, 461.
(369) Yasuda, K.; Taniguchi, A.; Akita, T.; Ioroi, T.; Siroma, Z. *J. Electrochem. Soc.* **2006**, *153*, A1599.
(370) Landsman, D. A.; Luczak, F. J. In *Handbook of Fuel Cells—Fundamentals, Technology, and Applications*; Vielstich, W., Gasteiger, H. A., Lamm, A., Eds.; John Wiley and Sons Ltd.: West Sussex, England, 2003; Vol. 4.
(371) Gasteiger, H. A.; Kocha, S.; Sompalli, B.; Wagner, F. T. *Appl. Catal., B* **2005**, *56*, 9.
(372) Jalan, V.; Taylor, E. J. *J. Electrochem. Soc.* **1983**, *130*, 2299.
(373) Stamenkovic, V.; Schmidt, T. J.; Ross, P. N.; Markovic, N. M. *J. Phys. Chem. B* **2002**, *106*, 11970.
(374) Koh, S.; Leisch, J.; Toney, M. F.; Strasser, P. *J. Phys. Chem. C* **2007**, *111*, 3744.
(375) Piela, P.; Eickes, C.; Brosha, E.; Garzon, F.; Zelenay, P. *J. Electrochem. Soc.* **2004**, *151*, A2053.
(376) Antolini, E.; Salgado, J. R. C.; Gonzalez, E. R. *J. Power Sources* **2006**, *160*, 957.
(377) Yu, P.; Pemberton, M.; Plasse, P. *J. Power Sources* **2005**, *144*, 11.
(378) Colon-Mercado, H. R.; Popov, B. N. *J. Power Sources* **2006**, *155*, 253.
(379) Ball, S.; Hudson, S.; Theobald, B.; Thompsett, D. *ECS Trans.* **2006**, 1.
(380) Wikander, K.; Ekstr, H.; Palmqvist, A. E. C.; Lindbergh, G. *Electrochim. Acta* **2007**, *52*, 6848.
(381) Borup, R.; Davey, J.; Garzon, F. H. *ECS Trans.* **2006**, *3*, 879.
(382) Garzon, F. H.; Davey, J.; Borup, R. *ECS Trans.* **2005**, *1*, 153.

(383) Ascarelli, P.; Contini, V.; Giorgi, R. *J. Appl. Phys.* **2002**, *91*, 4556.
(384) Giorgi, R.; Ascarelli, P.; Turtu, S. *Appl. Surf. Sci.* **2001**, *178*, 149.
(385) Blom, D. A.; Dunlap, J. R.; Nolan, R. A.; Allard, L. F. *J. Electrochem. Soc.* **2003**, 150.
(386) More, K. L.; Reeves, K. S. *Microsc. Microanal.* **2005**, 11.
(387) More, K. L.; Reeves, K. S. *DOE Hydrogen Program Review*, 2005.
(388) More, K. L.; Borup, R.; Reeves, K. S. *ECS Trans.* **2006**, 3.
(389) Bi, W.; Gray, G.; Fuller, T. *Electrochem. Solid-State Lett.* **2007**, *10*, B101.
(390) Borup, R. *Hydrogen, Fuel Cells and Infrastructure Technologies Annual Progress Report*, 2006.
(391) More, K. E. *DOE Hydrogen Program Annual Progress Report*, 2006.
(392) Yu, P. T.; Gu, W.; Makharia, R.; Wagner, F. T.; Gasteiger, H. A. *ECS Trans.* **2007**, *3*, 797.
(393) Kinoshita, K. *Carbon: Electrochemical and Physicochemical Properties*; Wiley: New York, 1988.
(394) Roen, L. M.; Paik, C. H.; Jarvi, T. D. *Electrochem. Solid-State Lett.* **2004**, *7*, A19.
(395) Tang, H.; Qi, Z.; Ramani, M.; Elter, J. F. *J. Power Sources* **2006**, *158*, 1306.
(396) Gruver, G. A. *J. Electrochem. Soc.* **1978**, *125*, 1719.
(397) Alderucci, V.; Recupero, V.; Pino, L.; Leonardo, R. D.; Cocke, D. L.; Giordano, N. *J. Appl. Electrochem.* **1990**, *20*, 811.
(398) Alderucci, V.; Passalacqua, E.; Giordano, N. *J. Appl. Electrochem.* **1990**, *20*, 235.
(399) Paffett, M. T.; Hutchinson, W.; Farr, J. D.; Papin, P.; Beery, J. G.; Gottesfeld, S.; Feret, J. *J. Power Sources* **1991**, *36*, 137.
(400) Mitsuda, K.; Murahashi, T. *J. Appl. Electrochem.* **1991**, *21*, 524.
(401) Mitsuda, K.; Murahashi, T. *J. Appl. Electrochem.* **1993**, *23*, 19.
(402) Lee, S.-B.; Pyun, S.-I. *J. Appl. Electrochem.* **2000**, *30*, 795.
(403) Binder, H.; Kohling, A.; Richter, K.; Sandstede, G. *Electrochim. Acta* **1964**, *9*, 255.
(404) Kinoshita, K.; Bett, J. *Carbon* **1973**, *11*, 237.
(405) Kinoshita, K.; Bett, J. A. S. *Carbon* **1973**, *11*, 403.
(406) McBreen, J.; Olender, H.; Srinivasan, S.; Kordesch, K. V. *J. Appl. Electrochem.* **1981**, *11*, 787.
(407) Stonehart, P. *Carbon* **1984**, *22*, 423.
(408) Antonucci, P. L.; Romeo, F.; Minutoli, M.; Alderucci, E.; Giordano, N. *Carbon* **1988**, *26*, 197.
(409) Passalacqua, E.; Antonucci, P. L.; Vivaldi, M.; Patti, A.; Antonucci, V.; Giordano, N.; Kinoshita, K. *Electrochim. Acta* **1992**, *37*, 2725.
(410) Pyun, S.-I.; Lee, E.-J.; Kim, T.-Y.; Lee, S.-J.; Ryu, Y.-G.; C.-S., K. *Carbon* **1994**, *32*, 155.
(411) Pyun, S.-I.; Ryu, Y.-G.; Choi, S.-H. *Carbon* **1994**, *32*, 161.
(412) Kiho, M.; Matsunaga, K.; Morikawa, S.; Kato, O. *Electrochemistry* **2001**, *69*, 580.
(413) Boehm, H. P. *Carbon* **2002**, *40*, 145.
(414) Willsau, J.; Heitbaum, J. *J. Electroanal. Chem.* **1984**, *161*, 93.
(415) Kangasniemi, K. H.; Condit, D. A.; Jarvi, T. D. *J. Electrochem. Soc.* **2004**, *151*, E125.
(416) Siroma, Z.; Ishii, K.; Yasuda, K.; Miyazaki, Y.; Inaba, M.; Tasaka, A. *Electrochem. Commun.* **2005**, *7*, 1153.
(417) Kinumoto, T.; Takai, K.; Iriyama, Y.; Abe, T.; Inaba, M.; Ogumi, Z. *J. Electrochem. Soc.* **2006**, *153*, A58.
(418) Chaparro, A. M.; Mueller, N.; Atienza, C.; Daza, L. *J. Electroanal. Chem.* **2006**, *591*, 69.
(419) Wang, X.; Li, W.; Chen, Z.; Waje, M.; Yan, Y. *J. Power Sources* **2006**, *158*, 154.
(420) Laser, D.; Ariel, M. *J. Electroanal. Chem.* **1974**, *52*, 291.
(421) Neffe, S. *Carbon* **1988**, *26*, 687.
(422) Barbero, C.; Kötz, R. *J. Electrochem. Soc.* **1993**, *140*, 1.
(423) Swain, G. M. *J. Electrochem. Soc.* **1994**, *141*, 3382.
(424) Yang, Y.; Lin, Z. G. *J. Appl. Electrochem.* **1995**, *25*, 259.
(425) Alliata, D.; Häring, P.; Haas, O.; Kötz, R.; Siegenthaler, H. *Electrochem. Solid-State Lett.* **1999**, *2*, 33.
(426) Sullivan, M. G.; Schnyder, B.; Bärtsch, M.; Alliata, D.; Barbero, C.; Imhof, R.; Kötz, R. *J. Electrochem. Soc.* **2000**, *147*, 2636.
(427) Weinberg, N. L.; Reddy, T. B. *J. Appl. Electrochem.* **1973**, *3*, 73.
(428) Neffe, S. *Carbon* **1987**, *25*, 761.
(429) Yue, Z. R.; Jiang, W.; Wang, L.; Gardner, S. D.; Pittman, J. C. U. *Carbon* **1999**, *37*, 1785.
(430) Goss, C. A.; Brumfield, J. C.; Irene, E. A.; Murray, R. W. *Anal. Chem.* **1993**, *65*, 1378.
(431) Hathcock, K. W.; Brumfield, J. C.; Goss, C. A.; Irene, E. A.; Murray, R. W. *Anal. Chem.* **1995**, *67*, 2201.
(432) Gewirth, A. A.; Bard, A. J. *J. Phys. Chem.* **1988**, *92*, 5563.
(433) Zhang, B.; Wang, E. *Electrochim. Acta* **1995**, *40*, 2627.
(434) Serp, P.; Corrias, M.; Kalck, P. *Appl. Catal. A* **2003**, *253*, 337.
(435) Lee, K.; Zhang, J. J.; Wang, H. J.; Wilkinson, D. P. *J. Appl. Electrochem.* **2006**, *36*, 507.
(436) Bessel, C. A.; Laubernds, K.; Rodriguez, N. M.; Baker, R. T. K. *J. Phys. Chem. B* **2001**, *105*, 1115.
(437) Carmo, M.; Paganin, V. A.; Rosolen, J. M.; Gonzalez, E. R. *J. Power Sources* **2005**, *142*, 169.
(438) Figueiredo, J. L.; Pereira, M. F. R.; Serp, P.; Kalck, P.; Samant, P. V.; Fernandes, J. B. *Carbon* **2006**, *44*, 2516.
(439) Frackowiak, E.; Lota, G.; Lota, K.; Beguin, F. *AIP Conf. Proc.* **2004**, *723*, 532.
(440) Gennett, T.; Landi, B. J.; Elich, J. M.; Jones, K. M.; Alleman, J. L.; Lamarre, P.; Morris, R. S.; Raffaelle, R. P.; Heben, M. J. *Mater. Res. Soc. Symp. Proc.* **2003**, *756*, 379.
(441) Liang, Y. M.; Zhang, H. M.; Yi, B. L.; Zhang, Z. H.; Tan, Z. C. *Carbon* **2005**, *43*, 3144.
(442) Maiyalagan, T.; Viswanathan, B.; Varadaraju, U. *Electrochem. Commun.* **2005**, *7*, 905.
(443) Moloney, P.; Huffman, C.; Springer, M.; Gorelik, O.; Nikolaev, P.; Sosa, E.; Arepalli, S.; Yowell, L. *Mater. Res. Soc. Symp. Proc.* **2006**, *885*, 75.
(444) Pan, M.; Tang, H. L.; Mu, S. C.; Yuan, R. Z. *J. Mater. Res.* **2004**, *19*, 2279.
(445) Rajesh, B.; Karthik, V.; Karthikeyan, S.; Thampi, K. R.; Bonard, J. M.; Viswanathan, B. *Fuel* **2002**, *81*, 2177.
(446) Sasaki, K.; Shinya, K.; Tanaka, S.; Furukawa, A.; Ando, K.; Kuroki, T.; Kusaba, H.; Teraoka, Y. *206th Meeting Electrochem. Soc.* **2004**, 1912.
(447) Shao, Y.; Yin, G.; Zhang, J.; Gao, Y. *Electrochim. Acta* **2006**, *51*, 5853.
(448) Steigerwalt, E. S.; Deluga, G. A.; Lukehart, C. M. *J. Phys. Chem. B* **2002**, *106*, 760.
(449) Wu, G.; Chen, Y. S.; Xu, B. Q. *Electrochem. Commun.* **2005**, *7*, 1237.
(450) Xu, B. Q.; Xu, J. B.; Hua, K. K.; Sun, G. Z.; Wang, C.; Lv, X. Y.; Wang, Y. J. *Electrochem. Commun.* **2006**, *8*, 982.
(451) Yuan, F. L.; Ryu, H. J. *Nanotechnology* **2004**, *15*, S596.
(452) Yuan, F. L.; Sasikumar, G.; Ryu, H. *J. New Mater. Electrochem. Syst.* **2004**, *7*, 311.
(453) Yuan, F. L.; Yu, H. K.; Ryu, H. J. *Electrochim. Acta* **2004**, *50*, 685.
(454) Wang, C.; Waje, M.; Wang, X.; Tang, J. M.; Haddon, R. C.; Yan, Y. S. *Nano Lett.* **2004**, *4*, 345.
(455) Zhang, Y.; Li, X.; Wu, X.; Xu, M.; Deng, L. *J. Rare Earths* **2005**, *23*, 40.
(456) Chen, C. C.; Chen, C. F.; Hsu, C. H.; Li, I. H. *Diamond Relat. Mater.* **2005**, *14*, 770.
(457) Hyeon, T.; Han, S.; Sung, Y. E.; Park, K. W.; Kim, Y. W. *Angew. Chem.* **2003**, *42*, 4352.
(458) Park, K. W.; Sung, Y. E.; Han, S.; Yun, Y.; Hyeon, T. *J. Phys. Chem. B* **2004**, *108*, 939.
(459) Yoshitake, T.; Shimakawa, Y.; Kuroshima, S.; Kimura, H.; Ichihashi, T.; Kubo, Y.; Kasuya, D.; Takahashi, K.; Kokai, F.; Yudasaka, M.; Iijima, S. *Physica B* **2002**, *323*, 124.
(460) Piao, Y. Z.; An, K. J.; Kim, J. Y.; Yu, T. Y.; Hyeon, T. H. *J. Mater. Chem.* **2006**, *16*, 2984.
(461) Kim, C.; Kim, Y. J.; Kim, Y. A.; Yanagisawa, T.; Park, K. C.; Endo, M.; Dresselhaus, M. S. *J. Appl. Phys.* **2004**, *96*, 5903.
(462) Wang, M. Y.; Chen, J. H.; Fan, Z.; Tang, H.; Deng, G. H.; He, D. L.; Kuang, Y. F. *Carbon* **2004**, *42*, 3257.
(463) Rajalakshmi, N.; Ryu, H.; Shaijumon, M. M.; Ramaprabhu, S. *J. Power Sources* **2005**, *140*, 250.
(464) Li, X. G.; Hsing, I. M. *Electrochim. Acta* **2006**, *51*, 5250.
(465) Dieckmann, G. R.; Langer, S. H. *Electrochim. Acta* **1998**, *44*, 437.
(466) Hayase, M.; Kawase, T.; Hatsuzawa, T. *Electrochem. Solid-State Lett.* **2004**, *7*, A231.
(467) Wu, G.; Li, L.; Li, J. H.; Xu, B. Q. *Carbon* **2005**, *43*, 2579.
(468) Rajesh, B.; Thampi, K. R.; Bonard, J. M.; Mathieu, H. J.; Xanthopoulos, N.; Viswanathan, B. *Chem. Commun.* **2003**, 2022.
(469) Lefebvre, M. C.; Qi, Z. G.; Pickup, P. G. *J. Electrochem. Soc.* **1999**, *146*, 2054.
(470) Rajesh, B.; Thampi, K. R.; Bonard, J. M.; Mathieu, H. J.; Xanthopoulos, N.; Viswanathan, B. *J. Power Sources* **2005**, *141*, 35.
(471) Swathirajan, S.; Mikhail, Y. M. *J. Electrochem. Soc.* **1992**, *139*, 2105.
(472) Zhao, X. S.; Li, W. Z.; Jiang, L. H.; Zhou, W. J.; Xin, Q.; Yi, B. L.; Sun, G. Q. *Carbon* **2004**, *42*, 3263.
(473) Li, W. Z.; Liang, C. H.; Qiu, J. S.; Zhou, W. J.; Han, H. M.; Wei, Z. B.; Sun, G. Q.; Xin, Q. *Carbon* **2002**, *40*, 791.
(474) Tang, H.; Chen, J. H.; Huang, Z. P.; Wang, D. Z.; Ren, Z. F.; Nie, L. H.; Kuang, Y. F.; Yao, S. Z. *Carbon* **2004**, *42*, 191.
(475) Chen, G. Y.; Waraksa, C. C.; Cho, H. G.; Macdonald, D. D.; Mallouk, T. E. *J. Electrochem. Soc.* **2003**, *150*, E423.
(476) Ioroi, T.; Siroma, Z.; Fujiwara, N.; Yamazaki, S.; Yasuda, K. *Electrochem. Commun.* **2005**, *7*, 183.
(477) Kuroki, T.; Sasaki, K.; Kusaba, H.; Teraoka, Y. *Meeting abstracts* **2004**, 1527.
(478) Feng, C. H.; Xiao, Z. Y.; Chan, P. C. H.; Hsing, I. M. *Electrochem. Commun.* **2006**, *8*, 1235.
(479) Seo, Y. H.; Cho, Y. H. *Sens. Mater.* **2004**, *16*, 277.

(480) Min, K.; Tanaka, S.; Esashi, M. *J. Micromech. Microeng.* **2006**, *16*, 505.
(481) D'Arrigo, G.; Spinella, C.; Arena, G.; Lorenti, S. *Mater. Sci. Eng., C* **2003**, *23*, 13.
(482) Yeom, J.; Mozsgai, G. Z.; Flachsbart, B. R.; Choban, E. R.; Asthana, A.; Shannon, M. A.; Kenis, P. J. A. *Sens. Actuators, B* **2005**, *107*, 882.
(483) Rajesh, B.; Thampi, K. R.; Bonard, J. M.; Mathieu, H. J.; Xanthopoulos, N.; Viswanathan, B. *Electrochem. Solid-State Lett.* **2004**, *7*, A404.
(484) Wang, J.; Swain, G. M. *J. Electrochem. Soc.* **2003**, *150*, E24.
(485) Wang, J.; Swain, G. M.; Tachibana, T.; Kobashi, K. *J. New Mater. Electrochem. Syst.* **2000**, *3*, 75.
(486) Wang, J.; Swain, G. M.; Tachibana, T.; Kobashi, K. *Electrochem. Solid-State Lett.* **2000**, *3*, 286.
(487) Bennett, J. A.; Show, Y.; Wang, S. H.; Swain, G. M. *J. Electrochem. Soc.* **2005**, *152*, E184.
(488) Montilla, F.; Morallon, E.; Duo, I.; Comninellis, C.; Vazquez, J. L. *Electrochim. Acta* **2003**, *48*, 3891.
(489) Enea, O.; Riedo, B.; Dietler, G. *Nano Lett.* **2002**, *2*, 241.
(490) Gao, J. S.; Arunagiri, T.; Chen, J. J.; Goodwill, P.; Chyan, O.; Perez, J.; Golden, D. *Chem. Mater.* **2000**, *12*, 3495.
(491) Honda, K.; Yoshimura, M.; Rao, T. N.; Tryk, D. A.; Fujishima, A.; Yasui, K.; Sakamoto, Y.; Nishio, K.; Masuda, H. *J. Electroanal. Chem.* **2001**, *514*, 35.
(492) Gonzalez-Gonzalez, I.; Tryk, D. A.; Cabrera, C. R. *Diamond Relat. Mater.* **2006**, *15*, 275.
(493) Suffredini, H. B.; Tricoli, V.; Vatistas, N.; Avaca, L. A. *J. Power Sources* **2006**, *158*, 124.
(494) Parsonage, E. E.; Debe, M. K. U.S. Patent 5,338,430, 1994.
(495) Debe, M. K.; Poirier, R. J.; Wackerfuss, M. K.; Ziegler, R. J. U.S. Patent 5,879,828, 1999.
(496) Debe, M. K. In *Handbook of Fuel Cells Fundamentals, Technology and Applications*; Vielstich, W., Lamm, A., Gasteiger, H. A., Eds.; John Wiley & Sons: New York, 2003.
(497) Bonakdarpour, A.; Wenzel, J.; Stevens, D. A.; Sheng, S.; Monchesky, T. L.; Lobel, R.; Atanasoski, R. T.; Schmoeckel, A. K.; Vernstrom, G. D.; Debe, M. K.; Dahn, J. R. *J. Electrochem. Soc.* **2005**, *152*, A61.
(498) Debe, M. *DOE Hydrogen Program Review*, 2005.
(499) Johnson Matthey Precious Metals Marketing, 2007, http://www.platinum.matthey.com/prices/price_charts.html.
(500) Kinoshita, K. *J. Electrochem. Soc.* **1990**, *137*, 845.
(501) Zhang, J.; Lima, F. H. B.; Shao, M. H.; Sasaki, K.; Wang, J. X.; Hanson, J.; Adzic, R. R. *J. Phys. Chem. B* **2005**, *109*, 22701.
(502) Fernandez, J. L.; Raghuveer, V.; Manthiram, A.; Bard, A. J. *J. Am. Chem. Soc.* **2005**, *127*, 13100.
(503) Raghuveer, V.; Manthiram, A.; Bard, A. J. *J. Phys. Chem. B* **2005**, *109*, 22909.
(504) Zhang, J.; Mo, Y.; Vukmirovic, M. B.; Klie, R.; Sasaki, K.; Adzic, R. R. *J. Phys. Chem. B* **2004**, *108*, 10955.
(505) Alonso-Vante, N.; Malakhov, I. V.; Nikitenko, S. G.; Savinova, E. R.; Kochubey, D. I. *Electrochim. Acta* **2002**, *47*, 3807.
(506) Vante, N. A.; Tributsch, H. *Nature* **1986**, *323*, 431.
(507) Cao, D. X.; Wieckowski, A.; Inukai, J.; Alonso-Vante, N. *J. Electrochem. Soc.* **2006**, *153*, A869.
(508) Zhang, L.; Zhang, J. J.; Wilkinson, D. P.; Wang, H. J. *J. Power Sources* **2006**, *156*, 171.
(509) Houston, J. E.; Laramore, G. E.; Park, R. L. *Science* **1974**, *185*, 258.
(510) Colton, R. J.; Huang, J.-T.; Rabalais, J. W. *Chem. Phys. Lett.* **1975**, *34*, 337.
(511) Bennett, L. H.; Cuthill, J. R.; McAlister, A. J.; Erickson, N. E.; Watson, R. E. *Science* **1974**, *184*, 563.
(512) Colton, R. J.; Rabalais, J. W. *Inorg. Chem.* **1976**, *15*, 236.
(513) Levy, R. B.; Boudart, M. *Science* **1973**, *181*, 547.
(514) Binder, H.; Köhling, A.; Kuhn, W.; Lindner, W.; Sandstede, G. *Nature* **1969**, *224*, 1299.
(515) Kawamura, G.; Okamoto, H.; Ishikawa, A.; Kudo, T. *J. Electrochem. Soc.* **1987**, *137*, 1653.
(516) Okamoto, H.; Kawamura, G.; Ishikawa, A.; Kudo, T. *J. Electrochem. Soc.* **1987**, *134*, 1649.
(517) Okamoto, H.; Kawamura, G.; Ishikawa, A.; Kudo, T. *J. Electrochem. Soc.* **1987**, *134*, 1345.
(518) Kudo, T.; Kawamura, G.; Okamoto, H. *J. Electrochem. Soc.* **1983**, *130*, 1491.
(519) Machida, K.; Enyo, M. *J. Electrochem. Soc.* **1990**, *137*, 871.
(520) Palanker, V. S.; Gajyev, R. A.; Sokolsky, D. V. *Electrochim. Acta* **1977**, *22*, 133.
(521) Silberberg, E.; Arbib, M.; Reniers, F.; Buess-Herman, C. *Proceedings of the second international symposium on new materials fuel cell and modren battery systems* **1997**, 693.
(522) Armstrong, R. D.; Douglas, A. F.; Keene, D. E. *J. Electrochem. Soc.* **1971**, *118*, 568.
(523) Böhm, H. *Electrochim. Acta* **1970**, *15*, 1273.
(524) Ilchenko, N. I.; Pyatinitsky, Yu. I. *Carbides of transition metals as catalysts for oxidation reactions*; Blackie Academic & Professional: Glasgow, 1996.
(525) Scholl, H.; Hofman, B.; Kupis, J.; Polaski, K. *Electrochim. Acta* **1994**, *39*, 115.
(526) Scholl, H.; Hofman, B.; Rauscher, A. *Electrochim. Acta* **1992**, *37*, 447.
(527) Voorhies, J. D. *J. Electrochem. Soc.* **1972**, *119*, 219.
(528) Yoneyama, H.; Kaneda, M.; Tamura, H. *Denki Kagaku* **1973**, *41*, 719.
(529) Yoneyama, H.; Murakami, S.; Tamura, H. *Denki Kagaku* **1974**, *42*, 178.
(530) Bianchi, V. G.; Mazza, F.; Trasatti, S. *Z. Phys. Chem.* **1964**, *Bd.226*, 40.
(531) Armstrong, R. D.; Douglas, A. F. *J. Appl. Electrochem.* **1972**, *2*, 143.
(532) Morita, M.; Iwakura, C.; Yoneyama, H.; Tamura, H. *Denki Kagaku* **1975**, *43*, 740.
(533) Tamari, N.; Kato, A. *Denki Kagaku* **1976**, *44*, 477.
(534) Cowling, R. D.; Hintermann, H. E. *J. Electrochem. Soc.* **1970**, *117*, 1447.
(535) Cowling, R. D.; Hintermann, H. E. *J. Electrochem. Soc.* **1971**, *118*, 1912.
(536) Lavrenko, V. A.; Lysenko, E. V.; Bochko, A. V.; Knyazeva, E. N.; Frantsevich, I. N. *Dokl. Akad. Nauk SSSR* **1982**, *267*, 1395.
(537) Yoneyama, H.; Ishikawa, Y.; Tamura, H. *Denki Kagaku* **1971**, *39*, 816.
(538) Tomashov, N. D.; Chuhalovskaya, T. V.; Medova, I. L.; Egorov, F. F. *Zashch. Met.* **1985**, *21*, 682.
(539) Tomashov, N. D.; Chuhalovskaya, T. V.; Chebotareva, N. P.; Kudryavtsev, V. I. *Zashch. Met.* **1989**, *25*, 911.
(540) Mazza, F.; Trasatti, S. *J. Electrochem. Soc.* **1963**, *110*, 847.
(541) Voïnov, M.; Bühler, D.; Tannenberger, H. *J. Electrochem. Soc.* **1971**, *118*, 1137.
(542) Scholta, J.; Wendt, H. *Inst. Chem. Eng. Symp. Ser.* **1992**, *No.127*, 237.
(543) Lee, K.; Ishihara, A.; Mitsushima, S.; Kamiya, N.; Ota, K. *Electrochim. Acta* **2004**, *49*, 2479.
(544) Ota, K.; Ishihara, A.; Mitsushima, S.; Lee, K.; Suzuki, Y.; Horibe, N.; Nakagawa, T.; Kamiya, N. *J. New Mater. Electrochem. Syst.* **2005**, *8*, 25.
(545) Ishihara, A.; Lee, K.; Doi, S.; Kim, J.-H.; Liu, Y.; Mitsushima, S.; Kamiya, N.; Ota, K. *Papers of EXPO World Conference on Wind energy, Renewable energy, Fuel cell & Exhibition* **2005**, 5010.
(546) Bhattarai, J.; Akiyama, E.; Habazaki, H.; Kawashima, A.; Asami, K.; Hashimoto, K. *Corros. Sci.* **1998**, *40*, 757.
(547) Šepa, D. B.; Damjanovic, A.; Bockris, J. O'M. *Electrochim. Acta* **1967**, *12*, 746.
(548) Niedrach, L. W.; Zeliger, H. I. *J. Electrochem. Soc.* **1969**, *116*, 152.
(549) Broyde, B. *J. Catal.* **1968**, *10*, 13.
(550) Damjanovic, A.; Sepa, D.; Bockris, J. O'M. *J. Res. Inst. Catal., Hokkaido Univ.* **1968**, *16*, 1.
(551) Fishman, J. H.; Henry, J. F.; Tessore, S. *Electrochim. Acta* **1969**, *14*, 1314.
(552) McHardy, J.; Bockris, J. O'M. *J. Electrochem. Soc.* **1973**, *120*, 53.
(553) Bockris, J. O. M.; McHardy, J. *J. Electrochem. Soc.* **1973**, *120*, 61.
(554) Appleby, A. J.; Drunen, C. V. *J. Electrochem. Soc.* **1976**, *123*, 200.
(555) Liu, L.; Ishihara, A.; Mitsushima, S.; Kamiya, N.; Ota, K. *Electrochem. Solid-State Lett.* **2005**, *8*, A400.
(556) Yato, K.; Doi, S.; Ishihara, A.; Mitsushima, S.; Kamiya, N.; Ota, K. *Suiso enerugi shisutemu* **2006**, *31*, 58.
(557) Doi, S.; Liu, Y.; Ishihara, A.; Mitsushima, S.; Kamiya, N.; Ota, K. *ECS Trans.* **2006**, *1*, 17.
(558) Ishihara, A.; Doi, S.; Mitsushima, S.; Kamiya, N.; Ota, K. *ECS Trans.* **2006**, *1*, 51.
(559) Kim, J.-H.; Ishihara, A.; Mitsushima, S.; Kamiya, N.; Ota, K. *Electrochemistry*, in press.
(560) Shibata, Y.; Ishihara, A.; Mitsushima, S.; Kamiya, N.; Ota, K. *Electrochem. Solid-State Lett.* **2007**, *10*, B43.
(561) Ishihara, A.; Lee, K.; Doi, S.; Mitsushoma, S.; Kamiya, N.; Ota, K. *Proc. 15th World Hydrogen Energy Conf.* **2004**, *29K-09*.
(562) Ishihara, A.; Lee, K.; Doi, S.; Mitsushima, S.; Kamiya, N.; Hara, M.; Domen, K.; Fukuda, K.; Ota, K. *Electrochem. Solid-State Lett.* **2005**, *8*, A201.
(563) Azuma, M.; Nakato, Y.; Tsubomura, H. *J. Electroanal. Chem.* **1987**, *220*, 369.
(564) Azuma, M.; Nakato, Y.; Tsubomura, H. *J. Electroanal. Chem.* **1988**, *225*, 179.
(565) Azuma, M.; Nakato, Y.; Tsubomura, H. *Mater. Res. Bull.* **1987**, *22*, 527.
(566) Azuma, M.; Kashihara, M.; Nakato, Y.; Tsubomura, H. *J. Electroanal. Chem.* **1988**, *250*, 73.

(567) Zhong, H.; Zhang, H.; Liu, G.; Liang, Y.; Hu, J.; Yi, B. *Electrochem. Commun.* **2006**, *8*, 707.
(568) Faubert, G.; Lalande, G.; Cote, R.; Guay, D.; Dodelet, J. P.; Weng, L. T.; Bertrand, P.; Denes, G. *Electrochim. Acta* **1996**, *41*, 1689.
(569) Lalande, G.; Cote, R.; Tamizhmani, G.; Guay, D.; Dodelet, J. P.; Dignardbailey, L.; Weng, L. T.; Bertrand, P. *Electrochim. Acta* **1995**, *40*, 2635.
(570) Lefevre, M.; Dodelet, J. P. *Electrochim. Acta* **2003**, *48*, 2749.
(571) Lefevre, M.; Dodelet, J. P.; Bertrand, P. *J. Phys. Chem. B* **2002**, *106*, 8705.
(572) Lefevre, M.; Dodelet, J. P.; Bertrand, P. *J. Phys. Chem. B* **2000**, *104*, 11238.
(573) Medard, C.; Lefevre, M.; Dodelet, J. P.; Jaouen, F.; Lindbergh, G. *Electrochim. Acta* **2006**, *51*, 3202.
(574) Fournier, J.; Lalande, G.; Cote, R.; Guay, D.; Dodelet, J. P. *J. Electrochem. Soc.* **1997**, *144*, 218.
(575) Wang, H.; Cote, R.; Faubert, G.; Guay, D.; Dodelet, J. P. *J. Phys. Chem. B* **1999**, *103*, 2042.
(576) Villers, D.; Jacques-Bedard, X.; Dodelet, J. P. *J. Electrochem. Soc.* **2004**, *151*, A1507.
(577) Jaouen, F.; Lefevre, M.; Dodelet, J.-P.; Cai, M. *J. Phys. Chem. B* **2006**, *110*, 5553.
(578) Faubert, G.; Cote, R.; Dodelet, J. P.; Lefevre, M.; Bertrand, P. *Electrochim. Acta* **1999**, *44*, 2589.
(579) Jaouen, F.; Marcotte, S.; Dodelet, J. P.; Lindbergh, G. *J. Phys. Chem. B* **2003**, *107*, 1376.
(580) Jasinski, R. *Nature* **1964**, *201*, 1212.
(581) Jasinski, R. *J. Electrochem. Soc.* **1965**, *112*, 526.
(582) Elzing, A.; Vanderputten, A.; Visscher, W.; Barendrecht, E. *J. Electroanal. Chem. Interfacial Electrochem.* **1986**, *200*, 313.
(583) Wang, B. *J. Power Sources* **2005**, *152*, 1.
(584) Gouerec, P.; Savy, M. *Electrochim. Acta* **1999**, *44*, 2653.
(585) Sawai, K.; Suzuki, N. *J. Electrochem. Soc.* **2004**, *151*, A682.
(586) Matter, P. H.; Ozkan, U. S. *Catal. Lett.* **2006**, *109*, 115.
(587) Matter, P. H.; Wang, E.; Arias, M.; Biddinger, E. J.; Ozkan, U. S. *J. Phys. Chem. B* **2006**, *110*, 18374.
(588) Matter, P. H.; Wang, E.; Ozkan, U. S. *J. Catal.* **2006**, *243*, 395.
(589) Matter, P. H.; Zhang, L.; Ozkan, U. S. *J. Catal.* **2006**, *239*, 83.
(590) Posudievsky, O. Y.; Kurys, Y. I.; Pokhodenko, V. D. *Synth. Met.* **2004**, *144*, 107.
(591) Bashyam, R.; Zelenay, P. *Nature* **2006**, *443*, 63.
(592) Bashyam, R.; Johnston, C. M.; Conradson, S. D.; Zelenay, P. *233rd Am. Chem. Soc. Natl. Meet.* **2007**.
(593) Zelenay, P.; Bashyam, R.; Brosha, E.; Choi, J.-H.; Garzon, F.; Conradson, S.; Johnston, C.; Mukundan, R.; Ramsey, J. *U.S. DOE, Hydrogen Annual Progress Report*, 2006, http://www.hydrogen.energy.gov/pdfs/progress06/v_c_7_zelenay.pdf.
(594) Lefevre, M.; Dodelet, J. P. *Electrochim. Acta* **2003**, *48*, 2749.
(595) Faubert, G.; Lalande, G.; Cote, R.; Guay, D.; Dodelt, J. P.; Weng, L. T.; Bertrand, P.; Denes, G. *Electrochim. Acta* **1996**, *41*, 1689.
(596) Lalande, G.; Cote, R.; Tamizhmani, G.; Guay, D.; Dodelet, J. P.; Dignardbailey, L.; Weng, L. T.; Bertrand, P. *Electrochim. Acta* **1995**, *40*, 2635.
(597) Maruyama, J.; Abe, I. *Chem. Mater.* **2006**, *18*, 1303.
(598) Maruyama, J.; Abe, I. *Chem. Mater.* **2005**, *17*, 4660.
(599) Zelenay, P.; Brosha, E.; Choi, J.-H.; Davey, J.; Garzon, F.; Hamon, C.; Piela, B.; Ramsey, J.; Uribe, F. *U.S. DOE, Hydrogen Annual Progress Report*, 2005, http://www.hydrogen.energy.gov/pdfs/progress05/vii_c_7_zelenay.pdf.
(600) Nguyen, T. V. *J. Electrochem. Soc.* **1996**, *143*, L103.
(601) You, L.; Liu, H. *Int. J. Heat Mass Transfer* **2002**, *45*, 2277.
(602) Natarajan, D.; Nguyen, T. V. *J. Power Sources* **2003**, *115*, 66.
(603) Weber, A. Z.; Darling, R. M.; Newman, J. *J. Electrochem. Soc.* **2004**, *151*, A1715.
(604) Williams, M. V.; Kunz, H. R.; Fenton, J. M. *J. Electrochem. Soc.* **2004**, *151*, A1617.
(605) Pasaogullari, R.; Wang, C.-Y. *J. Electrochem. Soc.* **2004**, *151*, A399.
(606) Pasaogullari, U.; Wang, C.-Y. *J. Electrochem. Soc.* **2005**, *152*, A380.
(607) Weber, A. Z.; Newman, J. *J. Electrochem. Soc.* **2005**, *152*, A677.
(608) Yi, J. S.; Nguyen, T. V. *J. Electrochem. Soc.* **1999**, *146*, 38.
(609) Li, G.; Pickup, P. G. *J. Electrochem. Soc.* **2003**, *150*, C745.
(610) Williams, M. V.; Kunz, H. R.; Fenton, J. M. *J. Electrochem. Soc.* **2005**, *152*, A635.
(611) Wood, D. L.; Grot, S. A.; Fly, G. U.S. Patent No. 6,350,539, 2002.
(612) Tseng, C.-J.; Lou, S.-K.; Yan, Y.-Y.; Sung, L. Y. *Proc. Int. Hydrogen Energy Congr. Exhibition* **2005**, 1.
(613) Yu, J.; Matsuura, T.; Yoshikawa, Y.; Islam, M. Z.; Hori, M. *Electrochem. Solid-State Lett.* **2005**, *8*, A156.
(614) Wood, D. L.; Wilde, P. M.; Mändle, M.; Murata, M. *Abstracts of the 2002 Fuel Cell Seminar* **2002**, 41.
(615) Bluemle, M. J.; Gurau, V.; Mann, J. A., Jr.; Zawodzinski, T. A., Jr.; De Castro, E. S.; Tsou, Y.-M. *Electrochem. Soc Joint Int. Meet.* **2004**, Abstract No. 1932.
(616) Liu, W.; Moore, D.; Murthy, M. *2004 Electrochem. Soc. Joint Int. Meet.* **2004**, Abstract No. 1930.
(617) Jordan, L. R.; Shukla, A. K.; Behrsing, T.; Avery, N. R.; Muddle, B. C.; Forsyth, M. *J. Power Sources* **2000**, *86*, 250.
(618) Dohle, H.; Jung, R.; Kimiaie, N.; Mergel, J.; Müller, M. *J. Power Sources* **2003**, *124*, 371.
(619) Ihonen, J.; Mikkola, M.; Lindbergh, G. *J. Electrochem. Soc.* **2004**, *151*, A1152.
(620) Weber, A. Z.; Newman, J. *Chem. Rev.* **2004**, *104*, 4679.
(621) Bernardi, D. M.; Verbrugge, M. W. *J. Electrochem. Soc.* **1992**, *139*, 2477.
(622) Springer, T. E.; Wilson, M. S.; Gottesfeld, S. *J. Electrochem. Soc.* **1993**, *140*, 3513.
(623) Springer, T. E.; Zawodzinski, T. A.; Wilson, M. S.; Gottesfeld, S. *J. Electrochem. Soc.* **1996**, *143*, 587.
(624) Nam, J. H.; Kaviany, M. *Int. J. Heat Mass Transfer* **2003**, *46*, 4595.
(625) Kumbur, E. C.; Sharp, K. V.; Mench, M. M. *J. Power Sources* **2006**, *161*, 333.
(626) Kumbur, E. C.; Sharp, K. V.; Mench, M. M. *J. Electrochem. Soc.*, Submitted.
(627) Hou, J.; Yu, H.; Zhang, S.; Sun, S.; Wang, H.; Yi, B.; Ming, P. *J. Power Sources* **2006**, *162*, 513.
(628) St-Pierre, J.; Wilkinson, D. P.; Knights, S.; Bos, M. L. *J. New Mater. Electrochem. Syst.* **2000**, *3*, 99.
(629) Wood, D.; Davey, J.; Garzon, F.; Atanassov, P.; Borup, R. *Proc. Fuel Cell Seminar* **2005**.
(630) Liu, D.; Case, S. *J. Power Sources* **2006**, *162*, 521.
(631) Kuriki, H. H.; Fukumoto; Yoshioka, S.; Matsumoto, S. *Proc. Fuel Cell Seminar 2006* **2006**.
(632) Yan, Q. G.; Toghiani, H.; Lee, Y. W.; Liang, K. W.; Causey, H. *J. Power Sources* **2006**, *160*, 1242.
(633) Lee, W. K.; Ho, C. H.; Van, Zee, J. W.; Murthy, M. *J. Power Sources* **1999**, *84*, 45.
(634) Kitahara, T.; Konomi, T.; Sasaki, Y. *Jpn. Soc. Mech. Eng.* **2006**, *72*, 192.
(635) Wilde, P. M.; Mändle, M.; Murata, M.; Berg, N. *Fuel Cells* **2004**, *4*, 180.
(636) Murata, M. *J. Soc. Automotive Eng. Jpn.* **2005**, *59*, 109.
(637) Kim, Y. S.; Chlistunoff, J.; Pivovar, B. 2006 DOE Hydrogen Program Review, Arlington, VA, 2006.
(638) Guo, Q. H.; Pintauro, P. N.; Tang, H.; O'Connor, S. *J. Membr. Sci.* **1999**, *154*, 175.
(639) Liu, B.; Guiver, M. D.; Kim, Y. S.; Pivovar, B. 232nd ACS National Meeting, San Francisco, 2006.
(640) Miyatake, K.; Oyaizu, K.; Tsuchida, E.; Hay, A. S. *Macromolecules* **2001**, *34*, 2065.
(641) Fang, J.; Guo, X.; Harada, S.; Watari, T.; Tanaka, K.; Kita, H.; Okamoto, K. *Macromolecules* **2002**, *35*, 9022.
(642) Almeida, S. H. d.; Kawano, Y. *J. Therm. Anal. Calorim.* **1999**, *58*, 569.
(643) Shi, Z.; Holdcroft, S. *Macromolecules* **2005**, *38*, 4193.
(644) Nasef, M. M. *Eur. Polym. J.* **2002**, *38*, 87.
(645) Calcagno, L.; Musumeci, P.; Percolla, R.; Foti, G. *Nucl. Instrum. Methods Phys. Res., Sect. B* **1993**, *91*, 461.
(646) Swier, S.; Chun, Y. S.; Gasa, J.; Shaw, M. T.; Weiss, R. A. *Polym. Eng. Sci.* **2005**, *45*, 1081.
(647) Marani, D.; Vona, M. L. D.; Traversa, E.; Licoccia, S.; Beurroies, I.; Llewellyn, P. L.; Knauth, P. *J. Phys. Chem. B* **2006**, *110*, 15817.
(648) Mitsushima, S.; Kawahara, S.; Ota, K. I.; Kamiya, N. *J. Electrochem. Soc.* **2007**, *154*, B153.

CR050182L